REFLECTANCE-BASED PULSE OXIMETER FOR THE CHEST AND WRIST

A Major Qualifying Project Report:

Submitted to the Faculty

Of the

WORCESTER POLYTECHNIC INSTITUTE

In partial fulfillment of the requirements for the

Degree of Bachelor of Science

By

Alexandra Fontaine

Arben Koshi

Danielle Morabito

Nicolas Rodriguez

Submitted on:

Approved by:

Professor Yitzhak Mendelson, Advisor, Dept. of Biomedical Engineering

APPLE 1042
Apple v. Masimo
IPR2024-00241

Authorship

Section	Author
Introduction	Nicolas Rodriguez, Danielle Morabito, Alex Fontaine, Arben Koshi
Literature Review	Nicolas Rodriguez, Danielle Morabito, Alex Fontaine, Arben Koshi
Design Approach	Alex Fontaine, Danielle Morabito
Device Development	Nicolas Rodriguez, Danielle Morabito
Methods	Nicolas Rodriguez, Danielle Morabito
Final Design	Arben Koshi, Nicolas Rodriguez, Danielle Morabito
Results	Alex Fontaine, Arben Koshi
Discussion	Arben Koshi, Alex Fontaine
Summary	Arben Koshi
Conclusion	Arben Koshi
Future Improvements	Arben Koshi, Nicolas Rodriguez
Appendix A	Danielle Morabito
Appendix B	Arben Koshi
Appendix C	Alex Fontaine
Appendix D	Arben Koshi

Abstract

Reflectance-based pulse oximetry is a technique used for noninvasively monitoring the oxygen saturation (SpO_2) and pulse rate (PR). However, there is little supporting evidence that it can accurately collect measurements from the chest and wrist. In this project, a reflectance-based pulse oximeter was built and used to collect measurements while sitting, standing, during self-induced hypoxia, and during self-induced hyperventilation then compared to the measurements taken by a HOMEDIC Deluxe Pulse Oximeter. The prototype was able to accurately measure within an error of $\pm$ 1% and ±3% for SpO_2 and PR respectively from the wrist while an error of ±1% and $\pm$4% for SpO_2 and PR respectively from the chest.

Acknowledgements

We would like to thank Professor Mendelson for advising this project. We would also like to acknowledge Dr. Adriana Hera and Lisa Wall for their support.

Executive Summary

Oxygen saturation (SpO_2) is the measurement of oxyhemoglobin (HbO_2) in arterial blood. SpO_2 is an important vital measurement because it shows the levels of blood oxygenation. Traditionally, SpO_2 is measured by invasively drawing blood samples. This method, however, is not ideal and it is unable to provide clinicians with real-time measurements. With the need for a noninvasive way to measure SpO_2, pulse oximetry was developed. The use of this technology allows clinicians to determine SpO_2 in patients that are sedated, anesthetized, unconscious, or unable to regulate their own oxygen supply.

Reflectance-based pulse oximetry allows measurements to be taken from areas of the body in which transmittance based pulse oximetry cannot be applied. In reflectance-based pulse oximetry, the incident light is passed through the skin and is reflected off the subcutaneous tissue and bone. To this day, being able to measure signals from the chest and wrist with one single device has not been successfully achieved. Such a device would allow patients to measure SpO_2 and pulse rate (PR) without hindering their normal day-to-day activities.

The prototype pulse oximeter constructed during this project consists of two hardware components and a programmed LabVIEW Virtual Instrument (VI). The hardware components consist of the sensor and a circuit which produces, collects, and processes photoplethysmographic (PPG) signals. The VI collects the PPG signals produced by the hardware and process them in order to produce numerical results for PR and SpO_2 . The optical sensor is made up of two Light Emitting Diodes (LEDs), a red LED, with a peak emission wavelength of 660 nm, and an infrared emitter with a peak emission wavelength of 940 nm. These LEDs are positioned next to each other in the center of a circular Printed Circuit Board (PCB) and surrounded by 8 photodiodes (PD). The circuitry for the sensor consists of an Arduino Duo Microprocessor which is programmed to light up the red and infrared LEDs intermittently at a frequency of 100Hz. The PDs are connected in photovoltaic mode in order to produce a voltage output. Operational amplifiers are utilized to amplify the photodiode output. Once amplified, the red and infrared PPG signals obtained from the photodetectors are sent through two Sample-and-Hold circuits to separate the signals into their respective alternating current (AC) and direct current (DC) components for further filtering and amplification.

The four input signals sent to the LabVIEW software : AC red, AC infrared, DC red and DC infrared access the VI via a National Instruments (NI) Data Acquisition (DAQ) system. The AC components of the red and infrared PPGs are measured using a peak-to-peak detection algorithm, while the DC components are measured by finding their respective averages. Once the signals are processed, SpO_2 is calculated by obtaining the ratio of the AC and DC components of the red PPG and dividing that by the ratio of the AC and DC components of the infrared PPG. To calculate PR, the frequency of the infrared AC signal is measured using frequency measurement parameters in LabVIEW and then

multiplied by 60 to display PR in beats per minute (bpm). To compare the measurants taken from the pulse oximeter prototype, a transmission-type finger HOMEDICS Deluxe Pulse Oximeter was utilized as reference. The reliability of the Deluxe Pulse Oximeter was tested against a Biopac ECG model 100C module and was concluded that the HOMEDICS Deluxe Pulse Oximeter was provided accurate enough measurements for pulse rate.

For testing, the sensor was strapped to the wrist and chest of each subject using a Velcro strap while the HOMEDICS Deluxe Pulse Oximeter was placed on the subject's index finger. The VI was set up to collect, average and display SpO_2 and PR data every 10 seconds throughout a 6 minute timespan accounting for 36 measurements. At this point, a second individual that was monitoring the reference device recorded the corresponding SpO_2 and PR values displayed by the HOMEDICS pulse oximeter. Subjects were tested on the chest and wrist while sitting, standing, during self-induced hyperventilation, and during self-induced hypoxia.

While collecting data, it was noticed that the PR measurements collected from the chest had significantly larger margins of error compared to those from the wrist. One possible explanation for this discrepancy deals with the LabVIEW algorithm for PR calculation. Instead of doing peak-peak analysis, we opted to use a search tool which graphs a power spectrum of the data and searches for the highest amplitude frequency between 0.75Hz and 2.25Hz. This method is very effective at PR values ranging between 45 and 135 bpm, but loses its accuracy at higher PR values. Measurements above 135 bpm were detected by the reference, but not accurately detected by the prototype.

Margins of error obtained from the standing and sitting measurement tests on the wrist included 0.6%, and 0.2% for SpO_2 and 0.2%, 1.1% for PR respectively. Measurements from the chest displayed errors of 0.4% and 0.3% for SpO_2 and 0.1%, and 0.7% for PR while standing and sitting respectively. Based on this data, our prototype for a reflectance-based pulse oximeter for the chest and wrist was successful in measuring PR and SpO_2.

Table of Contents

Authorship i
Abstract ii
Acknowledgements iii
Executive Summary iv
Table of Figures viii
Table of Tables x
Abbreviations xi
1 Introduction 12
2 Literature Review 13
2.1 Oxygen Saturation 13
2.2 Pulse Oximetry 13
2.2.1 Principle of a Pulse Oximeter 15
2.2.2 Methods of Light Detection 16
2.2.3 Photoplethysmogram 17
2.2.4 Wavelength Optimization 17
2.2.5 Limitations and Applications of Pulse Oximetry 17
2.3 Reflectance vs. Transmittance Pulse Oximetry 18
2.4 New Studies for Pulse Oximeters 19
3 Design Approach 21
3.1 Initial Client Statement 21
3.2 Clinical Need 21
3.3 Design Parameters 21
3.3.1 Objectives 21
3.3.2 Constraints 22
3.3.3 Functions 22
3.3.4 Design Specifications 23
3.4 Revised Client Statement 25
4 Device Development 27
4.1 Device Alternatives 27
4.1.1 Sensor Design 1 27
4.1.2 Sensor Design 2 28
4.2 Software Design 29
5 Methods 30

5.1 Photodetection Unit 30
5.2 PPG 30
5.3 Filter Design 30
5.4 Software 31
5.4.1 Incoming Signals 32
5.4.2 Filtering 34
5.4.3 Frequency of Pulse Rate 35
5.4.4 Pulse Rate Calculation 36
5.4.5 Spectral Measurements 37
5.4.6 SpO_2 Calculation 39
5.4.7 Preliminary VI Test 44
5.5 Experimentation/Testing 48
6 Final Design 51
6.1 Device Hardware 51
6.1.1 Sensor 51
6.1.2 Circuitry 52
6.2 Software 56
7 Results 59
7.1 Comparison Graphs 61
7.2 Dynamic Response Plots 73
7.3 Residual Plots 91
8 Discussion 98
10 Summary 101
11 Conclusion 103
12 Future Improvements 104
References 106
Appendix A: Description of LabVIEW 107
Appendix B: Bill of Materials 117
Appendix C: Data Sets 118
Appendix D: Filter Bode Plots 128

Table of Figures

Figure 2.1: Arterial blood changing over time, PPG [11] 14
Figure 2.2: Optical absorption spectra of Hb, HbO_2, MetHb, and BbCO [11] 15
Figure 2.3: Transmittance pulse oximetry 18
Figure 2.4: Reflectance pulse oximetry 18
Figure 2.5: Forehead pulse oximeter 19
Figure 3.1: Objective tree 22
Figure 5.1: Unfiltered output of a PPG signal with an AC component riding on top of a DC component 30
Figure 5.2: Configuration of functions to separate incoming signals 33
Figure 5.4: Filter function and graph 35
Figure 5.5: Tone measurements output frequency 35
Figure 5.6: Configure tone measurements parameters 36
Figure 5.7: Functions used to calculate pulse rate 37
Figure 5.8: Amplitude and level measurements functions with numeric indicators 38
Figure 5.9: Configure amplitude and level measurements set to mean (DC) 39
Figure 5.10: SpO_2 calculation 40
Figure 5.11: The configuration of function that limit the displayed SpO_2 41
Figure 5.12: VI Block Diagram 42
Figure 5.13: VI Front Panel 43
Figure 5.14: Front panel for the simulated hypoxia test with low amplitude 45
Figure 5.15: Front panel for the simulated hypoxia test with high amplitude 46
Figure 5.16: Block diagram for the simulated hypoxia test 47
Figure 5.17: Application of the sensor to the wrist (left) and the chest (right) 49
Figure 6.1: Top View of sensor module with photodiodes and LEDs. 51
Figure 6.2: Platform view of sensor module 52
Figure 6.3: Block diagram of the prototype pulse oximeter 53
Figure 6.4:LED driver timing diagram with 2.5ms time increments 54
Figure 6.5: Circuit design for pulse oximeter device 55
Figure 6.6: Block Diagram of Final VI 57
Figure 6.7: Front Panel of Final VI 58
Figure 7.1: Example of corrupted PPG 60
Figure 7.2: Comparison graph for the chest sitting tests. The solid line represents the regression line and the dashed line represents the identity line. 62
Figure 7.3: Comparison graph for the chest standing tests. The solid line represents the regression line and the dashed line represents the identity line. 64
Figure 7.4: Comparison graph for the wrist sitting tests. The solid line represents the regression line and the dashed line represents the identity line. 66
Figure 7.5: Comparison graph for the wrist standing tests. The solid line represents the regression line and the dashed line represents the identity line. 68
Figure 7.6: Comparison graph for hyperventilation tests 70
Figure 7.7: Comparison graph for hypoxia tests. The solid line represents the regression line and the dashed line represents the identity line. 72
Figure 7.8: Oxygen saturation measurement validation plot for the chest standing test 74
Figure 7.9: Pulse rate measurement validation plot for the chest standing test 75
Figure 7.10: Oxygen saturation measurement validation plot for the chest sitting test 77
Figure 7.11: Pulse rate measurement validation plot for the chest sitting test 78
Figure 7.12: Pulse rate measurement validation plot 1 for hyperventilation test 80
Figure 7.13: Pulse rate measurement validation plot 2 for hyperventilation test 81
Figure 7.14: Pulse rate measurement validation plot for the wrist sitting test 83
Figure 7.15: Oxygen saturation measurement validation plot for the wrist sitting test 84
Figure 7.16: Oxygen saturation measurement validation plot for the wrist standing test 86
Figure 7.17: Pulse rate measurement validation plot for the wrist standing test 87
Figure 7.18: Oxygen saturation measurement validation plot 1 for hypoxia test 89

Figure 7.19: Oxygen saturation measurement validation plot 2 for hypoxia test *90*
Figure 7.20: Residual plot for hyperventilation testing for data set 1 (dotted lines: ± 2SD, solid line: average of differences) *92*
Figure 7.21: Residual plot for hyperventilation testing for data set 2(dotted lines: ± 2SD, solid line: average of differences) *93*
Figure 7.22: Residual plot for hyperventilation testing for data set 3 (dotted lines: ± 2SD, solid line: average of differences) *94*
Figure 7.23: Residual plot for hypoxia testing for data set 1 (dotted lines: ± 2SD, solid line: average of differences) *96*
Figure 7.24: Residual plot for hypoxia testing for data set 2 (dotted lines: ± 2SD, solid line: average of differences) *97*

Table of Tables

Table 3.1: Respironic's WristOx Ambulatory Finger Pulse Oximeter Specifications [21] 23
Table 3.2: Santa Medical's Finger Pulse Oximeter Specifications[7] 24
Table 3.3: Crucial Medical Systems Finger Pulse Oximeter Specifications [22] 24
Table 3.4: Project Specifications 25
Table 7.1: Calculated accuracy for the average SpO_2 and PR for each data set 59
Table 7.2: Prototype accuracy based on all data collected 60

Abbreviations

O_2: Oxygen
Hb: Hemoglobin
HbO_2: Oxyhemoglobin
SpO_2: Oxygen saturation
SaO_2: Oxygen saturation measured invasively
PR: Pulse rate
COHb: Carboxyhemoglobin
MetHb: Methyl hemoglobin
PPG: Photoplethysmogram
VI: Virtual Instrument

1 Introduction

One of the most important elements needed to sustain life is oxygen (O_2) because it is used by cells to turn sugars into useable energy. Oxyhemoglobin (HbO_2) is the protein hemoglobin, found in red blood cells, bounded to O_2 that delivers 98% of oxygen to cells. The measurement and calculation of the percentage of HbO_2 in arterial blood is known as oxygen saturation (SpO_2). [1]

Originally, SpO_2 was measured by taking samples of blood and measuring O_2 levels directly. This method was invasive and was unable to provide real-time measurements. This measuring technique made it impossible for SpO_2 to be recognized as an important measure of wellness until a non-invasive method of measuring SpO_2 in real-time was established. [2]

The need for a non-invasive method of measuring SpO_2 in real-time led to the development of pulse oximetry. Pulse oximetry derives SpO_2 and pulse rate (PR) from a photoplethysmogram (PPG). The PPG is obtained by measuring changes in light absorbed by the blood. Red and infrared wavelengths are used to obtain the PPG because these wavelengths are easily transmitted through tissues, allowing SpO_2 to be calculated from the ratio of the absorption of the red and infrared light.

The first device used to continuously measure blood oxygen saturation of human blood in vivo (SaO_2) was built by Karl Matthes in 1935. [2] However, it was not until 1983 that William New and Mark Yelderman, after recognizing the need of an accurate oximeter in the operating room evaluated and produced the pulse oximeter with aims to make it an intraoperative monitoring device. [2] Pulse oximetry allows for an accurate determination of O_2 levels in patients that are sedated, anesthetized, unconscious, and unable to regulate their own oxygen supply as well as provides information needed to avoid irreversible tissue damage. [2]

Since the invention of pulse oximetry, the measurement of SpO_2 has become an important part of the medical world. Nevertheless, improvements such as the application of the reflectance-based technique to measure SpO_2 from multiple locations on the body are still to be developed. This project demonstrates the use of reflectance-based pulse oximetry to obtain measurements for PR and SpO_2 from the chest and wrist. This development in pulse oximetry technology will pave the way for the development of new and novel pulse oximeters that can be worn as accessories, are easily concealed under clothing, and more acclimated to use outside of hospital settings.

2 Literature Review

This is a thorough literature review covering the necessary background needed to fully understand this project.

2.1 Oxygen Saturation

SpO_2 is the amount of O_2 that is carried in the blood. In the human body, SpO_2 is defined as the ratio of HbO_2 to the total concentration of Hb (reduced Hb + HbO_2) present in the blood [1].

$$Oxyhemoglobin\ Saturation\ (\%) = \frac{[HbO_2]}{[Hb]+[HbO_2]} * 100 \tag{1}$$

Hb is the iron-containing protein in red blood cells that transports O_2 to the tissues. This protein forms an unstable and reversible bond with O_2. Thus, Hb in its oxygenated state is called HbO_2 and exhibits a bright red color. Conversely, in its reduced state, it exhibits a purplish blue color [3]. Hb can carry up to four O_2 molecules.

In calculating the absorption of light at a specific wavelength by a homogeneous substance, the Beer-Lambert law can be used to show the basic relationship between the transmitted light intensity and the incident light:

$$I_t = I_o * 10^{-\varepsilon c d} \tag{2}$$

where 'I_t' is the intensity of transmitted light, 'I_o' is incident light intensity, 'ε' is the extinction coefficient (fraction of light absorbed at a specific wavelength), 'c' is the concentration of the sample, and 'd' is the length of the light path through the sample. However, this is difficult to use in pulse oximetry because the light scattering through the tissue cannot be distinguished from that of blood [1].

Two independent equations can be derived to describe the absorption of light by both Hb and HbO_2 at two distinct wavelengths. These equations can then be solved to find the concentration of Hb and HbO_2 in blood and establish the relationship,

$$SO_2 = A - B\frac{OD(\lambda_1)}{OD(\lambda_2)} \tag{3}$$

where A and B are functions of the extinction coefficients of Hb and HbO_2 while 'OD' is the optical density or the $\log(I_o/I_t)$. The relationship above is the underlying principle used by commercial pulse oximeters to measure SpO_2. [1]

2.2 Pulse Oximetry

Pulse oximetry was initially intended for monitoring hospitalized patients after surgery. However, after recognizing the importance of an accurate oximetry device during surgery in operating rooms, non-invasive pulse oximetry became a standard for anesthesiologists for intraoperative monitoring since 1990. By the use of this technique, physicians can determine the SpO_2 in patients that are sedated, anesthetized,

unconscious, and unable to regulate their own oxygen supply avoiding irreversible tissue damage [2].

It is not until 1935 that Karl Matthes used red and infrared wavelengths to build a device that continuously measured SaO_2 in vivo. Matthes stated that "the red light can pass through HbO_2, but reduced Hb absorbs it" [2]. Non-invasive oximetry evolved even further when Robert Brinkman and William Ziilstra began measuring SpO_2 from the forehead with the use of reflected light. Brinkman and Zijlstra made an additional modification when they divided the red signal by the infrared signal to show continuous measurements of SpO_2 [2,4]. However, differentiating various types of Hb was still a problem. This is when Robert Shaw invented an absolute reading ear oximeter in 1964. This device used eight different wavelengths to identify the separate Hb species present in the blood. Although expensive, this instrument was accurate down to 70% of SpO_2 and it was commercialized for use in physiology laboratories for pulmonary and cardiac applications. [2] In 1970, research performed by Takuo Aoyagi and his associates on dye-dylution techniques for measuring cardiac output led to the development of photoplethysmogram (PPG) ,which optically generates time dependent volumetric changes in living tissues leading to the development of pulse oximeter [1, 2]. Here, the time dependent changes are associated with arterial blood allowing for the measurement of SpO_2. Figure 2.1 shows the amount of light absorbed by tissue over time.

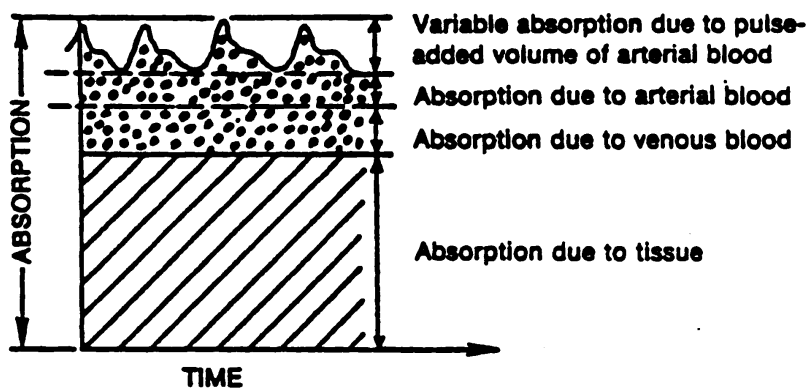

Figure 2.1: Arterial blood changing over time, PPG [11]

Aoyagi and his associates researched this technique even further and applied it to the already existent ear-piece oximeter [2]. Next, in 1977 Minolta Camera developed an oximeter using the same method with a fingertip probe and fiberoptic cables from the instrument. Finally, New and Yederman produced the Nellcor Pulse Oximeter in 1983 for patients admitted in clinic and hospitals sites [2]. Improvements on the idea of pulse oximetry led to its reliability to the extent that in 1990 the American Society of Anesthesiologists recognized the pulse oximeter as their standard for intraoperative monitoring [2].

2.2.1 Principle of a Pulse Oximeter

A noninvasive pulse oximeter relies on an optical sensor to detect SpO_2 and PR. This optical sensor is made up of a red and an infrared LED as well as silicone photodiodes (PD) [5]. In order to obtain SpO_2, the red wavelength must range within a region where the absorption of Hb and HbO_2 are markedly different. This is why a red light with a wavelength close to 660nm is chosen as shown in Figure 2. On the other hand, the region for the infrared light must revolve around a wavelength where the absorption coefficients of Hb and HbO_2 are practically the same. This happens between 940nm and 960nm as also shown in Figure 2.2 [1].

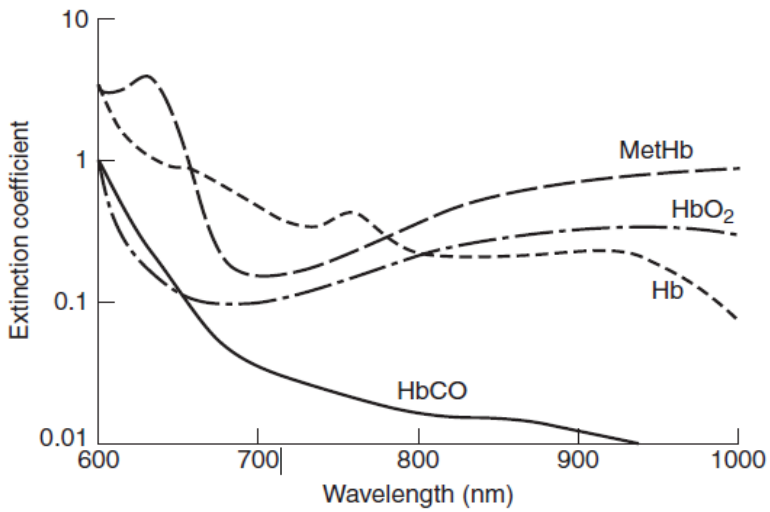

Figure 2.2: Optical absorption spectra of Hb, HbO_2, MetHb, and BbCO [11]

The sensor containing the red and infrared LED is applied over the radial artery on the wrist so arterial pulsation can be readily sensed. The PDs concentrically located around the LEDs will absorb the emission spectra of the red and infrared wavelengths when bounced back from the skin [5]. However, there are certain variables that could cause a barrier to the photodiodes from detecting light intensity. These include: the opacity of the skin, reflection of light by the bones, light scattered away through the tissues and the amount of blood in the vascular bed [5]. Furthermore, when blood flows into the vascular bed onto which the sensor is applied, the light emitted by the diodes will have a greater rate of absorption by the blood. The light absorbed when the tissue is either full or lacking blood with every heart beat will create an alternating light intensity signal. This difference in light intensity created by every heart beat accounts to approximately 0.05-1 percent of the whole light intensity that is either transmitted into the skin or backscattered into the photodetectors [5].

A pulse oximeter consists of a circuit that features a microprocessor used to light up the red and infrared LEDs one at a time in a synchronous manner, so that when the red light is turned on the infrared LED is turned off and vice versa [1]. With the use of sample-and-hold circuits, the overlapped signal acquired by the photodetector can be split into two different analog channels that correspond to the red and infrared PPGs [1]. The red and infrared PPG signals can be further amplified through the implementation of high and a low pass filters so that the AC and DC components for each PPG signal can be obtained [1]. The new four signals can be processed through a virtual instrument (VI) designed in a software program or a virtual instrument that calculates the ratio of AC red and DC red components and divides it by the ratio of AC infrared and DC infrared to produce SPO_2.

2.2.2 Methods of Light Detection

As previously discussed, pulse oximetry relies on the PPG signals produced by the difference in the amount of arterial blood, which in turn depends on the systolic and diastolic movements of the heart. Measurement of light by the photodetectors can be performed either in transmission or reflection modes. When the PPG is measured through transmission, the light source and the photodetectors are placed on opposite sides of the vascular bed so that the light travels across the pulsating blood. Thus, this method is limited to earlobes, feet, and fingertips. On the other side, reflectance pulse oximetry measures PPG signals with LEDs and photodetectors placed on the same side of the sensor surface. This method allows measurements to be taken from body parts where the transmission method cannot be used, for example on the chest, wrist, and forehead. [6]

2.2.2.1 Distance Between LED and Photodiode

In 1988, the effects of separation between the source and detector were studied [5]. Although it is understood that the farther away the photodiode and LED are from each other that the readings will degrade, it was demonstrated that larger PPGs can be detected by mounting the photodiode further from the LED. However, the tradeoff is that higher LED driving currents are required in order to overcome the absorption of incident light due to a longer optical path length. Mendelson also shows that by mounting more than one photodiode, a greater fraction of backscattered light can be collected and larger PPGs can be recorded. [5]

Furthermore, in 2010, there was a similar conclusion regarding the gap sizes between the LEDs and the photodiodes [7]. It was found that the amount of light backscattered from the skin on the optical module and that was absorbed by the PDs was directly proportional to the number of PDs surrounding the LEDs. Thus, the more PDs, the more light would be absorbed.[8] This research showed that 7mm was the optimal distance between the LED and PD and produced the highest AC signal. Similar to Mendelson's

research above, a higher current output obtained from a larger number of PDs was required in order to obtain a stronger AC components.

2.2.3 Photoplethysmogram

PPG is an optical measurement used to represent the volume of blood in vessels used to compute SpO_2 and PR based on the light absorbance of blood. During the cardiac cycle, the amount of blood in tissue varies in relation to each heartbeat, so a PPG signal is an optical representation of the cardiac cycle wave. This results in a distinguishable AC component. The PPG is usually taken at peripheral sites such as the finger, ear, or forehead. Since skin is perfused by blood, conventional pulse oximeters monitor the perfusion of blood in the dermis and subcutaneous tissue of the skin. The AC component of the oximeter signal is attributed to variation in blood volume and the DC component of the oximeter signal is generally attributed to skin tissue absorption. [9;10;11]

2.2.4 Wavelength Optimization

Although wavelengths at which the SpO_2 are typically measured are 660nm for red and 910 nm or 940 nm for infrared, it is possible to measure SpO_2 at different wavelengths and also with more than 2 wavelengths. In fact, the Hewlett-Packard model 47201 Ear Oximeter which debuted in the 1960s utilized 8 wavelengths. The advantage to using more than two wavelengths is that it makes it possible to measure saturation of more than just oxygen in the hemoglobin chains. However, for the purposes of measuring only SpO_2, two wavelengths are sufficient.

Nogawa, in 1998, also showed that by changing the two selected wavelengths from 665/910 nm to 730/880nm, a linear relationship could be established for oxygen saturation rates over the 100-30% range. In the 70-30% range, the improvement was significant with a standard error of 2.69% as compared to 9.49% for a sensor utilizing 665/910nm wavelengths. Results also showed that in the 100-70% range, the 730/880 nm sensor showed a slight improvement in the standard error, lowering it from 3.50 to 2.11%. [12]

2.2.5 Limitations and Applications of Pulse Oximetry

There are certain situations in which data processed by a pulse oximeter can be misinterpreted or difficult to acquire. Significant reduction in peripheral vascular pulsation due to hypotension, vasoconstriction or hypothermia can cause a small signal to be processed unreliably by a pulse oximetry [1]. Also, due to the small signal that is analyzed, only 1 to 2% of the PPG signal can be processed, motion artifacts can interfere with a proper PR signal reading if the patient is shivering or having a seizure. Increase in venous pulsations may also interfere with pulse oximetry resulting in artificially low SpO_2 readings [13]. Furthermore, large amounts of dysfunctional Hb, which is Hb derivatives that do not bind reversibly with O_2 like HbCO and MetHb, can lead to an incorrect oxygen saturation interpretation by the pulse oximeter

[1]. Compromised blood circulation, excessive contact pressure or weak PPG signals resulting from insufficient contact pressures may also yield to measurement errors [14]. Finally, one of the greatest limitations of transmittance pulse oximetry is movement of the patient. By being attached to the finger and the fact that extraneous movements can cause a change in absorbance of light by arterial blood flow, a conventional pulse oximeter hinders the user to perform regular daily activities [14;15].

2.3 Reflectance vs. Transmittance Pulse Oximetry

With recent achievements in pulse oximetry, the devices are generally characterized as transmission based and reflectance based. In transmission based pulse oximetry, LED and a photodiode are placed on opposite sides of a substrate, which in turn can be attached across the fingertip, earlobe, and foot.

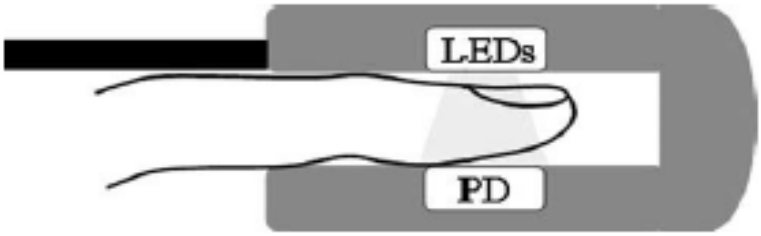

Figure 2.3: Transmittance pulse oximetry

In reflectance-based oximeters, the LED are placed together on the same probe surface. This method is mainly intended to be used on body locations where pulse oximetry through transmission is not feasible.

Figure 2.4: Reflectance pulse oximetry

Forehead reflection pulse oximetry is one example and is generally more accurate than transmission type pulse oximeters on patients with a low cardiac index or poor peripheral perfusion.[1]

Figure 2.5: Forehead pulse oximeter

2.4 New Studies for Pulse Oximeters

One such wrist based prototype relying on reflectance based oximetry is the AMON [19]. This prototype endeavored to measure blood oxygen saturation, pulse, blood pressure, skin temperature and ECG data using a single ECG lead. However, after conducting a study on 33 healthy volunteers, and comparing the data gathered by AMON to that of two commercially available pulse oximeters, the results weren't promising and not every type of measurement was able to be used. Results showed that blood pressure data and pulse measurements from SpO_2 were satisfactory and as expected, however SpO_2 measurements were far from expected due to significant deviation. As for ECG, although PR results could be obtained, there was no conformity in the QRS and QT complexes of the ECG as results, as well as high levels of measurement noise which degraded the results. The lack of conformity and noise made it difficult to distinguish the ECG as a waveform. The temperature sensor on the other hand was unsuccessful since the study showed no reliable correlation between the reading at the wrist and the core body temperature. [19]

A second wrist based pulse oximeter that showed potential is a prototype by Coker et al. in which the results were far more promising. For pulse measurements, Coker's prototype had an accuracy error of less than 2% as compared to two different commercial pulse oximeters while the averaged SpO_2 measurements had an accuracy error of less than 1%. However, it is noted that while the prototype provided accuracy competitive to that of commercial pulse oximeters, motion artifacts cause signal integrity issues and needs to be addressed. Some possible methods of addressing motion artifacts are through the use of a motion sensor to account for user movement or much more refined signal processing using filters to minimize noise and find the highest signal to noise ratio. [16]

Lastly, a sensor consisting of a multiple photodiode array was arranged concentrically around 4 LED's was tested on the forearm and calf [20]. This sensor however also utilizes a heating unit. Previous research has shown that heating the skin under the sensor increases the magnitude of the detected pulsatile component four- to five-fold. The purpose of this study however was to measure the effectiveness of the sensor under controlled hypoxia. Ten volunteers were studied and the inspired fraction of oxygen in the

breathing gas mixture was gradually lowered from 100 to 12%. Measurements were simultaneously taken from the forearm and calf then compared to SpO_2 measurements obtained by a finger sensor. Though the experiment was done while the volunteers were standing still and the results are not as ideal as the forehead reflectance oximeters [20].

3 Design Approach

Applying pulse oximetry technology to the chest and the wrist can provide the opportunity to create new noninvasive devices that will be less restrictive to a wears' movements and more comfortable. The combination of a different placement and design could further the monitoring of vital signs in settings other than hospitals.

3.1 Initial Client Statement

Develop a wearable, noninvasive reflectance-based pulse oximeter prototype that demonstrates accurate and precise measurements of arterial oxygen saturation and heart rate from the chest and/or wrist on healthy volunteers.

3.2 Clinical Need

Reflectance-based pulse oximetry allows measurements to be taken from areas of the body in which transmittance-based pulse oximetry cannot be used. Using reflectance-based pulse oximetry, the wavelengths are passed through the skin and reflect off the bone and tissue in the area of the measurement. Being able to receive signals from the chest and wrist has not yet been successfully achieved using reflectance-based pulse oximetry. It is difficult to receive signals from the chest and wrist because the light needed to create the signal must be reflected back which makes the signal weaker and more difficult to detect. Creating a method to obtain a PPG signal strong enough to process for SpO_2 and PR from the chest and wrist is the central dilemma behind this project. Achieving this could further the development of new devices that could be worn during daily activities and as a method of protecting servicemen in the field.

3.3 Design Parameters

In this section are outlined the various aspects of project designed to address the clinical need behind a reflectance-based pulse oximeter for the chest and wrist. These design parameters cover both the qualitative and quantitative pieces of the final design.

3.3.1 Objectives

The objectives consisted of three categories: 'Easy to use', 'Marketable', and 'Safe'. 'Easy to use' addresses the user friendly nature needed for the device to be useable by the large audience that is to be targeted. To be easy to use the device must be easy to wear, operate, or read. 'Marketable' addresses the need for the device to be successful and competitive on the market. This means that the device must be cost-efficient, manufacturable, portable, durable, and comfortable. 'Safe' addresses that device must be safe for the users. Thus the device must be secured against the user to avoid false measurements, be composed of biocompatible materials as not to cause the user adverse reactions, and conduct reliable readings.

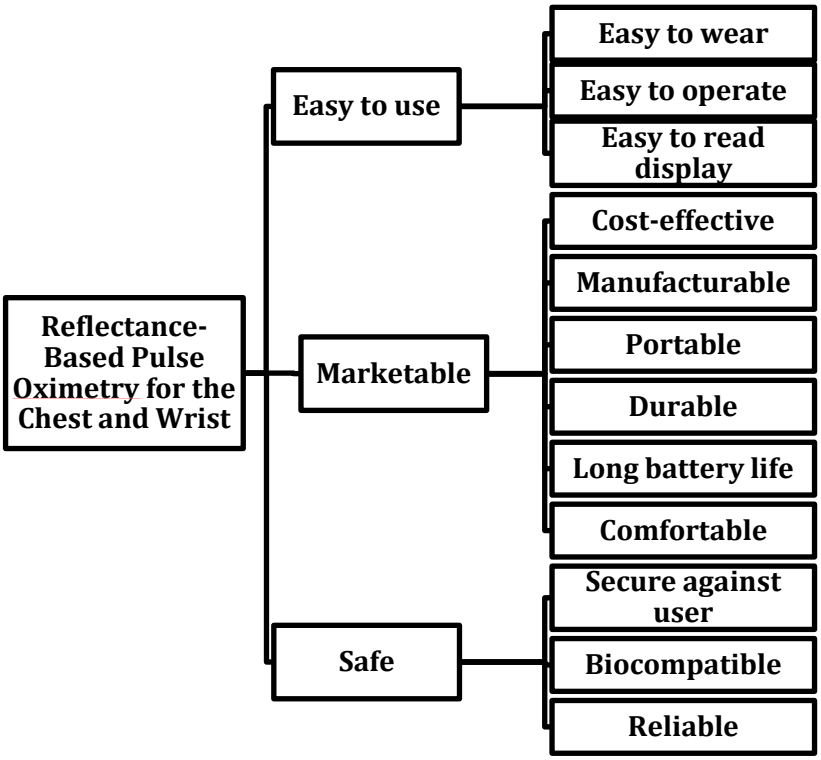

Figure 3.1: Objective tree

3.3.2 Constraints

Throughout the duration of our project, there were many constraints that the device must overcome. First, the device must not restrict the wearer from following their daily activities. There are many sizes the device could potentially be, however in order to keep the device from impacting a patients daily activities, the device must be kept to a small, concealable size. Second, the device must stay in constant contact with the skin. In order for the device to provide accurate results, it must not separate from the wearer at any time. The last constraint that the device must overcome is the regulatory requirements. The FDA has compiled a set of regulations, which include patient safety, performance requirements, and electrical, mechanical and environmental safety. In order for the device to be considered a success it must successfully overcome all of these constraints.

3.3.3 Functions

In this section is discussed the attributes that allow the prototype designed during this project to function properly.

3.3.3.1 Obtain Photoplethysmogram Signal

As dictated in the client statement, reflectance-based pulse oximetry was used to obtain the PPG signal necessary for computing SpO_2 and PR. The theory and method of reflectance-based pulse oximetry will

be used to do this from the chest and wrist.

3.3.3.2 Measure Heart Rate

In the AC component from the obtained PPG signal, the pulsatile pattern on the top of the PPG signal reflects the changing blood volume at the site of measurement with each cardiac beat. The signals are passed through a bandpass filter with a cut-off of about 1.5 Hz, to separate the AC pulses from the DC signals. The LabVIEW VI developed to process the PPG signal is then used to average the maximum frequency to determine the rate of the cardiac beat in hertz. This value was then multiplied by 60 to find the PR in beats per minute.

3.3.3.3 Measure Oxygen Saturation

SpO_2 is defined as the ratio of HbO_2 to the total concentration of Hb present in the blood [1]. After the LabVIEW VI processes the PPG signal, it calculates the ratio of red to infrared light used in the calculation for SpO_2.

3.3.4 Design Specifications

The specifications for this prototype were determined from the market standards by selecting several commercially available pulse oximeters specifications and examining them. One such device was the Respironics' WristOx™ Ambulatory Finger Pulse Oximeter which entered the market in October of 2003. Its specifications can be found in Table 3.1. [21]

Table 3.1: Respironic's WristOx Ambulatory Finger Pulse Oximeter Specifications [21]

Effective Measuring Range	
Saturation	0% to 100%
Pulse Rate	18 to 300 bpm
Resolution	1 digit
Accuracy	
Saturation	70 to 100% ± 2 digits
Pulse rate	±3%
Display	
Numerical	3-digit indicators
Pulse indicator	Pulse Strength Bar Graph
Power requirement	Two 1.5V alkaline N-cell batteries
Battery life	Minimum 24 hours continuous
Storage	9 months
Size	

Weight	~0.88 ounces (24.95g)
Dimensions (w/o sensor or strap)	1.75” wide x 2” high x 0.75” deep 4.45cm x 5.08cm x 1.905cm

Another device which is on the market and FDA approved is the Santa Medical’s Finger Pulse Oximeter. Its specifications can be found in Table 3.2. [7]

Table 3.2: Santa Medical's Finger Pulse Oximeter Specifications[7]

Effective Measuring Range	
Saturation	0% to 100%
Pulse Rate	18 to 254 bpm
Resolution	±1 digit
Accuracy	
Saturation	75 to 99% ±2 digits
Pulse rate	± 2bpm
Display	
Numerical	3-digit indicators
Pulse indicator	Pleth bar
Power requirement	Two AAA alkaline batteries or rechargeable batteries
Power consumption	Less than 30Ma 2.6-3.6V
Battery life	30 hours continuous
Size	
Weight	50g including batteries

The final device specifications examined are those of the Crucial Medical System’s Finger Pulse Oximeter which is also FDA approved. Its specifications can be found in Table 3.3. [22]

Table 3.3: Crucial Medical Systems Finger Pulse Oximeter Specifications [22]

Effective Measuring Range	
Saturation	35% to 99%
Pulse Rate	30 to 250 bpm
Resolution	±1 digit
Accuracy	

Saturation	70 to 99% ±2 digits
Pulse rate	± 2bpm
Display	
Numerical	3-digit indicators
Pulse indicator	Bar graph and perfusion index
Power requirement	Two AAA alkaline batteries
Power consumption	Less than 30Ma 2.6-3.6V
Battery life	30 hours continuous
Size	
Weight	1.8oz (50g) including batteries
Dimensions	58.5 x31 x32 mm

The standard parameters to make the prototype in this project competitive by market standards were determined after examining the specifications for the Respironics' WristOx™ Ambulatory Finger Pulse Oximeter, the Santa Medical's Finger Pulse Oximeter, and the Crucial Medical System's Finger Pulse Oximeter. The specifications table for this project's prototype can be found in Table 3.4.

Table 3.4: Project Specifications

Effective Measuring Range	
Saturation	70 to 100%
Pulse Rate	20 to 250 bpm
Resolution	1 digit
Accuracy	
Saturation	± 3% or ± 2 digits
Pulse rate	± 3% or ± 3 digits
Display	
Saturation	2 characters
Pulse Rate	3 characters
Power Requirement	3V lithium battery (coin sized batteries)
Battery Life	Minimum 24 hours continuous

3.4 Revised Client Statement

Develop a wearable, noninvasive reflectance-based pulse oximeter prototype that demonstrated reliably accurate and precise measurements SpO_2 and PR from the chest and wrist. The prototype connects to the computer generated program, LabVIEW, which displays the SpO_2 and PR graphically and numerically. The prototype measures SpO_2 within 70 to 100 percent and PR within 20 to 250 beats per minute having a

resolution of 1 digit and accuracy within ±3% or ±3 digits. This prototype should weigh less than 150 grams. The prototype must not cause any harm, such as burning the skin or allergic reactions. In order to provide the best results possible for SpO_2 and PR, the prototype must remain in constant contact with the skin. This prototype should be easy to use, requiring little to no training before use. Once the prototype is completed, testing for this device was conducted on healthy volunteers to test the accuracy and precision as well as proving that SpO_2 and PR can be measured from the chest and wrist.

4 Device Development

4.1 Device Alternatives

4.1.1 Sensor Design 1

This prototype design utilized a dual-wavelength LED surrounded by 4 photodiodes. These photodiodes were positioned at 90° increments around the LED. The LEDs transmitted at 660nm and 940nm. Many studies showed that better signal quality can be achieved when a ring of photodiodes are used to collect light from a central light source [23]. The separation distance between the LED and each photodiode were approximately 1 cm. As a result, the LED required a larger driving current so that more tissue is able to absorb and reflect light [5]. A bandpass filter was utilized at a cut off frequency of 2Hz and bandwidth of 3Hz. This sensor was compatible with flash memory and utilizes a serial connector interface so as to make it possible to connect the device to LabVIEW for signal analysis. Further signal processing was accomplished by using LabVIEW in order to minimize motion artifacts and noise.

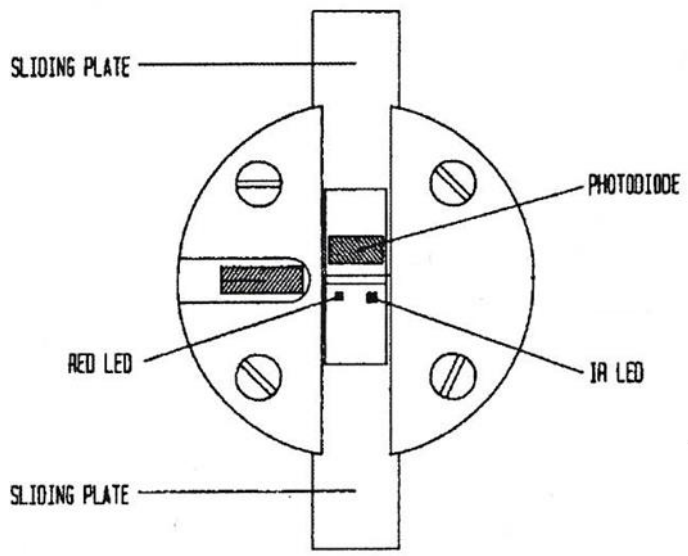

Figure 4.1: Sensor design 1.[5]

4.1.2 Sensor Design 2

The other prototype also utilized a dual-wavelength LED surrounded by 4 photodiodes. These photodiodes were positioned at 90° increments around the LED. The LEDs transmitted at 730nm and 880nm. These wavelengths have been shown to provide a more linear relationship for SpO_2 values less than 70%. Many studies showed that better signal quality can be achieved when a ring of photodiodes is used to collect light from a central light source [23]. The separation distance between the LED and each photodiode was approximately 1 cm. As a result, the LED required a larger driving current so that more tissue is able to absorb and reflect light [5]. A bandpass filter was utilized at a cut off frequency of 2Hz and bandwidth of 3Hz. This sensor was compatible with flash memory and utilized a serial connector interface so as to make it possible to connect the device to LabVIEW for signal analysis. Further signal processing was implemented using LabVIEW in order to minimize motion artifacts and noise.

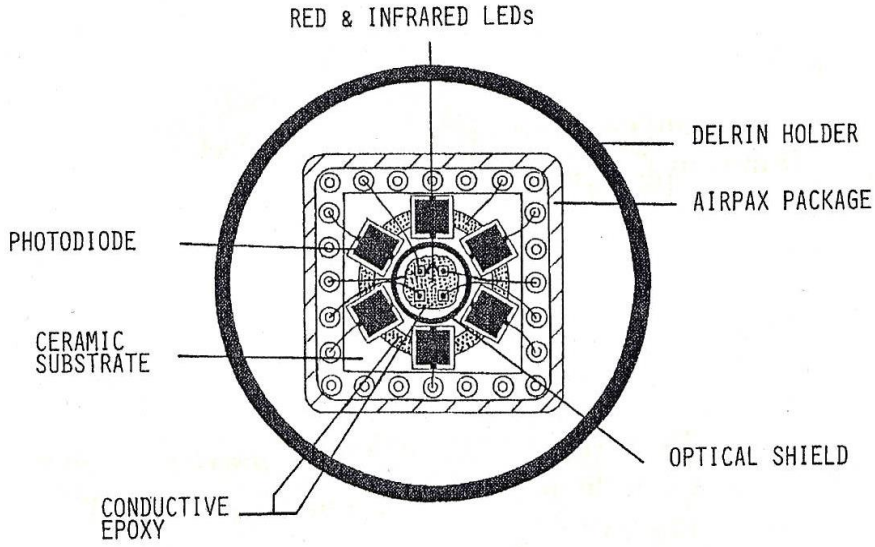

Figure 4.2: Diagram of sensor design 2.[5]

4.1.2.1 Evaluating Alternative Designs

The most significant difference between the two alternative designs above was the difference in wavelengths. In design 1, the most commonly wavelengths, 660nm and 940nm, for oximetry were used for the LEDs since they have been proven to work efficiently. In design 2, wavelengths 730nm and 880nm were explored and investigated to determine if these wavelengths would serve as more efficient substitutes. Nogawa showed that with a 730/880nm sensor, a linear relationship could be established for the oxygen saturation between 30-100% with the greatest improvement seen at oxygen saturation levels between 30-70% [12]. For the purpose of this project, the most commonly used wavelengths, 660nm and 940nm were selected. For a chest based pulse oximeter, research showed that the upper sternum provides decent readings when the user is still [24]. For the wrist based pulse oximeter, the desired measurement location was the radial artery which has shown some success over the ulnar artery on the wrist [25].

4.2 Software Design

The program used to compute SpO_2 and PR from the PPG signals gathered by the sensor is LabVIEW System Design Software from National Instruments. Each program created within LabVIEW is known as a virtual instrument (VI).

5 Methods

5.1 Photodetection Unit

The photodetection unit used in this project utilizes LEDs and photodiodes to collect backscattered light that travels from the LED, through skin and tissue and is reflected off the bones and subcutaneous tissues back into the photodiode. Our ability to measure the PPG and calculate SpO_2 comes from the varying absorption that occurs as the heart pumps blood through the arteries. For the photodetection unit to properly work, the LED and photodiode must be close enough to each other so the photodiode can pick up the greatest fraction of backscattered light for the highest possible output and signal to noise ratio.

5.2 PPG

The pulse oximeter makes it possible to observe the PPG signal due to the changing of absorbance because of arterial blood pulsating throughout the body. In Figure 5.1 below we can see that the PPG which is commonly referred to as the pulsatile component or the AC component, is a small percentage of the total signal output which is generally riding on top of a large DC offset. This DC offset occurs due to absorbencies that are not changing such as skin or other non-arterial tissues which maintain a constant absorbance. When attempting to amplify the PPG for closer inspection, it is generally the case that the DC component is also amplified and as a result ends up saturating the signal. To properly amplify the PPG signal it is best to filter out the DC component through the use of a bandpass or high pass filter. Once amplified, the PPG signal can then be used to calculate heart rate either visually or with the aid of special software that can calculate the frequency or count the number of peaks in a certain time interval.

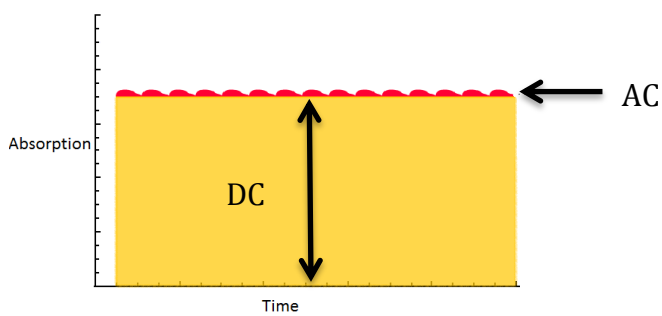

Figure 5.1: Unfiltered output of a PPG signal with an AC component riding on top of a DC component

5.3 Filter Design

To separate the PPG from the output of the photodiodes, it is necessary to filter the signal in such a way so that the PPG signal is preserved while other unwanted parts of the signal are attenuated. In the case of the PPG and the average pulse rate of a healthy patient, a bandpass filter with a cutoff frequency of 1.5-2Hz and a narrow bandwidth of 2-3Hz. This will allow for the separation of the AC and DC components which is necessary for SpO_2 and PR calculations.

5.4 Software

Signals were digitized and sampled using LabVIEW DAQ Assistant with analog inputs collected by a National Instrument's Data Acquisition Board with a sampling frequency of 100Hz. The functions of the software are described in Appendix A and can provide further detail into the design of the VI used for this prototype.

Figure is the summarized sequence of software processes which are applied to both the red and infrared PPGs.

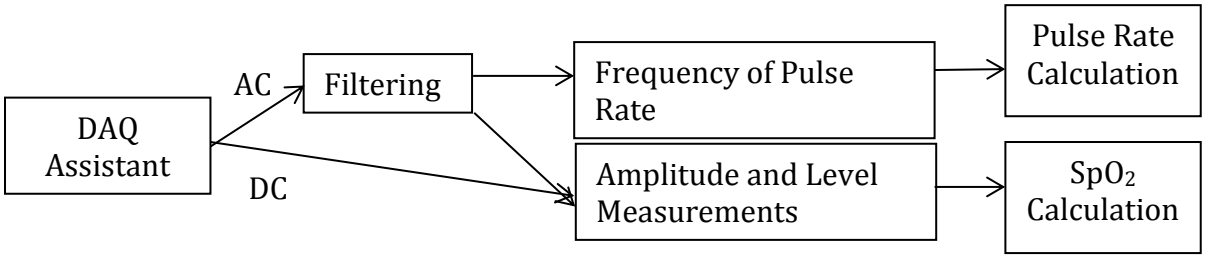

Figure 5.2: Software flow chart

5.4.1 Incoming Signals

The first block in the Software Flow Chart, in Figure 5.2 is to address the installation of the external DAQ Assistant and the completion of its internal task which includes identifying the connected external DAQ Assistant with the DAQ Assistant function in the Block Diagram, each of the incoming signal channels, and the sampling rate. Since the DAQ Assistant function combines the four incoming signals created by the sensor into a single output called data, four Select Signals functions are used to separate and identify the incoming signals. The Select Signal functions were used instead of a simple Split Signal function because they could be set to single out a one specific signal while a Split Signal would separate the signals, but provide no indication of which signal was being produced. To ensure that the DAQ Assistant external and internal system was receiving the signals correctly, Waveform Graphs were implemented at the output of each Select Signals which when the prototype was running would plot the AC and DC components of the red and infrared signals and be compared to the readings of an oscilloscope.

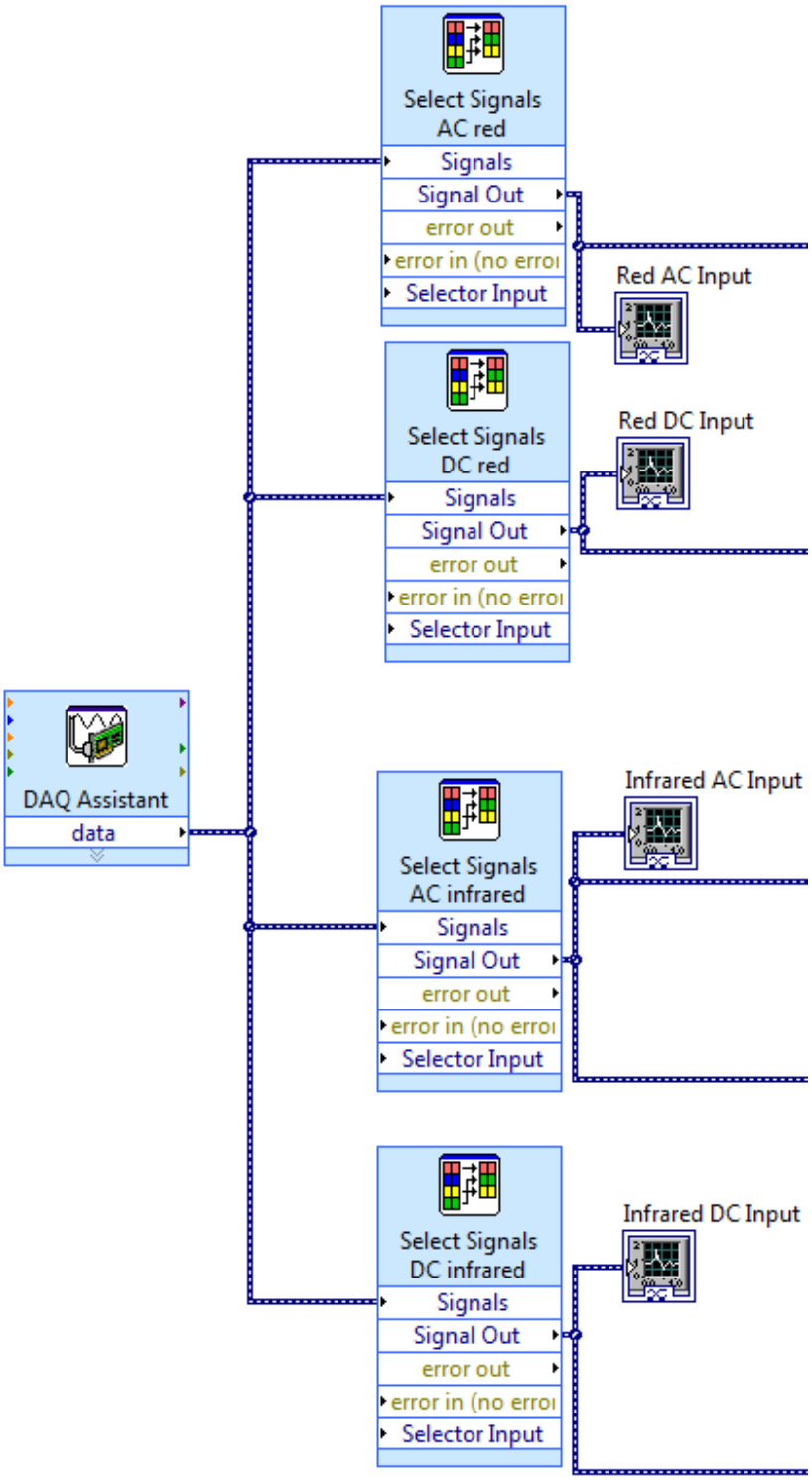

Figure 5.2: Configuration of functions to separate incoming signals

5.4.2 Filtering

Next, is the filtering of the red AC signal because of the extra noise that accompanies this signal. The infrared AC signal was not filtered digitally because it was a stronger signal due to infrared light not being as blood absorbent as red light. A bandpass filtering type was selected because it was necessary to eliminate extraneous signal samples above and below the main signal. Since an average pulse rate is approximately 60bpm, the amplitude of the signal necessary to produce the average pulse rate is between 1.5 -2 Hz. This provides the low cutoff with 0.75Hz which is about 40bpm and the high cutoff with 2.5Hz which is about 130bpm. The Chebyshev filter topology of the 7th order was implemented because it provides a steeper roll-off and minimizes the error between the idealized and the actual filter characteristic over the range of the filter. The impact of removing the noise from the signal by using these filter parameters can be seen on the sample graphs provided in the Configure Filter menu as seen below.

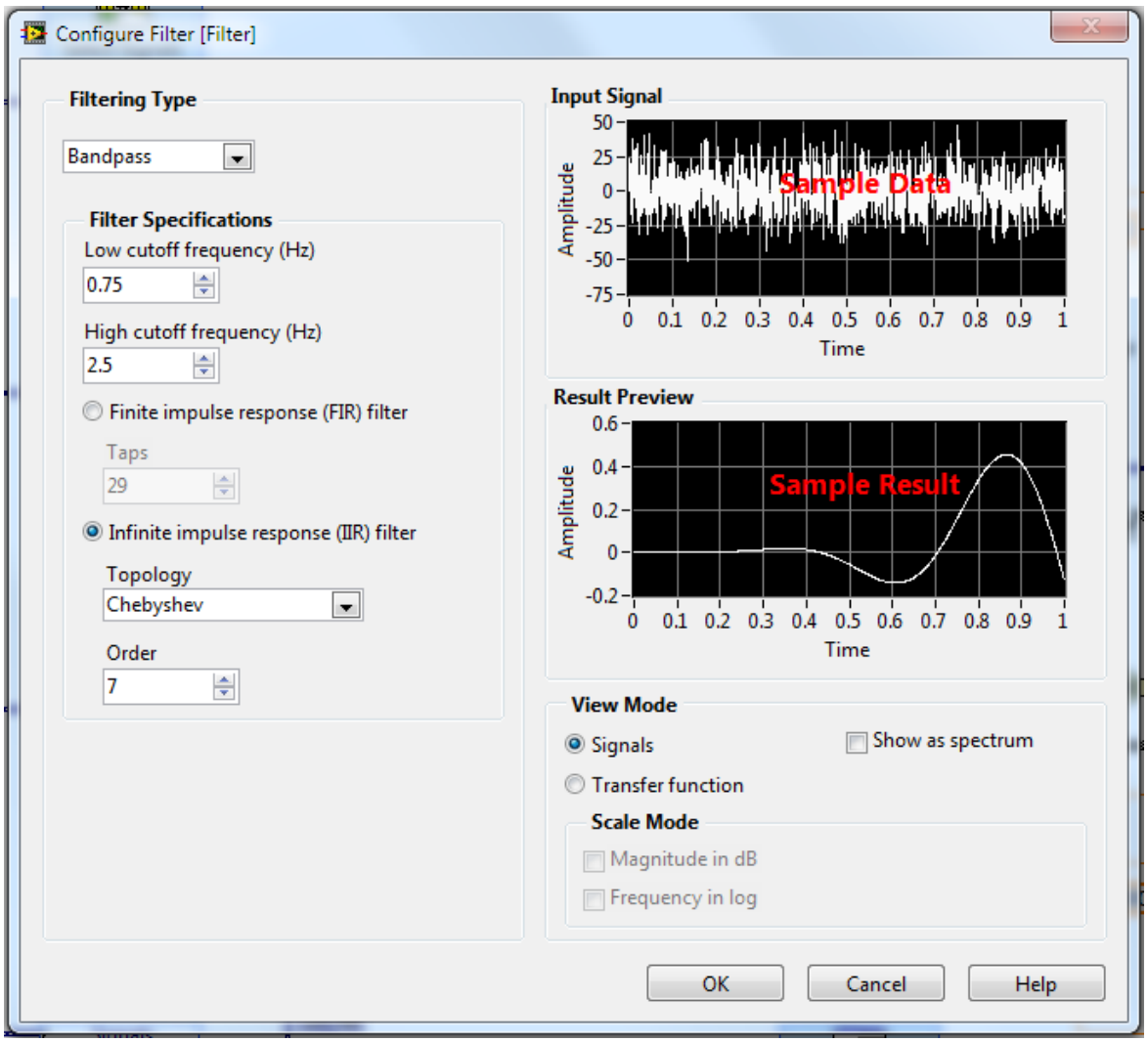

Figure 5.3: Configure filter menu

In Figure 5.4, the Filter function can be seen connected to a Waveform Graph which allows for the visualization of the change of the digital signal after it passes through the filter and confirmation that the filter was working.

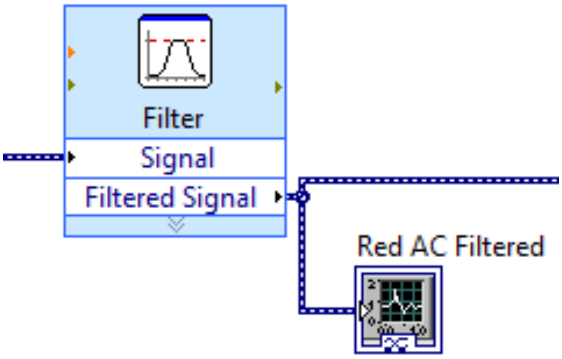

Figure 5.4: Filter function and graph

5.4.3 Frequency of Pulse Rate

Tone Measurements are the function used to determine the frequency of the Infrared AC signal which is needed to determine PR. This function has several measurements that it can perform, but for this VI, it is only used to measure frequency. Tone Measurements achieves this by searching for the set frequency, which is 2±50Hz. This range was chosen because a 2 Hz signal results in the average pulse rate of approximately 60bpm, but pulse rate can vary from 40bpm to 150bpm thus the ±50Hz range. In Figure 5.5, the Tone Measurement function can be seen connected to both a Numeric Indicator and Waveform Chart. In Figure 5.67, the configuration display for the Tone Measurement function is displayed with the settings used to measure frequency and plots of the signal before and after the function is applied.

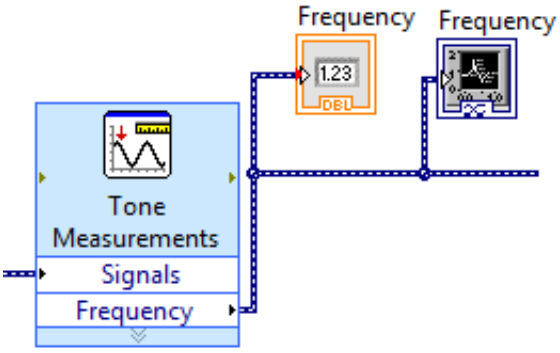

Figure 5.5: Tone measurements output frequency

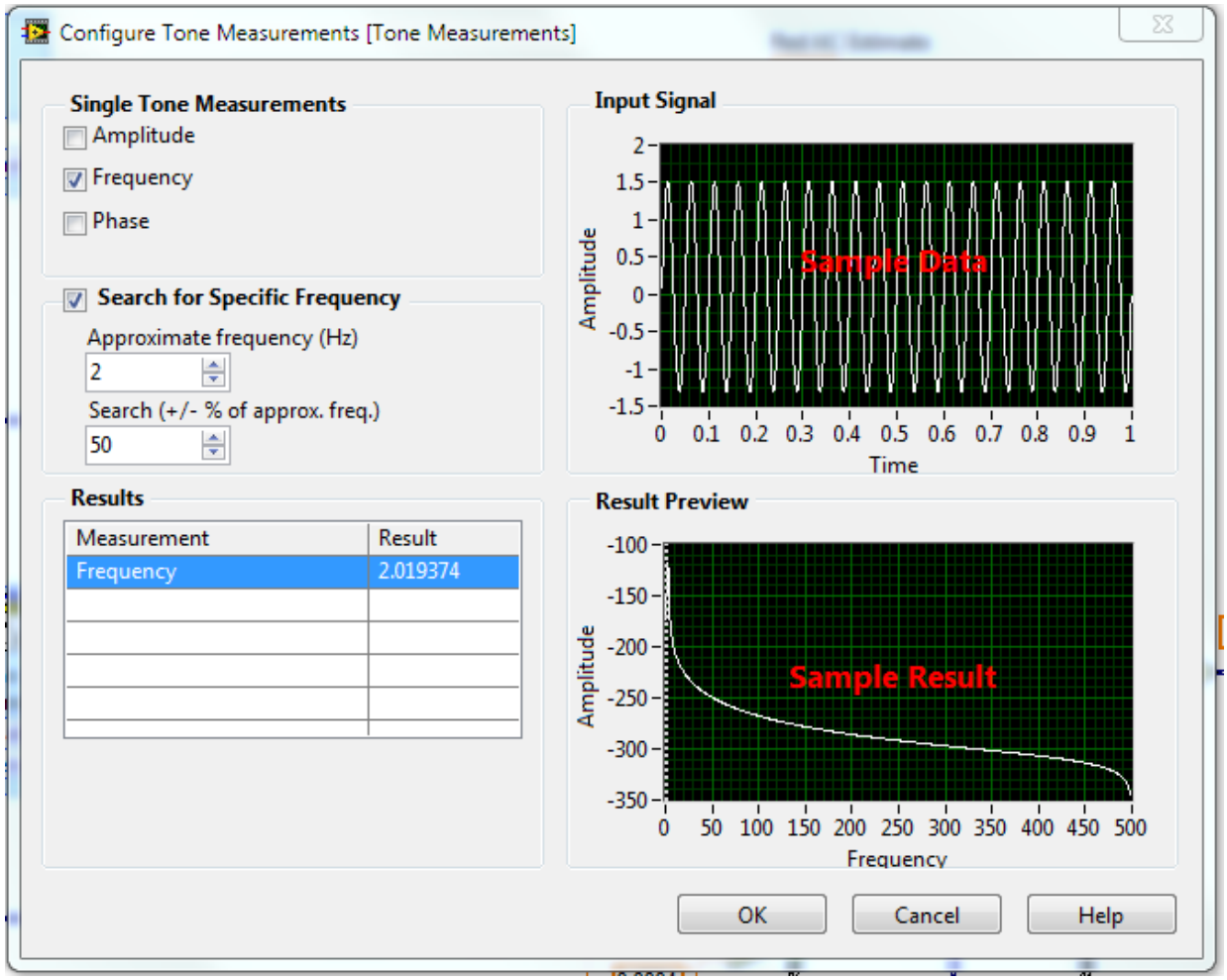

Figure 5.6: Configure tone measurements parameters

5.4.4 Pulse Rate Calculation

The PR calculation is the maximum average frequency of the infrared AC signals around 1.5 Hz with a ±50% search. The highest peaks can be assumed to be the PR because the raw graph of the AC signal, while having has some noise, is mostly representative of a clean PPG of the PR. The signal to noise ratio is very high resulting in the maximum average frequency measured being the PR.

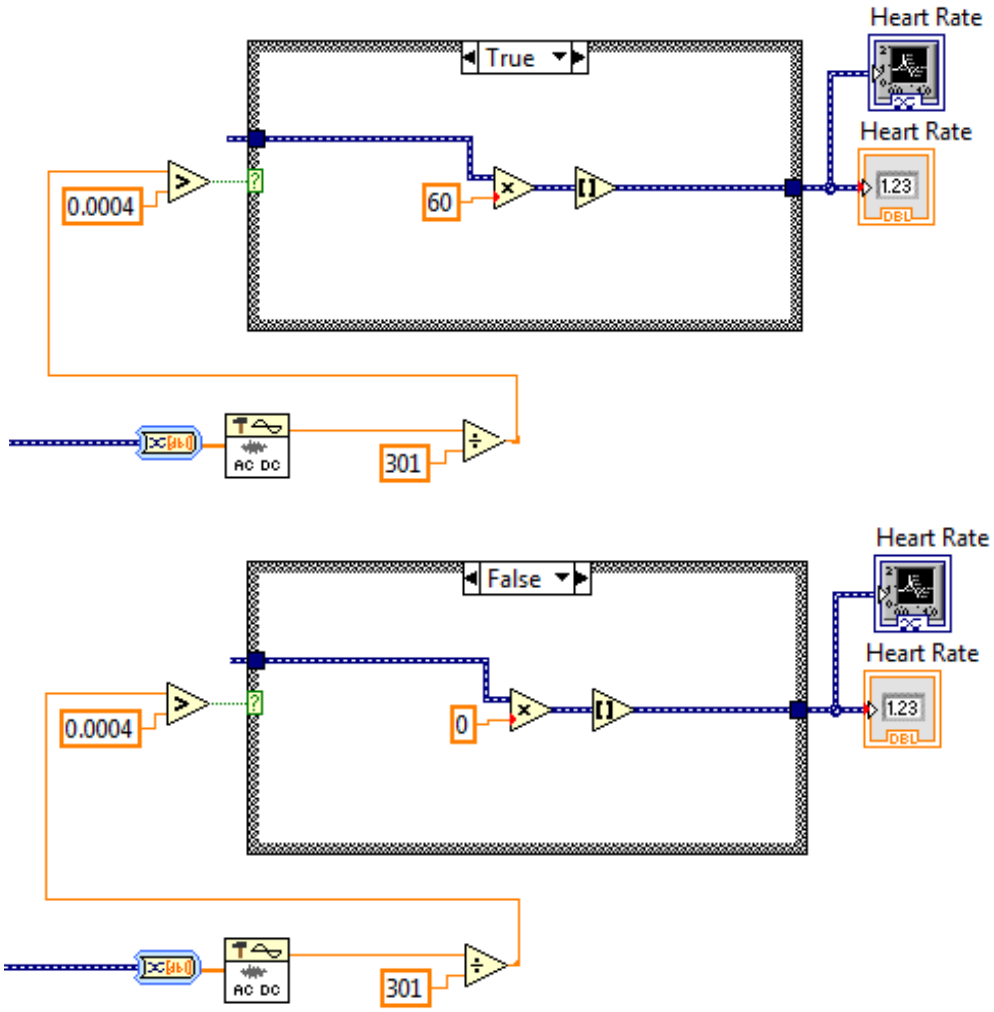

Figure 5.7: Functions used to calculate pulse rate

5.4.5 Spectral Measurements

Both the DC components of the red and infrared signals were averaged using the Amplitude and Level Measurement function and had these averages displayed with numeric indicators. This is necessary because to use the DC components of the signals, they need to be quantified into a signal value to be used in the SpO_2 calculation.

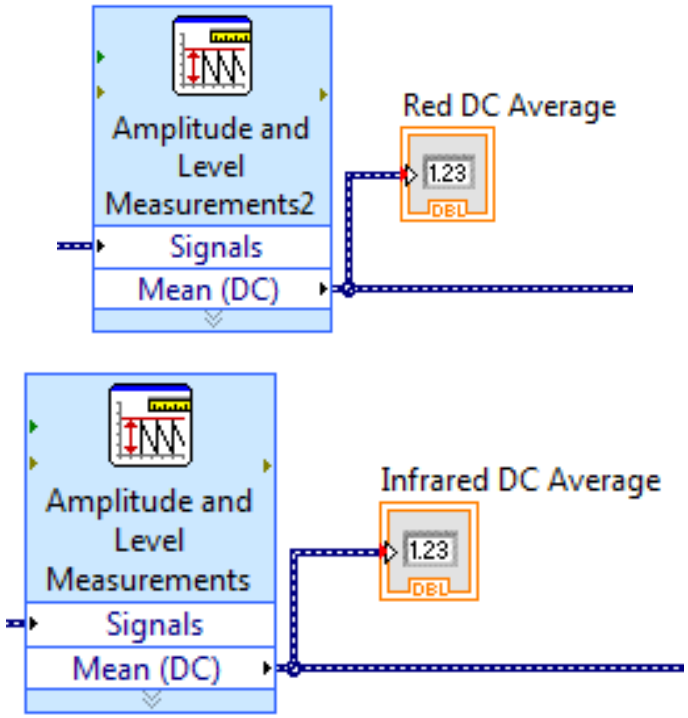

Figure 5.8: Amplitude and level measurements functions with numeric indicators

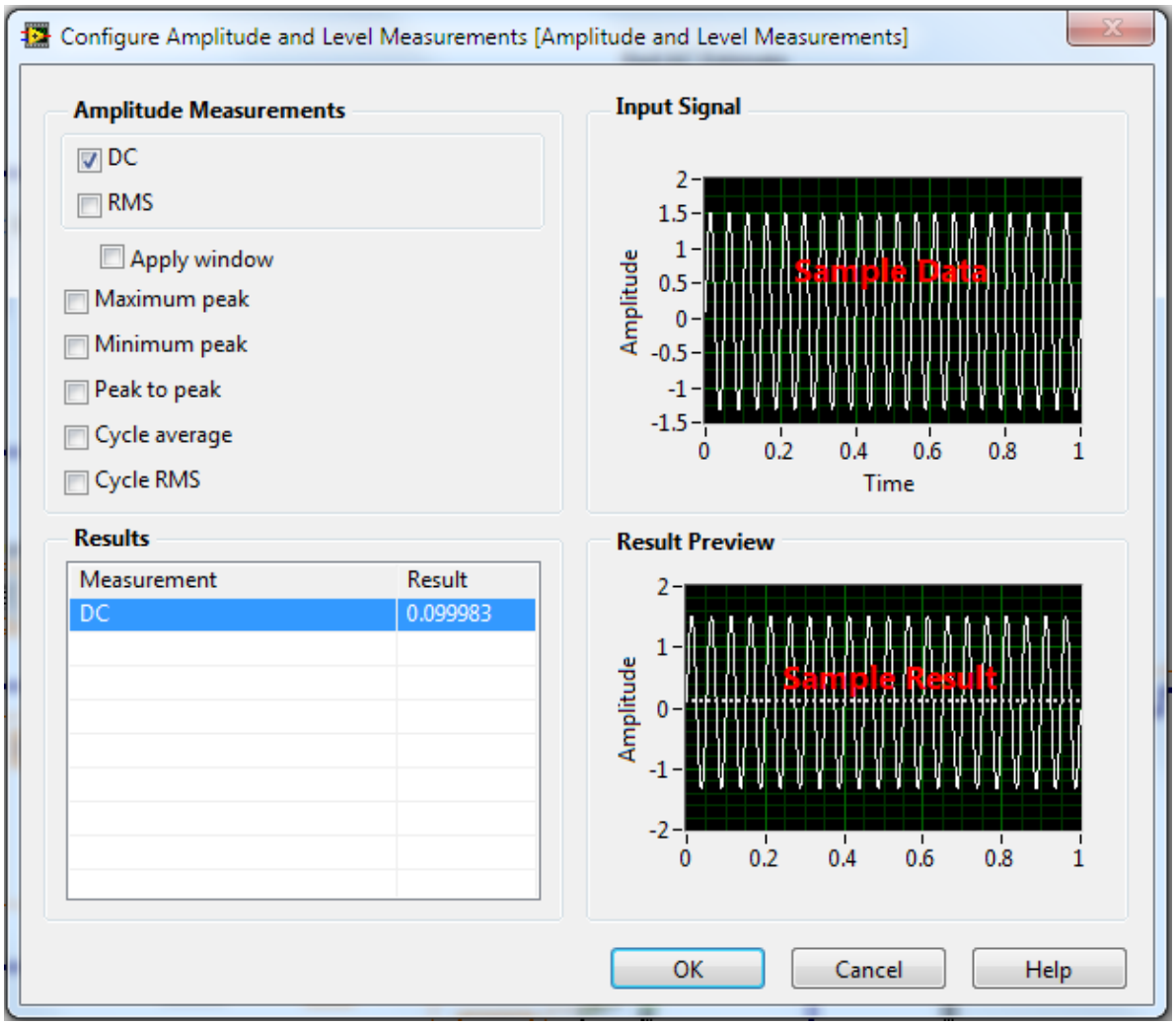

Figure 5.9: Configure amplitude and level measurements set to mean (DC)

5.4.6 SpO_2 Calculation

As mentioned previously, the SpO_2 calculation, with A = 110 and B = -25, is:

$$A + B\left(\frac{\left(\frac{AC}{DC}\right)_{Red}}{\left(\frac{AC}{DC}\right)_{IR}}\right) \tag{4}$$

To create this equation in LabVIEW, the divide, add, and multiply functions were used on the already processed AC and DC components of the red and infrared signals. At the end of the configuration of functions used to create the SpO_2 equation in LabVIEW, which can be seen in *Figure 5.11*, there is a numerical indicator and waveform chart so that the ratio $\left(\frac{\left(\frac{AC}{DC}\right)_{Red}}{\left(\frac{AC}{DC}\right)_{IR}}\right)$ is displayed on the Front Panel and monitored to ensure that this section of the VI is working.

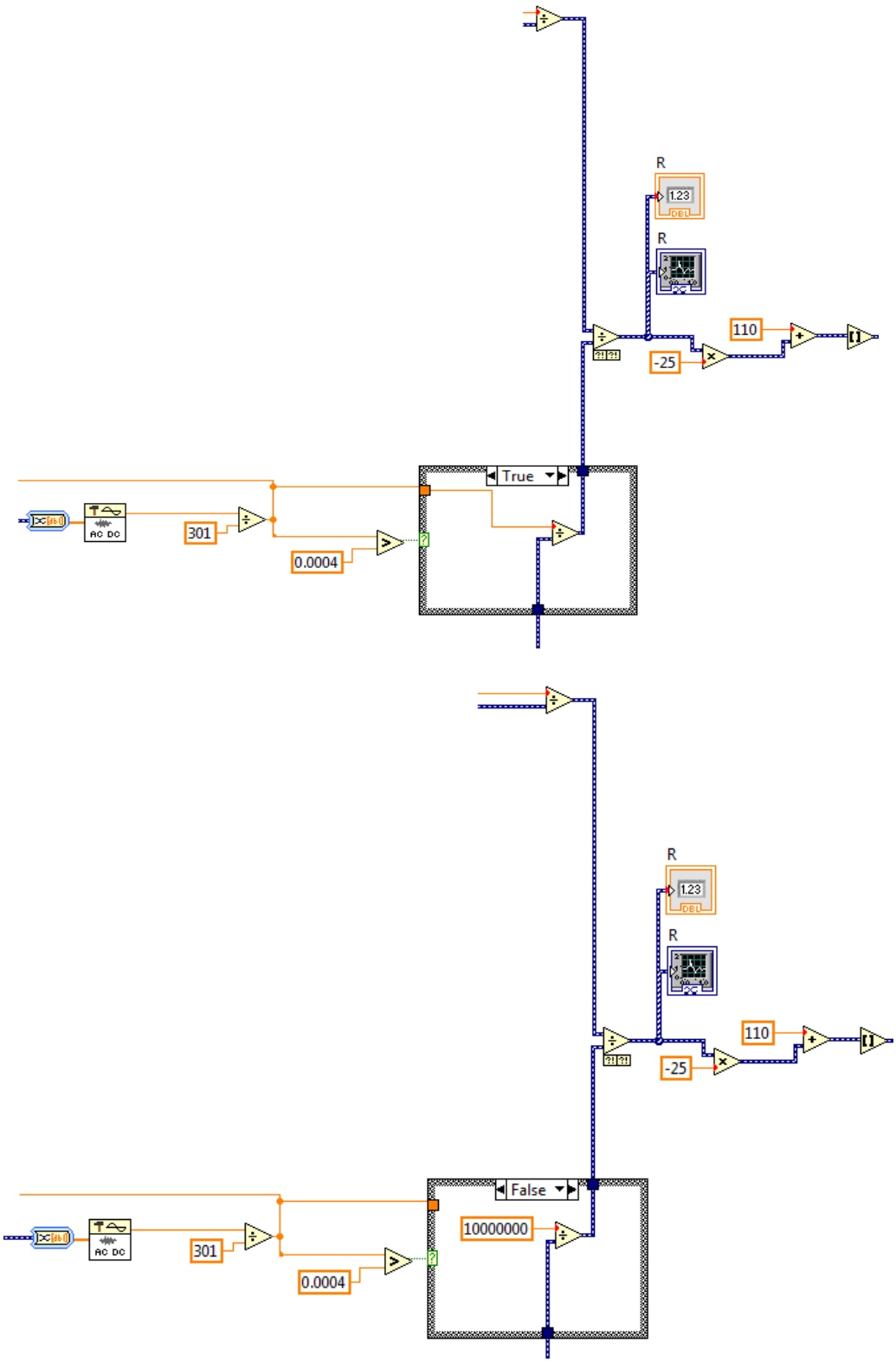

Figure 5.10: SpO_2 calculation

5.4.6.1 Limiting Range of SpO_2 Measurement

To receive the desired measurement range of 0-100 for SpO_2, the SpO_2 equation is first normalized by dividing the value produced by the SpO_2 equation by 110 and multiplying by 100. This value is then passed through a simple logic test. The logic test states if the value is greater than 0 and less than 100 it will be displayed on the SpO_2 gauge and waveform chart. Otherwise, the value is multiplied by 0 and then displayed on the SpO_2 gauge and waveform chart.

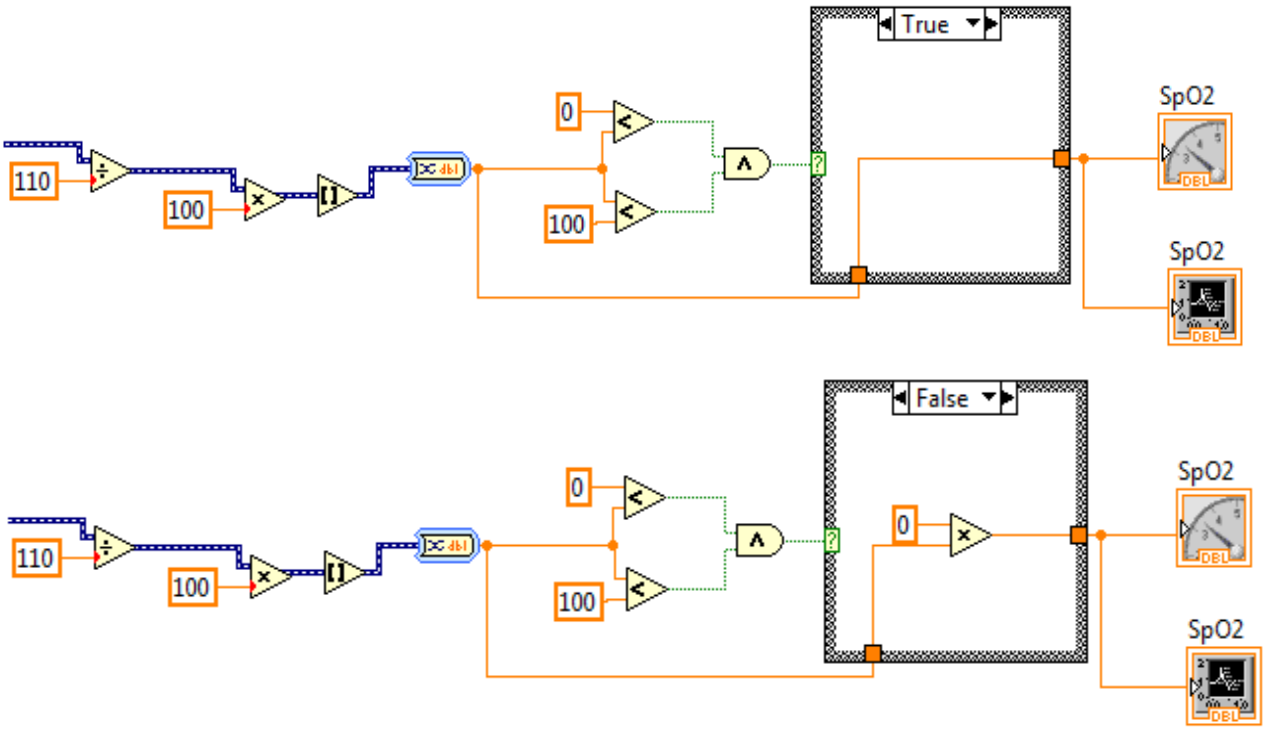

Figure 5.11: The configuration of function that limit the displayed SpO_2

Below are images of the block diagram and front panel of the full VI used in this project.

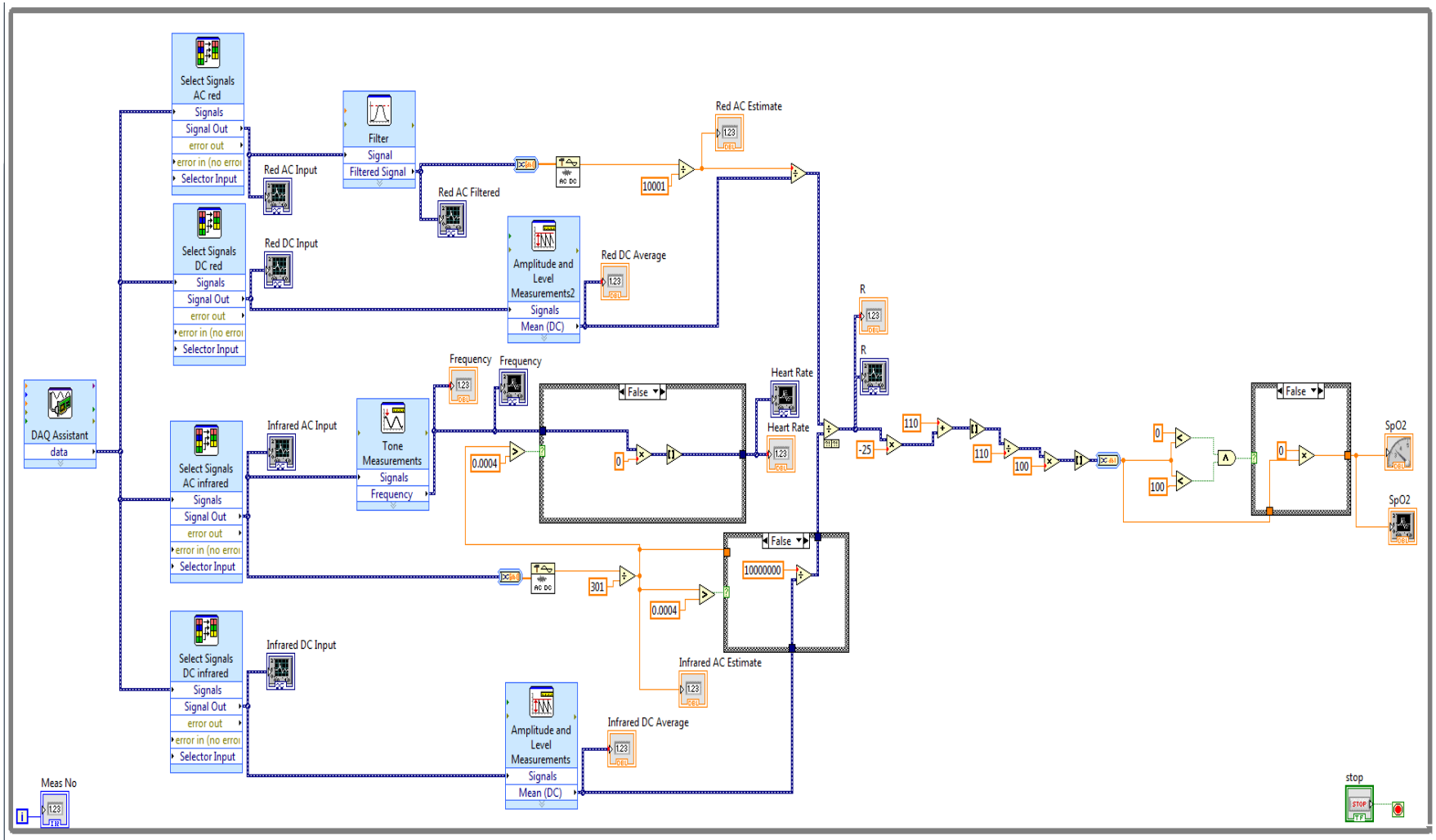

Figure 5.12: VI Block Diagram

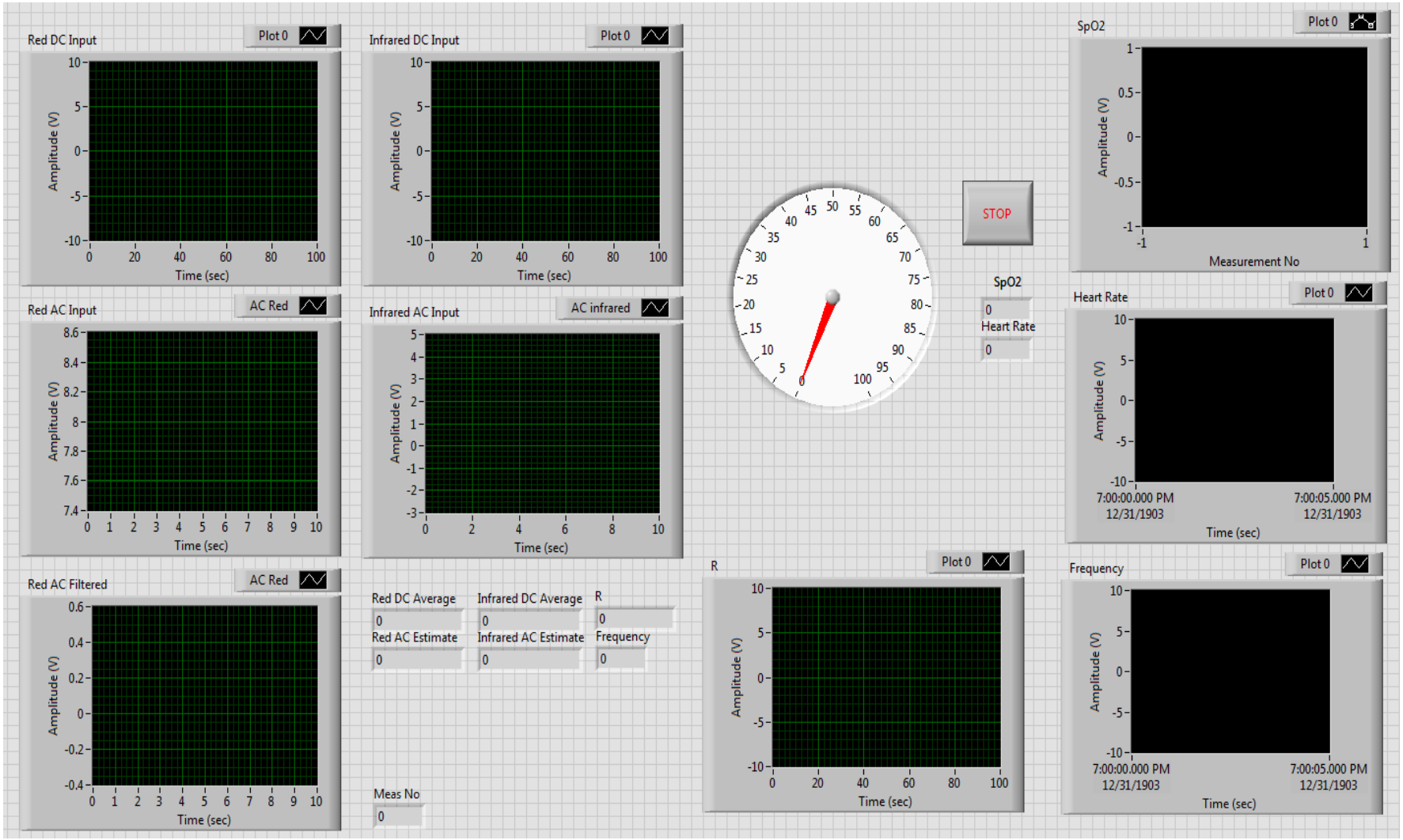

Figure 5.13: VI Front Panel

5.4.7 Preliminary VI Test

To test the VI, four digitally simulated signals were used with a control, a function in LabVIEW that will allow the manipulation of a variable while the VI is running, was placed on the amplitude of the red AC signal. This control was used to manually increase the red AC signal's amplitude causing the SpO_2 to decrease. This test of the VI replicated the oxygen decrease in the blood of a person who was hypoxic.

Below are images that demonstrate the success of this preliminary test of the VI. Figure 5.15, depicts the VI at the start of the test with the amplitude control at 0.5, the control can be seen below the SpO_2 gage and to the left of the LabVIEW stop button. Since the amplitude control has not been changed yet the SpO_2 graph in the upper right of the figure is a straight line and the AC Red Input and Red AC Filtered graphs have the relatively large amplitudes of 20Hz. As the amplitude control is slowly increased to 21, the SpO_2 graph in the upper right of Figure 5.16 shows a steady decrease and the AC Red Input and Red AC Filtered graphs now have amplitudes of 0.4Hz.

The "R" indicator, which displays the ratio value calculated during the SpO_2 calculation, is seen to increase between the two figures, as it was expected, because it is necessary for the ratio to increase for the resulting SpO_2 to decrease. The other graphs and indicators do not show a change in between Figure 5.15 and 5.16 because this was a controlled tested with simulated input signals.

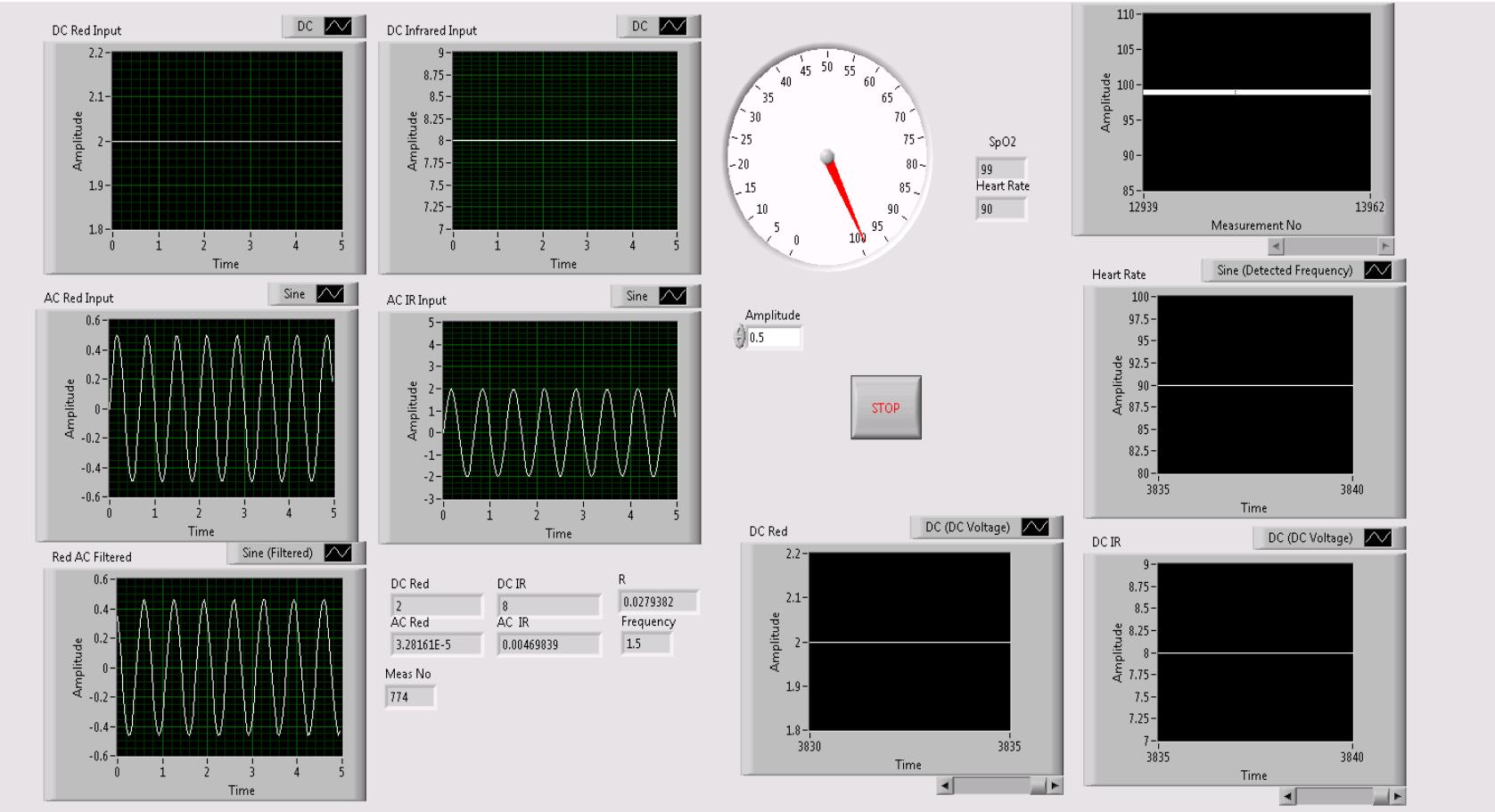

Figure 5.14: Front panel for the simulated hypoxia test with low amplitude

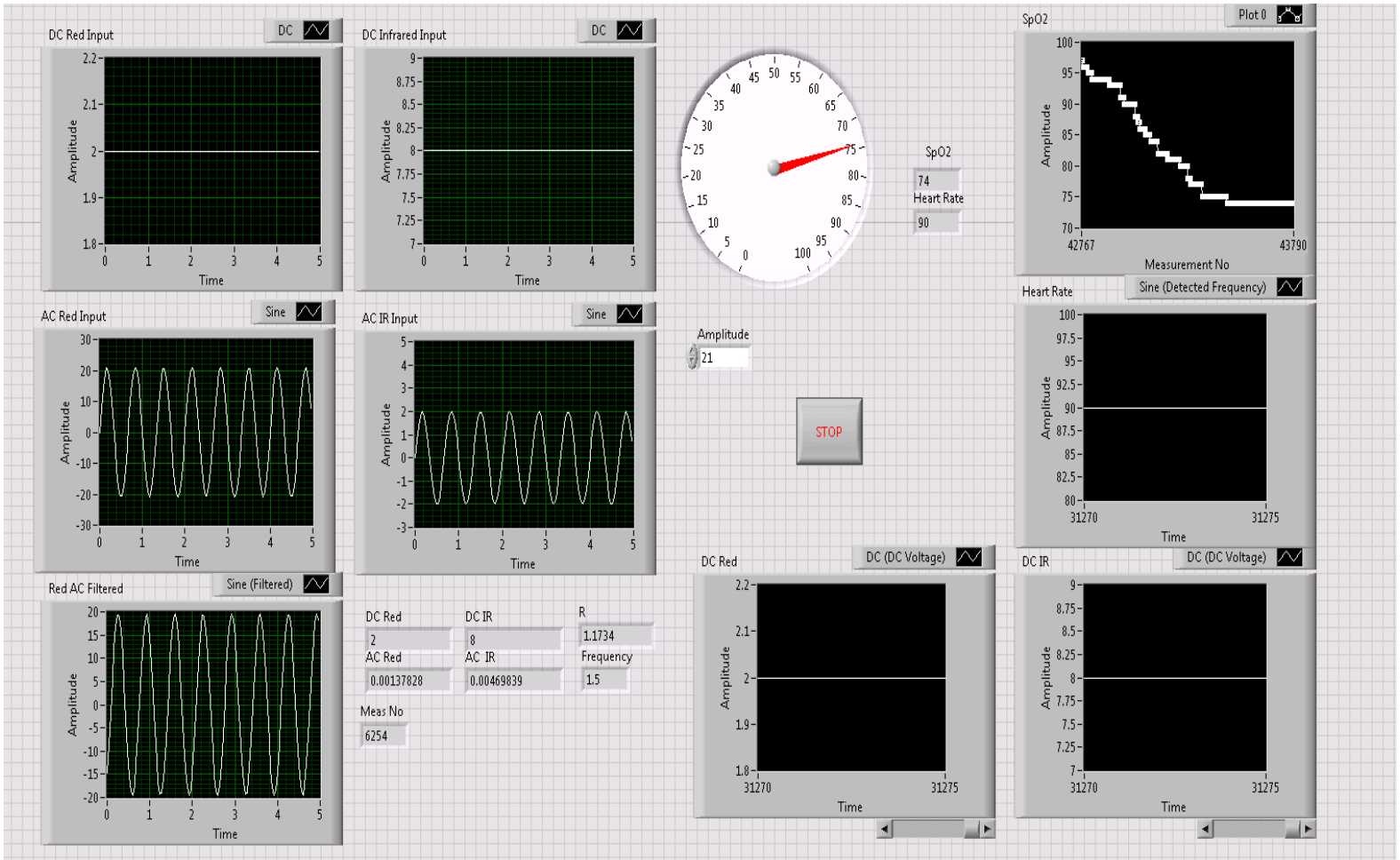

Figure 5.15: Front panel for the simulated hypoxia test with high amplitude

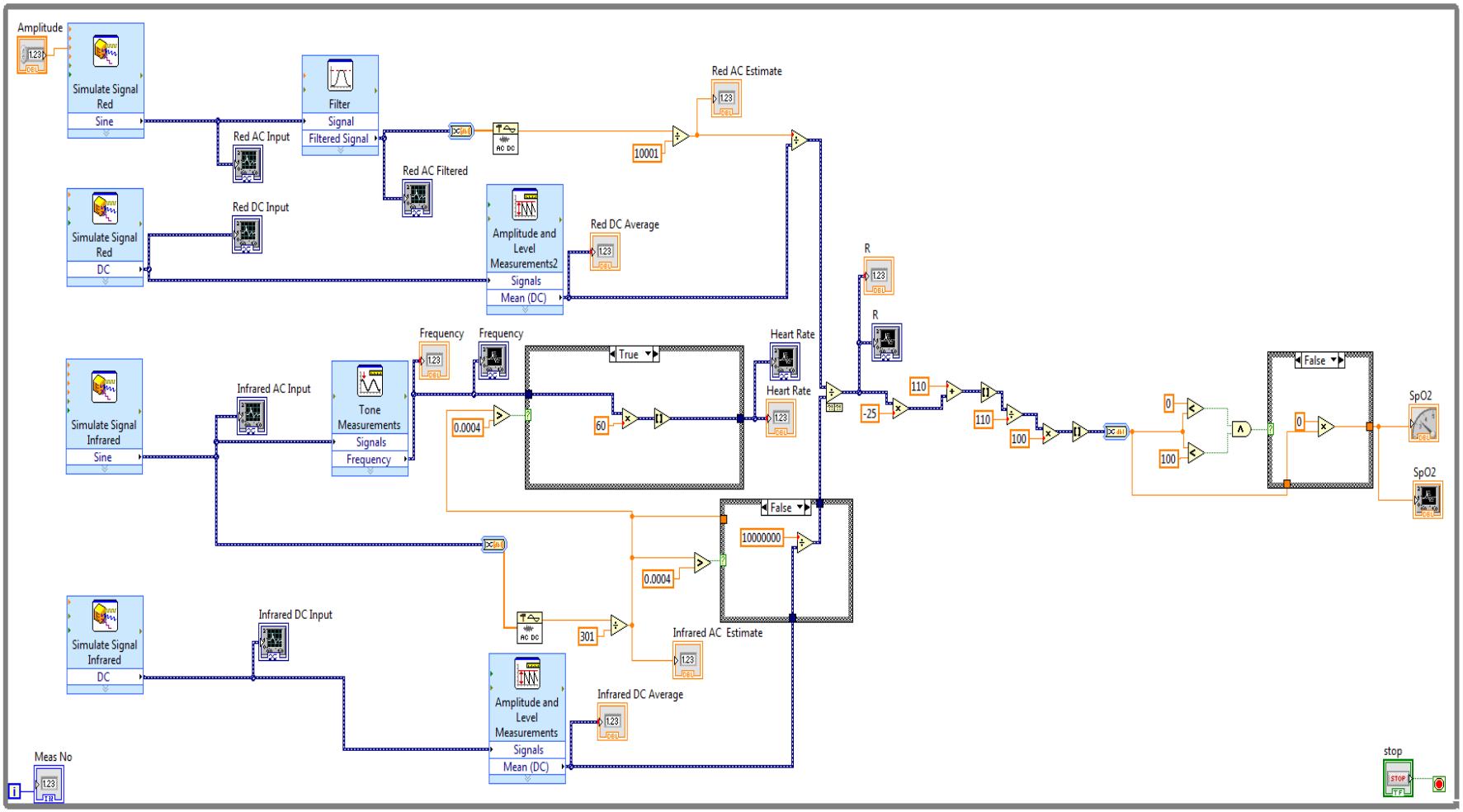

Figure 5.16: Block diagram for the simulated hypoxia test

5.5 Experimentation/Testing

5.5.1.1 ECG and Reference Pulse Oximeter Reliability Test

For measurement and comparison purposes a HOMEDICS Deluxe Pulse Oximeter with transmission method for the finger was utilized as a reference along with our pulse oximeter prototype. The reliability of the reference pulse oximeter was tested against an ECG Biopac module model 100C.

Three ECG electrodes were connected to each subject's right arm, left arm and left leg. Data collected from the ECG electrodes were displayed by the AcqKnowledge software and changes in PR were monitored on the screen using peak to peak analysis. The pulse oximeter was placed on the subject's index finger. The ECG Biopac module was turned on and one minute of data were collected while the PR was monitored by the finger pulse oximeter at the same time. Accuracy and error percentages were calculated from each measurement. We calculated the error to be less than $\pm$3%, which matches the finger pulse oximeter's specification sheet and deems it suitable to use as a reference.

5.5.1.2 Wrist Measurements

The probe of an oscilloscope was connected to the AC infrared outlet of the circuit and to common ground. The display of the oscilloscope was set up to segments of 500 milliseconds with amplitude of 2 volts so the blood pressure wave was clearly visualized. Since the AC component of the infrared outlet from the circuit showed a more defined representation of the blood pressure curve than the AC red component, the AC infrared component was utilized as a second visual reference for the testing phase of the prototype.

The sensor was strapped tightly to the wrist of the subject by means of a Velcro strap to maintain constant pressure while the subject was sitting with his/her arm resting on a table. Although we encouraged the subjects to place the sensor directly over the radial artery, the specific location and orientation of the sensor varied for each individual since PPG intensity can vary from person to person.

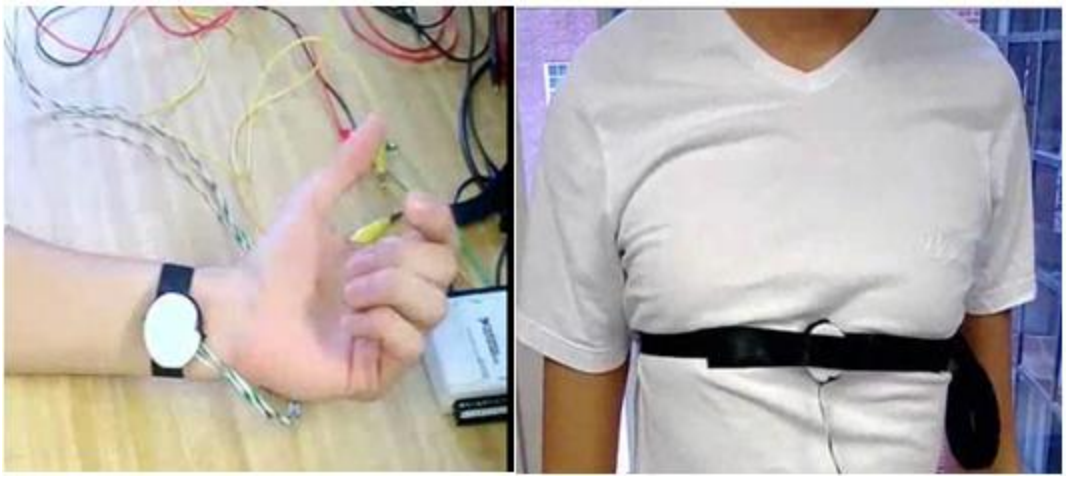

Figure 5.17: Application of the sensor to the wrist (left) and the chest (right)

The VI is setup to collect data in ten seconds intervals during six minutes. Measurements from the reference pulse oximeter, which was worn on the subject's finger, were taken at the same time that a new measurement appeared on our prototype VI. These results were recorded in an excel spreadsheet for the corresponding time. Measurants were recorded using the described procedure while sitting and standing.

5.5.1.3 Chest Measurements

The sensor was then attached to the chest using a longer Velcro strap and positioned directly over the sternum to obtain a strong PPG signal. The oscilloscope was set again with a window of 500 milliseconds and amplitude of 2 Volts. The pressure applied to the sensor on the chest varies depending on the subject's ability to display a continuous PR wave on the oscilloscope and their comfort level. The chest test was performed while the subjects were sitting and standing over six minutes.

5.5.1.4 Hypoxia Testing

The ability of the prototype to reproduce accurate low SpO_2 levels was also tested. Here, the sensor was strapped around the wrist and data were collected right after asking the subject to self-induce hypoxia by not breathing for 45 seconds. Hypoxia test were performed on four different sitting individuals. Only one individual was able to show a drop in SpO_2 levels after 45 seconds. The lowest SpO_2 value observed on the reference pulse oximeter was 91% while the VI displayed a value of 93%.

5.5.1.5 Hyperventilation Testing

The final test performed was a hyperventilation test in which we measured how well our prototype responding the changing values of PR. During this test four different subjects were asked to strap the sensor to the wrist and remain calm with their arm extended and relaxed on a table with the reference device attached to the finger. The subjects were asking to breathe normally for a 1-minute period to obtain

a stable PR. After the initial minute, each subject was then asked to begin hyperventilating for about 4 minutes. After the hyperventilation period the subjects were asked to breathe normally again for an additional minute to conclude the 6 min test and to show a declining PR. The results were compared to the reference device and plotted data were produced and shown in the results section.

6 Final Design

6.1 Device Hardware

For our final design, we took alternative design 1 and modified parts of it for efficiency. For the sensor block we increased the number of photodiodes surrounding the LEDs in order to obtain a lower degree of sensitivity that would otherwise be present with a smaller amount of photodiodes. More photodiodes also results in an increase in the total photodiode surface area which can capture reflected light.

6.1.1 Sensor

The design for the sensor module was based on the need for a concentric photodiode arrangement around two LEDs, one infrared and one red. Since that a larger number of photodiodes would only benefit the device, the group decided to utilize 8 surface photodiodes instead of the 4 that was designated in alternative design 1. In Figure 6.1 Figure 6.1 below, we can see the top view of the sensor module that the group developed. The red and infrared LEDs are placed in the center of 8 photodiodes which are able to pick up light from nearly every angle. The added effect of the photodiodes is also a benefit since summing up the current from all eight photodiodes maximizes the fraction of total backscattered light collected by the sensor.

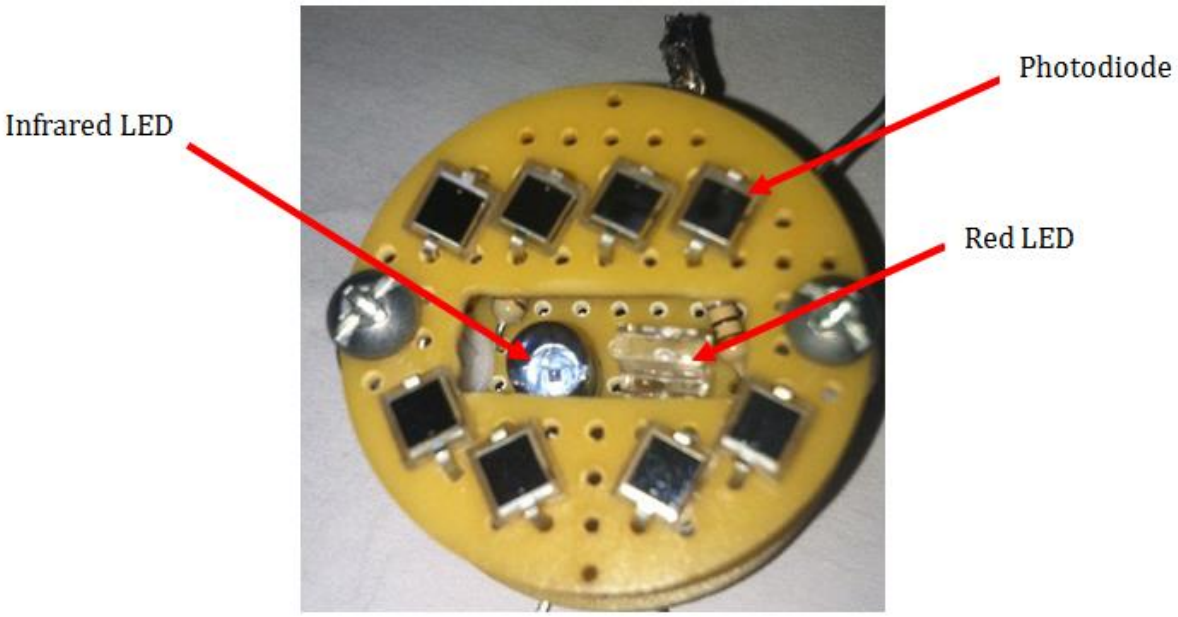

Figure 6.1: Top View of sensor module with photodiodes and LEDs.

The placement of the LEDs relative to the photodiodes was also important. Since the LEDs were much larger than the photodiodes, we had to consider how we could design the sensor so that the LEDs and photodiodes were the same level when placed on the skin. Our solution for this was using a two

platform design. In Figure 6.2Figure 6.2, we present a side view image of our sensor module with each platform labeled.

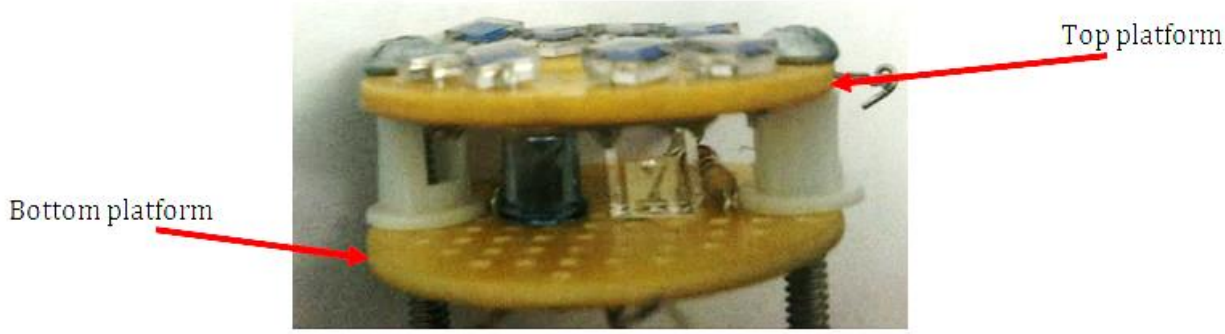

Figure 6.2: Platform view of sensor module

The top platform, which is the surface of the device that is placed against the skin, was used primarily for the placement of the photodiodes. A rectangular opening was then made in the center of the board to allow for the LEDs placed on the bottom platform to protrude through and allow the light to pass through the skin. To allow for portability and to reduce the weight of the sensor, we separated the sensor module from the actual circuitry and connected 4 wires from the sensor to the circuitry board.

6.1.2 Circuitry

To process the signals obtained from the sensor module, we implemented several different signal processing techniques which helped to simplify the programming required in the VI. The block diagram in Figure 6.3Figure 6.3 shows a simplified view of our circuitry and how it is connected.

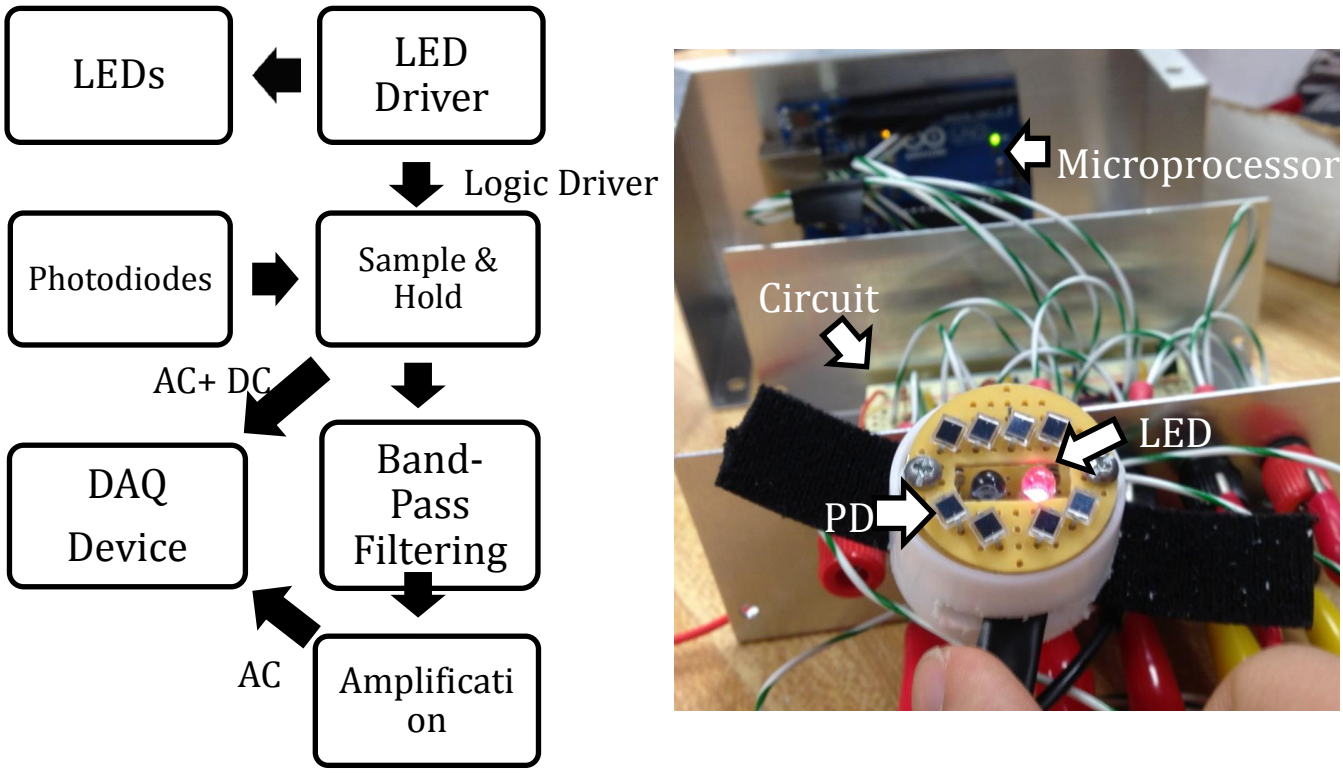

Figure 6.3: Block diagram of the prototype pulse oximeter

The LEDs in the sensor module are driven at alternating frequencies of 100Hz with a 2.5ms delay between each LED as it is turned on. Figure 6.4 displays the timing diagram of the Arduino Microcontroller which is used as an LED driver. The board was programmed so that the first channel (in yellow) is ON for 2.5ms and OFF for 7.5ms while the second channel (in green) is OFF for 5ms, ON for 2.5ms and then OFF for 2.5ms.

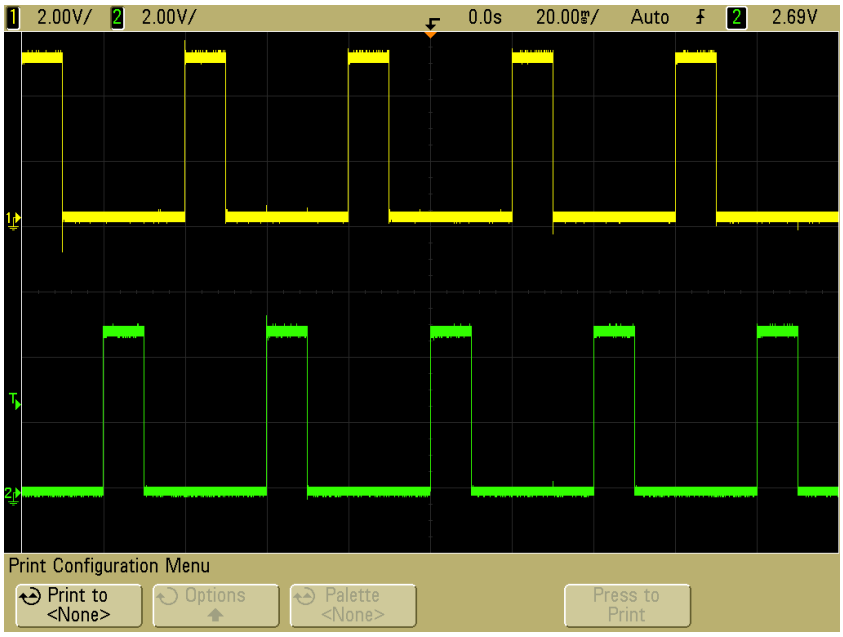

Figure 6.4:LED driver timing diagram with 2.5ms time increments

For the photodiodes, we used an op-amp in photovoltaic mode so that the current output of the photodiodes is converted to a voltage. The voltage, which is directly related to the amount of light collected, is then sent through two Sample-and-Hold ICs (LF398) (S/H) to separate the red and infrared signals. To accomplish this, the voltage output by the photodiodes were connected simultaneously connected to both S/H and used the LED driver signals for the red and infrared LEDs as the logic driver for each S/H respectively. Each S/H is able to sample the respective LED to which they are connected to and hold that value until the next time the LED is turned on. The output of each S/H provided the AC and DC components of the PPG required for calculating oxygen saturation. However, because the AC component is generally very tiny compared to the DC component, it was necessary to filter this signal further so that the DC component can be removed and the AC component is amplified. The circuit in Figure 6.55 Figure 6.5a detailed diagram for each signal processing stage in the block diagram.

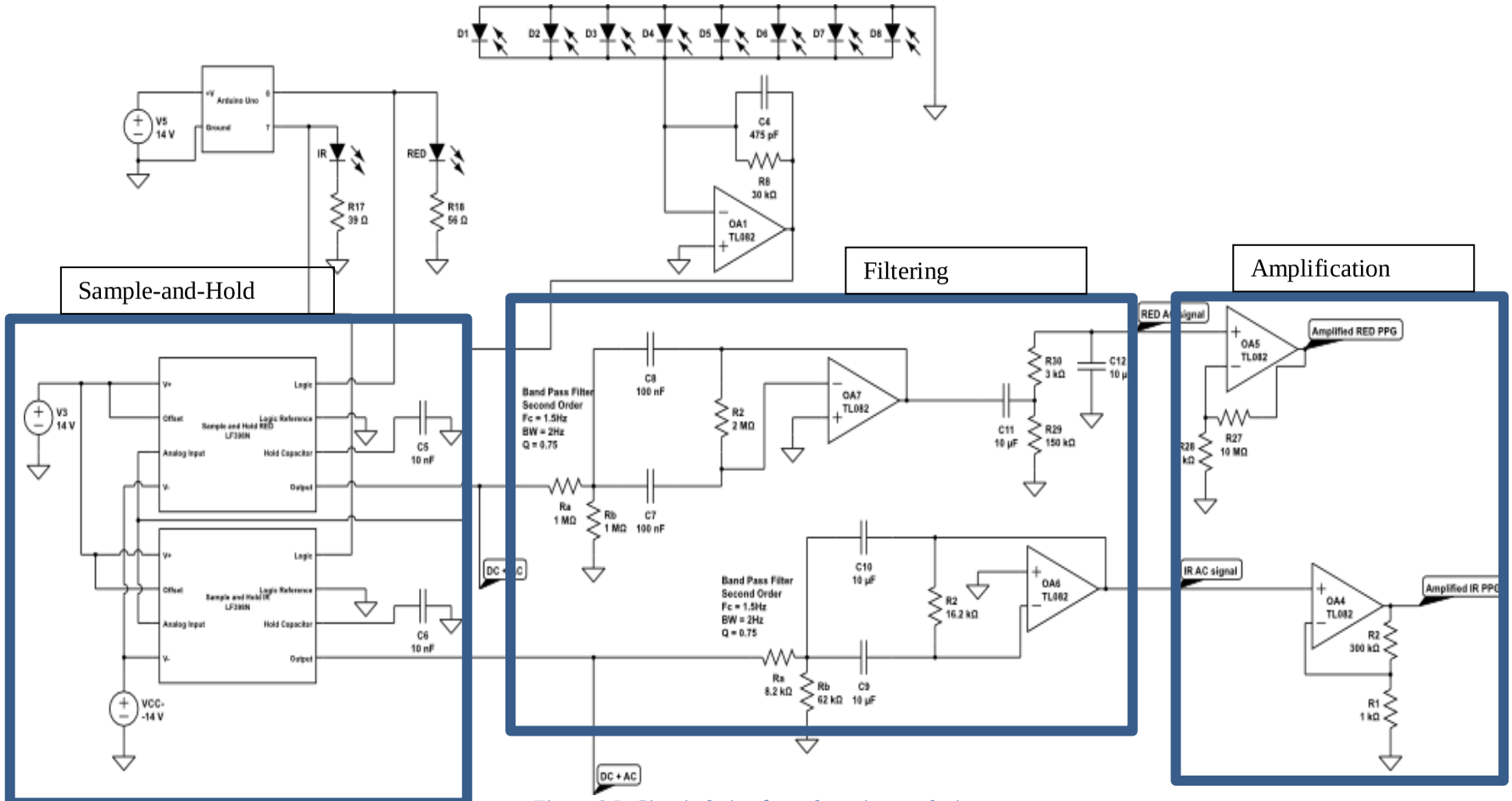

Figure 6.5: Circuit design for pulse oximeter device

To filter and separate the AC component from the AC and DC components, obtained from the S/H, each respective signal red and infrared was processed through a 2nd order bandpass filter. Both bandpass filters were designed with a frequency cutoff of 1.5Hz and bandwidth of 1.5Hz. The rationale behind the selected characteristics is that a range between 0.75Hz and 2.25Hz should be enough to capture and amplify the signals of almost any individual who is at rest. Although the ideal use for any pulse oximeter is to work efficiently at rest and in motion, we felt for the purpose of this project this frequency range would be enough to prove a concept and provide accurate enough readings for individuals with PR between 45bpm and 135bpm.

Seeing a lot of high frequency noise riding on top of a DC offset present in the red signal, we then implemented an additional high pass and low pass filter for the red AC signal so that the DC offset could first be removed and then second so that the high frequency noise could also be filtered out. The last stage in the signal processing is the amplification of the respective red and infrared AC signals at which point they are ready to be interfaced with the DAQ and processed by the VI.

6.2 Software

The final design of the block diagram and front panel of the VI can be seen below. The VI starts by accessing the signals from the sensor with the DAQ Assistant and then separating the signals by implementing select signals. Once the signals are separated and identified the AC components of the red and infrared signals are measured using the peak-to-peak method while the DC components were measured by finding their respective averages. The peak-to-peak method was chosen for the AC components because it is a straightforward measurement which can be compared to the readings of an oscilloscope. Averaging the DC components was necessary because it provided a single value to be used in the SpO_2 calculation for each data set sampled.

Once the signals are processed SpO_2 can be calculated as the ratio of the red AC/DC divided by the infrared AC/DC multiplied by -25 and added to 110. To provide a SpO_2 measurement between 0 and 100, the SpO_2 calculation is then divided by110 and multiplied by 100 so that the value is normalized. To calculate the PR, the frequency of the AC infrared signal was measured using the tone measurements function and then multiplied by 60 to calculate the PR in beats per minute.

Since the VI is constantly sampling data as long as the sensor and a power supply is connected to it, the VI samples noise and runs the computations for PR and SpO_2 even if the sensor is not being worn. To avoid this, case structures were used to introduce thresholds which allow the VI to calculate measurements when the amplitude of the red and IR AC signals were above a certain level and to output 0 when these conditions were not met.

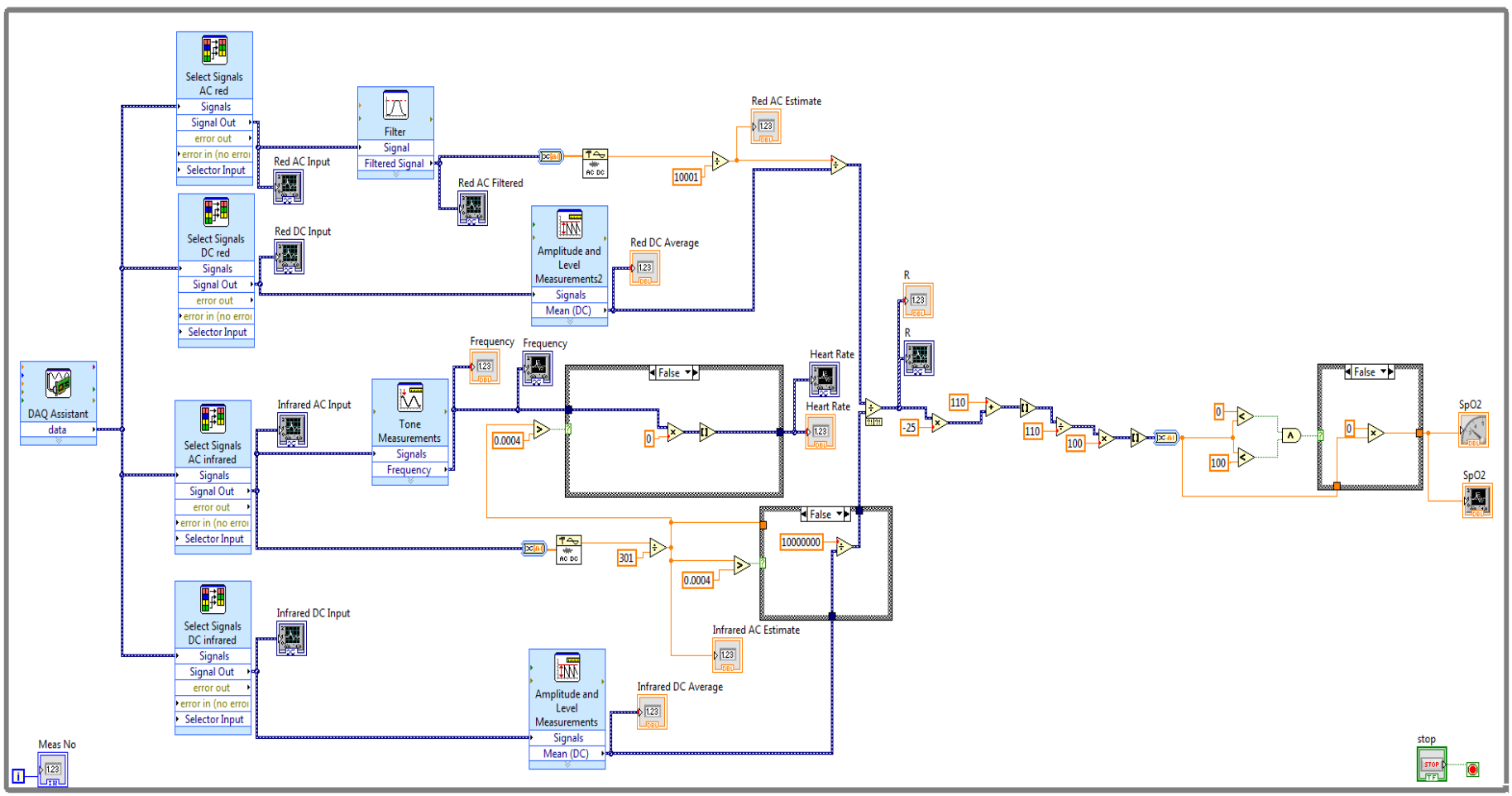

Figure 6.6: Block Diagram of Final VI

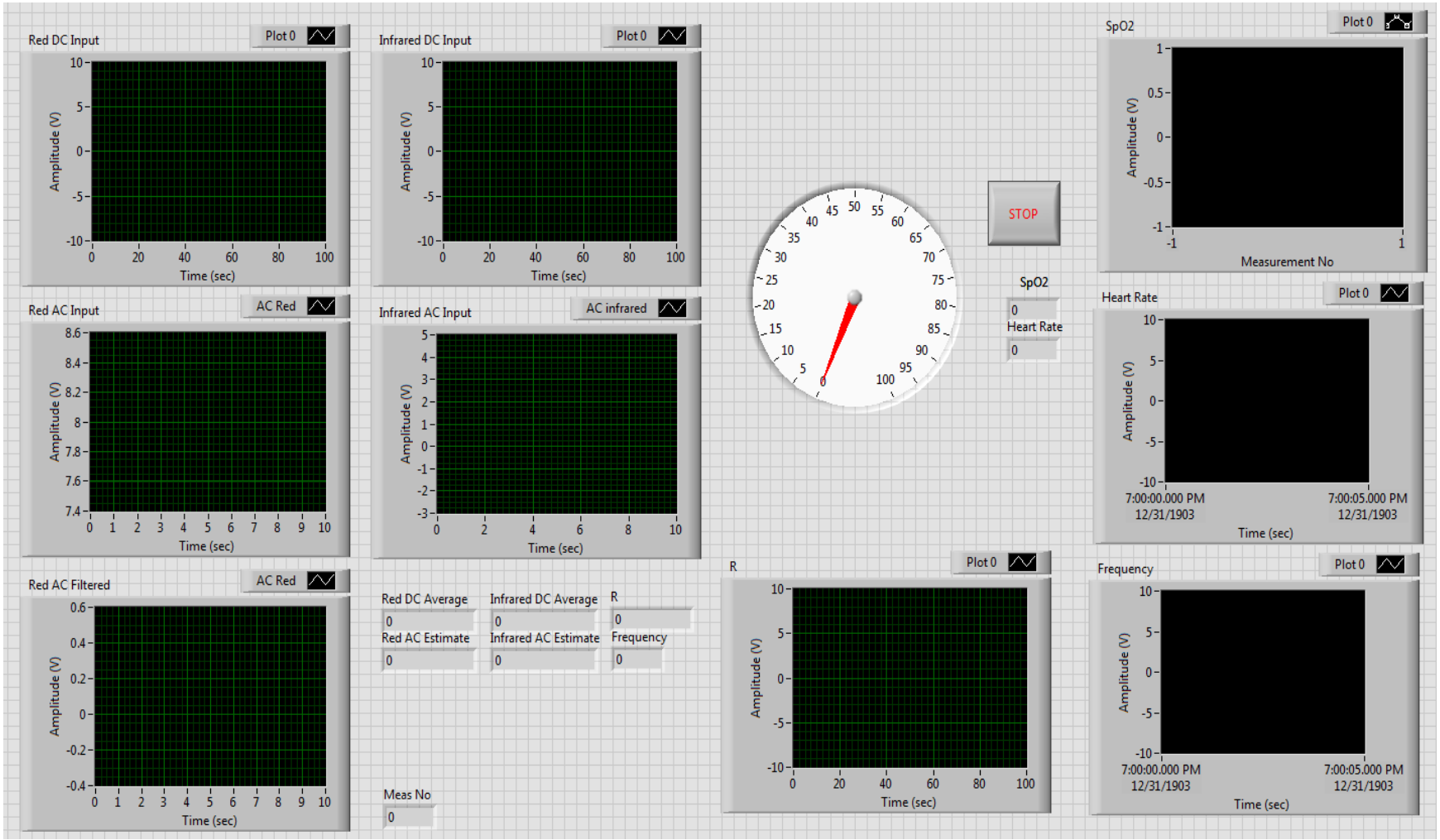

Figure 6.7: Front Panel of Final VI

7 Results

The VI was set to collect and average data every 10 seconds throughout a 6 minute timespan accounting for 36 measurements per data set. The VI was programmed to output SpO_2 and PR every 10 seconds at which point a second individual that was monitoring the control device recorded the corresponding SpO_2 and PR values displayed by the HOMEDICS pulse oximeter. Subjects were tested while sitting, standing, hyperventilating, and during self-induced hypoxia. PPG readings were acquired from both the chest and wrist. Each subject was asked to hyperventilate to mimic an increase in pulse rate and each of the subjects was also asked to hold their breath for 30 to 40 seconds after a full exhale to induce hypoxia. These tests showed the devices ability to detect increasing and decreasing levels of PR and SpO_2 respectively. To compare the accuracy of our prototype to that of the reference pulse oximeter we calculated the average SpO_2 and PR for each data set, and then calculated the percent error using the accuracy equation below summarized in Table 7.1.

$$Percent\ Accuracy = \frac{X_{actual} - X_{measured}}{X_{actual}} * 100 \qquad (5)$$

Table 7.1: Calculated accuracy for the average SpO_2 and PR for each data set

Average Measurements	**Reference**		**Prototype**		**Percent Errors**	
	SpO_2 (%)	PR (bpm)	SpO_2 (%)	PR (bpm)	SpO_2	PR
Wrist Standing	97.9	92.6	97.3	92.8	0.6	0.2
Wrist Sitting	98.2	82.4	98.4	83.3	0.2	1.1
Chest Standing	98.1	96.7	98.5	96.5	0.4	0.1
Chest Sitting	97.8	83.8	98.1	83.9	0.3	0.1

This method was only used for the standing and sitting positions for both chest and wrist readings. To calculate the percent error for all the data collected with our prototype, we first used the

accuracy equation on every individual measurement taken for each data set and averaged the percent error per measurement. To calculate the prototype's accuracy, we then averaged the percent error for each data set to obtain a single value. The accuracy of each data set and the prototype's final accuracy are shown in Table 7.2. Due to the fact that we were focusing primarily on SpO_2 for hypoxia and PR for hyperventilation, we chose to collect only those measurants during our testing and did not take measurements for PR and SpO_2 respectively.

Table 7.2: Prototype accuracy based on all data collected

Measurement	**Position**	**Accuracy (Percent Error %)**	
		SpO_2	***PR***
Chest	Sitting	0.76	3.15
	Standing	0.60	3.09
Wrist	Sitting	0.24	4.14
	Standing	0.76	3.75
Hypoxia		1.50	
Hyperventilation			5.32
Prototype Accuracy		0.77	3.89

As seen in a couple of the graphs in the sections below, there were examples of outliers in some of the data. These outliers were linked to a corrupted PPG signal in which the PPG was somehow affected by factors such as motion artifact or inconsistent pressure. Figure 7.1 shows an example of a corrupted PPG, in turn compromising the accuracy of that data point.

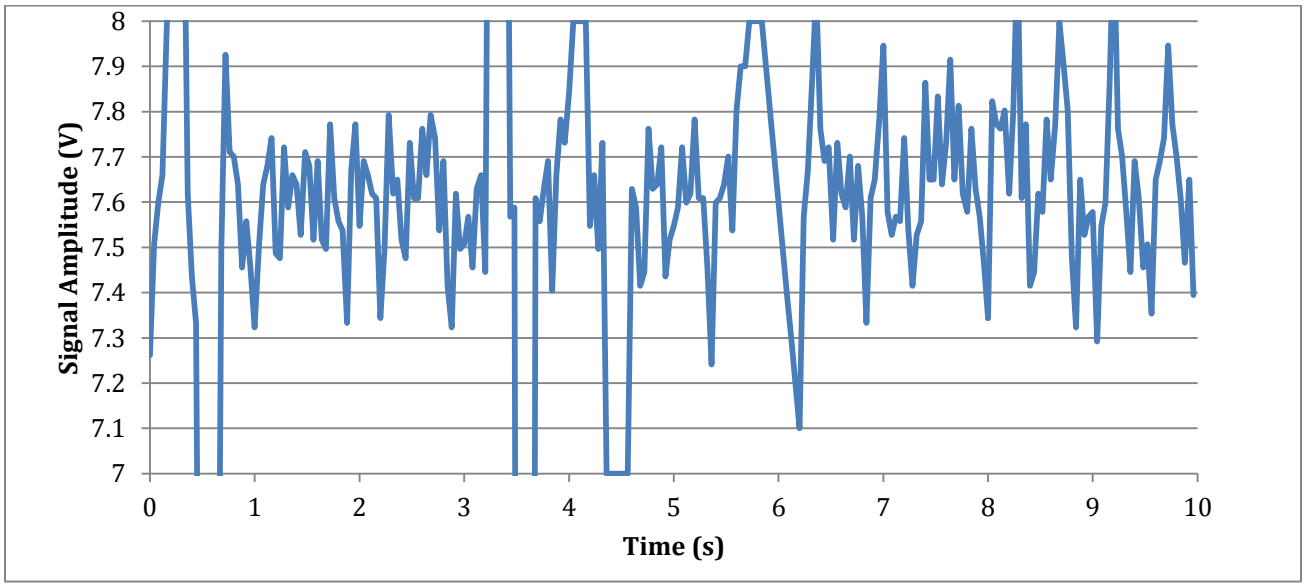

Figure 7.1: Example of corrupted PPG

7.1 Comparison Graphs

Comparison graphs are a useful tool when graphically representing our data because it enables to compare all the data sets for the prototype and reference devices for one test as a whole. Figure 7.2 displays a regression line for the PR data collected from our pulse oximeter prototype on the chest of four different subjects over a six-minute period while sitting. The data are clustered in four different groups, each one having a distinctive symbol corresponding to the subject tested. The total PR data obtained from our prototype for all four subjects ranges from 55 to approximately 105 bpm. The linear regression equation obtained from the data points as well as the statistical coefficient R^2 that determines how well the regression line approximates a linear trend are shown on the upper left corner of the graph. Table 7.1 shows that the PR measurements taken from the chest while sitting has a low percent error of less than 1% when looking at the average of the data and 3% when calculating the accuracy of each individual data point.

The fact that R^2 is close to 1 and the slope of the regression line is also very close to 1 show that the measurements picked up by the prototype appear to be well correlated with the measurements picked up by the reference pulse oximeter. This can also be observed visually by looking at how closely the regression line is to the line of identity.

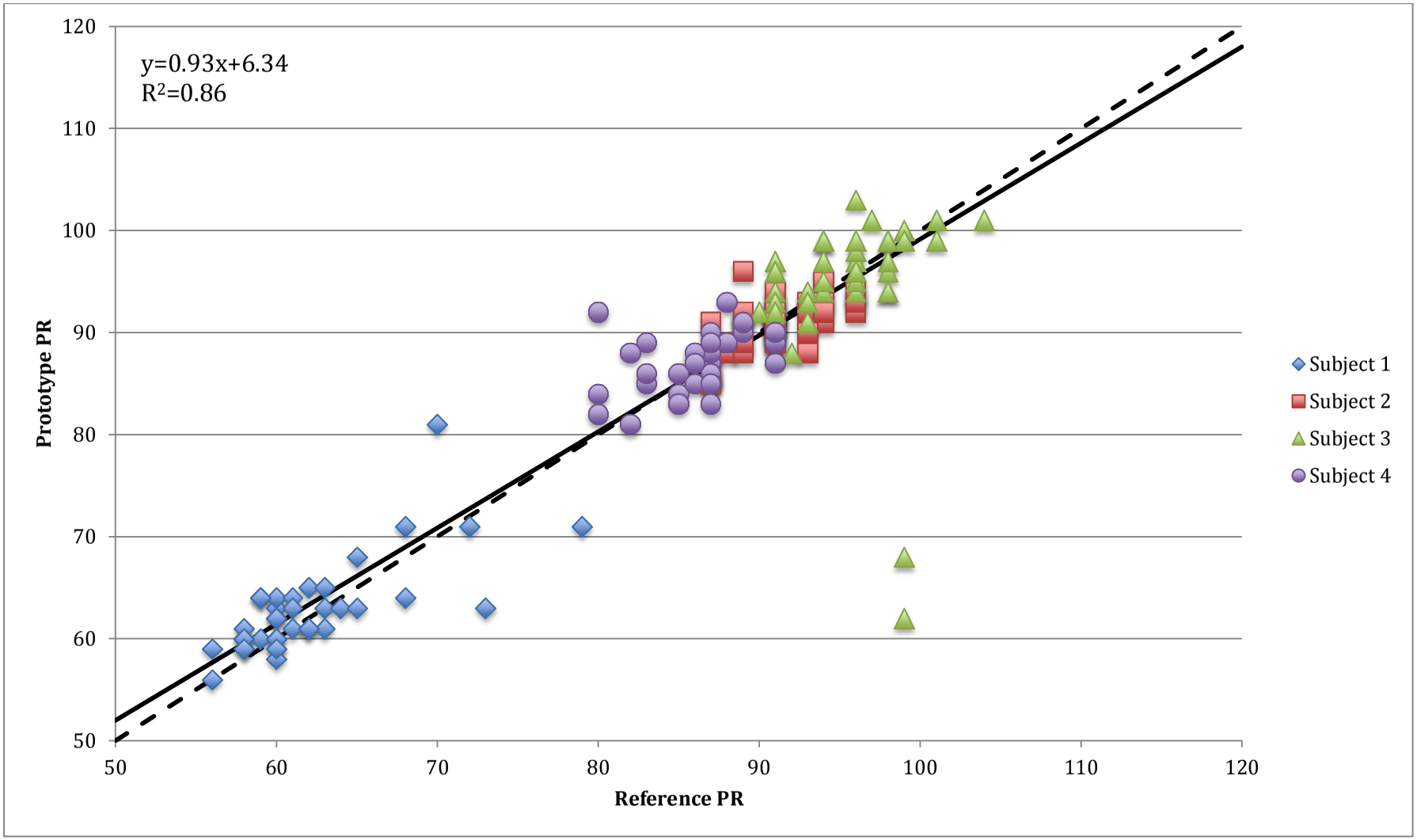

Figure 7.2: Comparison graph for the chest sitting tests. The solid line represents the regression line and the dashed line represents the identity line.

In Figure 7.3, a comparison plot referencing the data collected from our prototype on the chest of four different subjects while standing over a six minute period is displayed. The measuring scale ranges from 80 to 120 bpm with increments of 5 bpm. The linear regression equation and best fit coefficient are shown at the upper left corner. Similar to the regression line presented in Figure 7.2, the regression line in this comparison graph shows a slope very close to 1. The statistical coefficient of determination R^2, which is used in the context of statistical modeling for predictions, is a measure of how good a predicted value might be construed from the modeled values. A lower R^2 also shows that the correlation coefficient denoted as R, is lower than the sitting measurement shown in Figure 7.2.

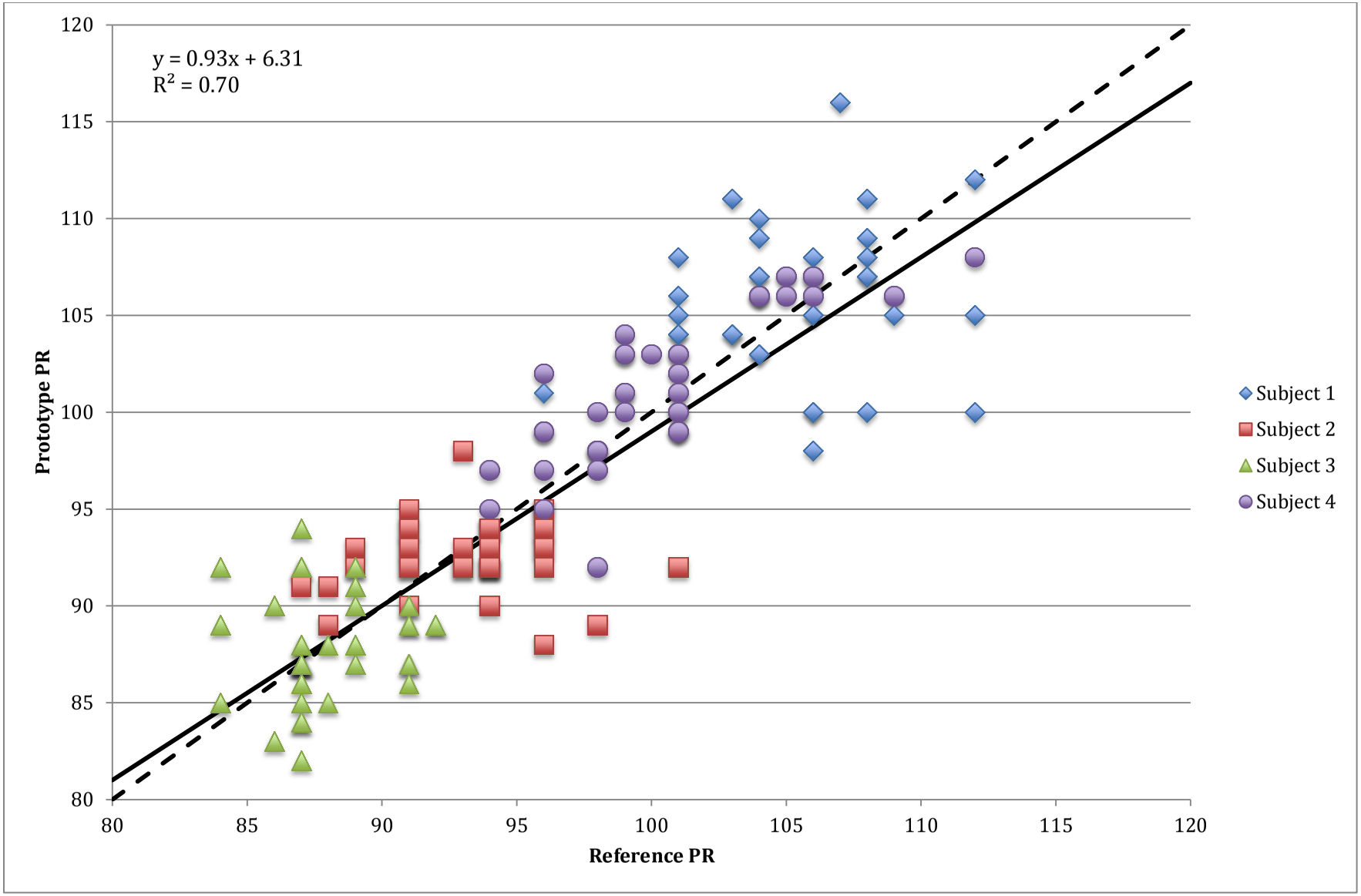

Figure 7.3: Comparison graph for the chest standing tests. The solid line represents the regression line and the dashed line represents the identity line.

Figure 7.4 displays a regression line for the PR data collected from our pulse oximeter prototype on the wrist against the HOMEDICS reference finger pulse oximeter on four different subjects over a six minute period while sitting. The data are clustered in four different groups, each one having a distinctive symbol corresponding to the subject tested. The measuring scale ranges from 50 to 120 bpm with increments of 10 bpm. The total PR data obtained from our prototype for all four subjects ranged from 52 to approximately 105 bpm. The graph displays the linear regression line and R^2 on the upper left corner. In this set of data we observed that the coefficient of variance, R^2, and in turn the coefficient of correlation, R, to be slightly lower than the values observed from the chest while sitting. When visually comparing the regression line to the line of identity, we can conclude that these measurements were not as accurate compared to the reference pulse oximeter.

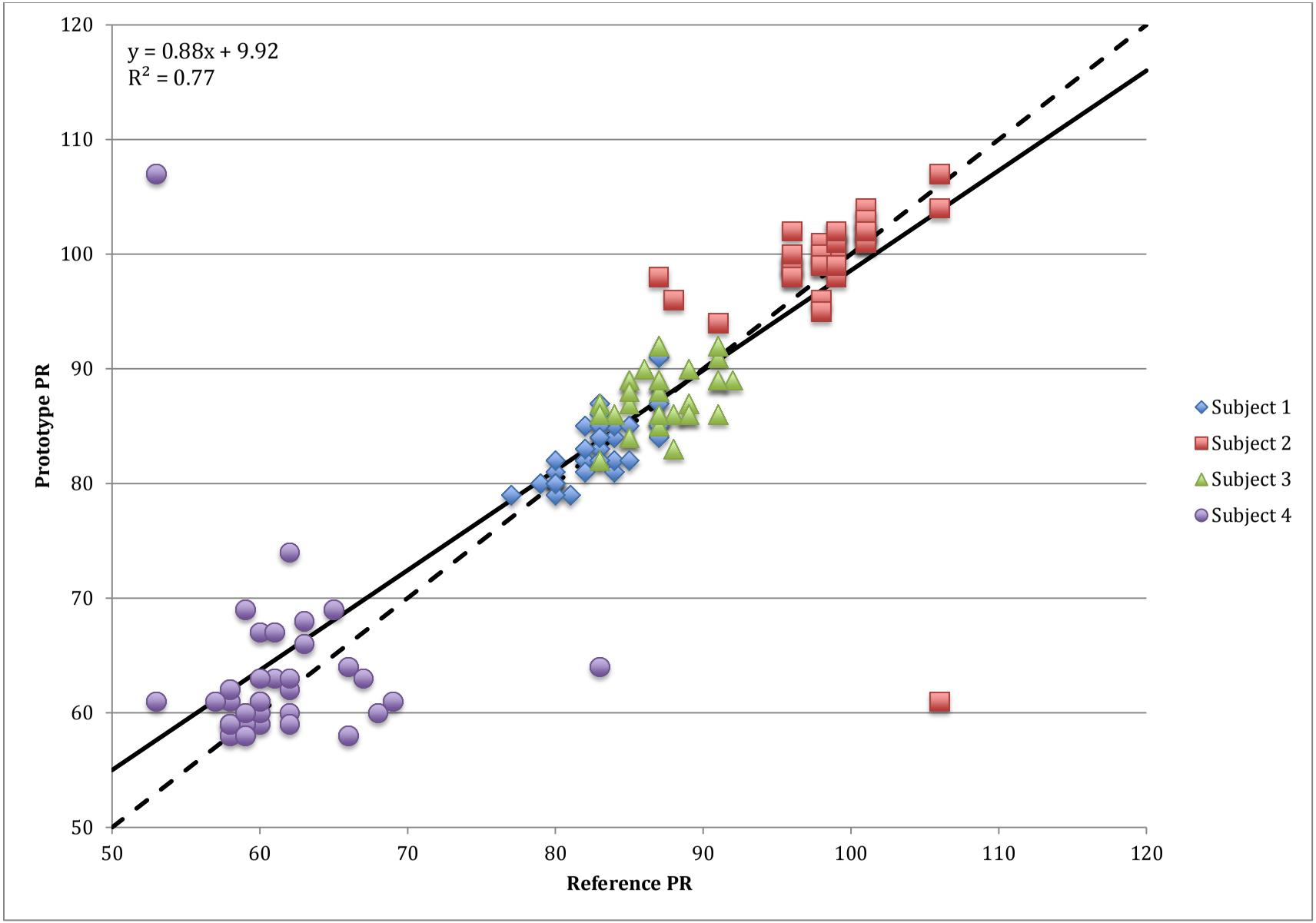

Figure 7.4: Comparison graph for the wrist sitting tests. The solid line represents the regression line and the dashed line represents the identity line.

In Figure 7.5 a comparison plot referencing the data collected from our prototype on the wrist of four different subjects over a six minute period while standing is displayed. The measuring scale ranges from 60 to 120 bpm with increments of 10 bpm. The linear regression equation and best fit coefficient are shown on the upper left corner. When comparing the standing wrist measurements to the sitting wrist measurements shown in Figure 7.4, we saw that the measurements obtained from the wrist while standing appeared to be the least correlated data set. Visually, there appears to be more variations between the identity line and the regression line than in other comparison graphs.

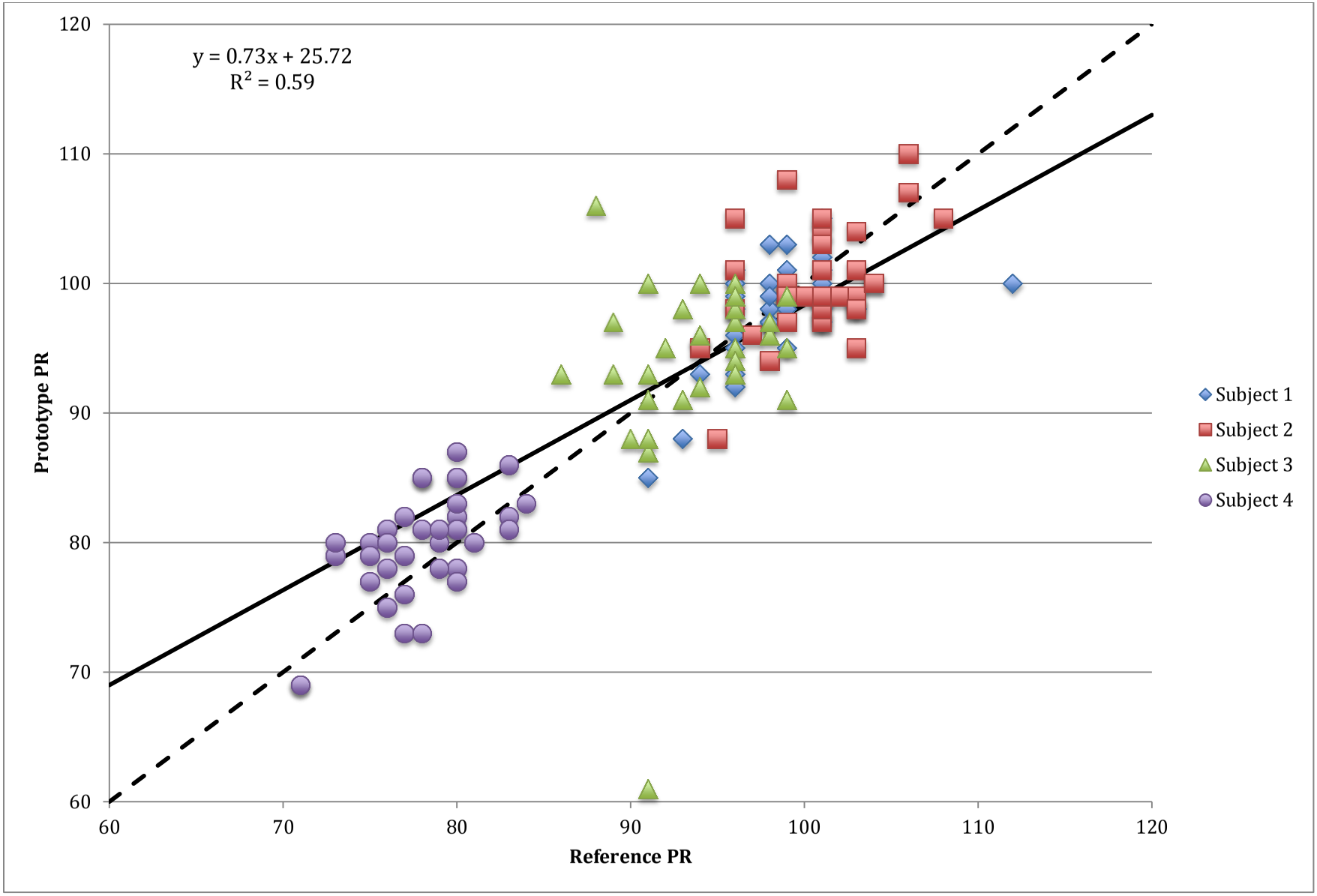

Figure 7.5: Comparison graph for the wrist standing tests. The solid line represents the regression line and the dashed line represents the identity line.

The plot displayed on Figure 7.6 shows the data points collected from our prototype on the wrist of four different subjects over a six minute period with the HOMEDICS reference device attached to the finger while hyperventilating. The measuring scale ranges from 50 to 140 bpm with increments of 10 bpm. The linear regression equation and best fit coefficient are shown at the upper left corner. One characteristic that is quickly observed when looking at this graph is that there is a lower accuracy in these measurements than in the previous graphs. This is visible in how the data points are distributed and the distance between points. Another aspect of these graphs that was noticed was that there appeared to be more outliers present in the data than in the other data sets.

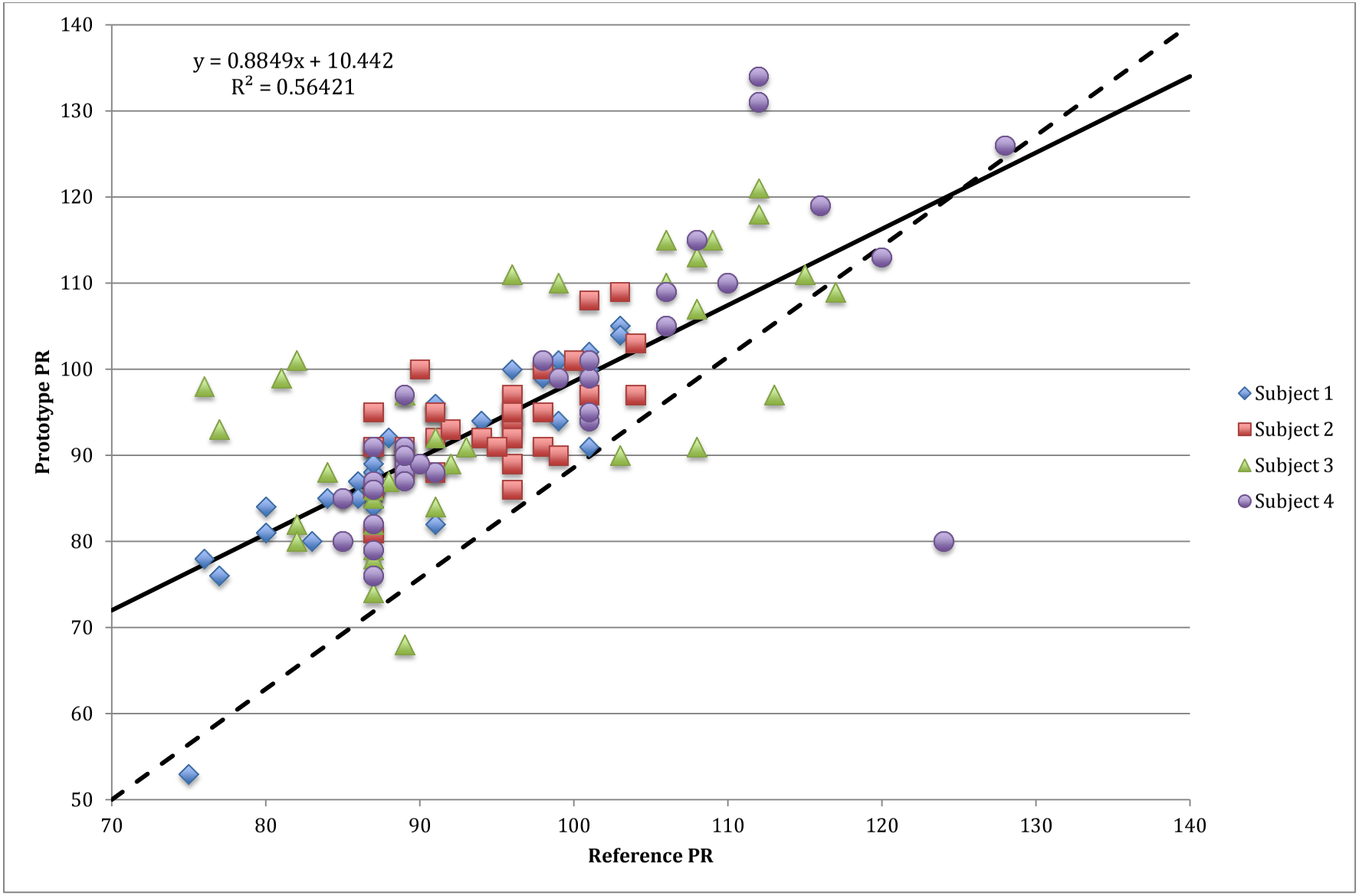

Figure 7.6: Comparison graph for hyperventilation tests

The hypoxia testing graph shown in Figure 7.7 was performed on 2 subjects capable of holding their breath for more than 40 seconds. SpO_2 readings were collected by our prototype pulse oximeter as well as by the reference HOMEDICS device. The measuring percentage scale ranged from 90 to 100 with increments of 1%. Regression line equation and best fit line coefficient are given at the upper left corner. For the purpose of plotting a regression line for SpO_2 we found it very difficult to correctly plot a regression line when the data had only a 10% range. Considering that for the majority of testing the subjects maintained a SpO_2 level of 97 or 98% we were only able to measure several small dips to assess the responsiveness of our device to changing SpO_2 levels. To correctly plot a regression line, one would need to change the SpO_2 levels over a larger range such as 70-100% in order to have a better idea of how well our device compares to the reference pulse oximeter.

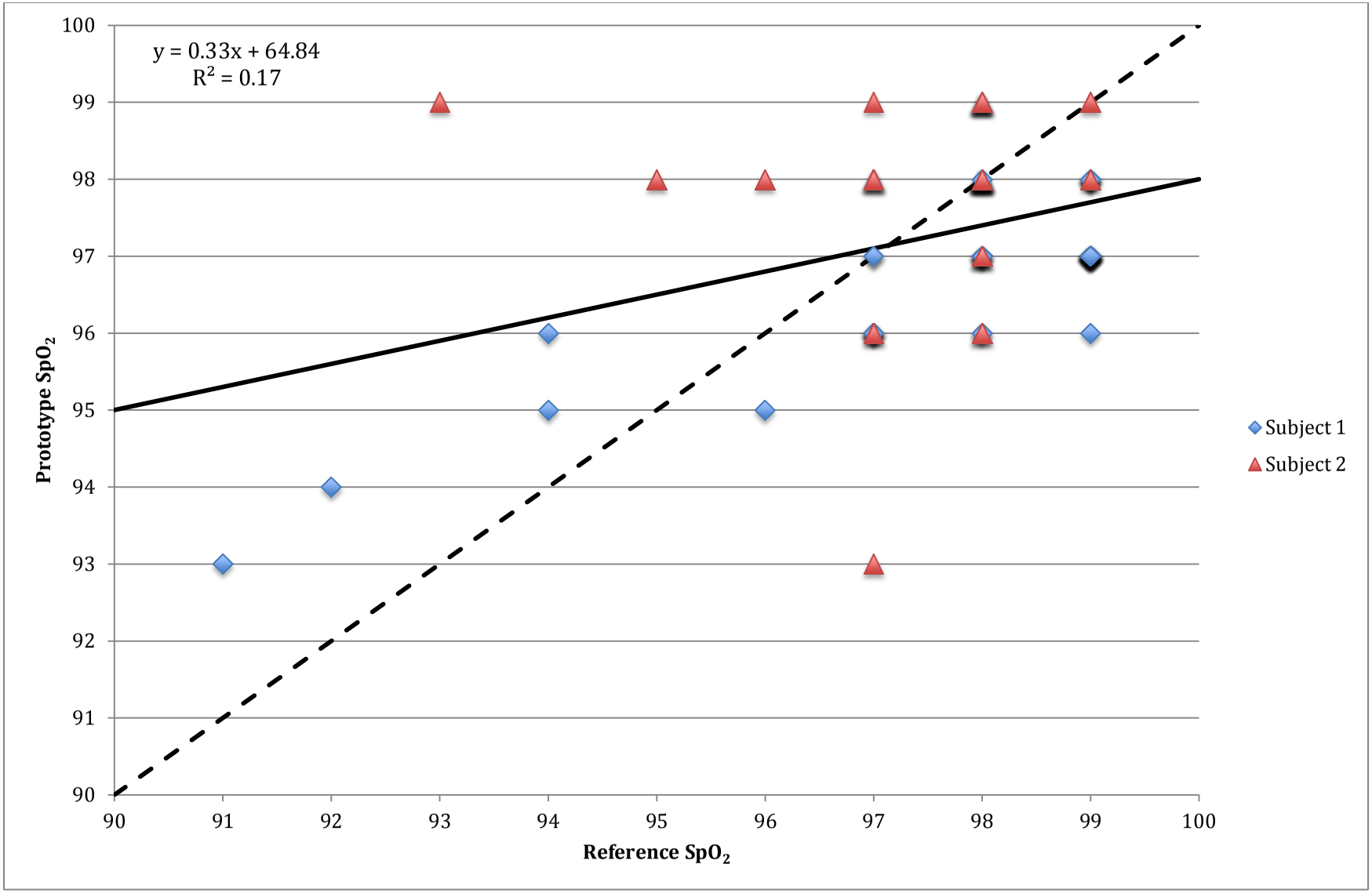

Figure 7.7: Comparison graph for hypoxia tests. The solid line represents the regression line and the dashed line represents the identity line.

7.2 Dynamic Response Plots

Dynamic response plots were utilized in analyzing the data because they show the prototype's response to changing levels of PR and SpO_2 over time. These plots in particular were utilized for all of the measurements to better understand how our device reacts to varying PR. The fact that the SpO_2 levels varied very little in most of the measurements doesn't provide any real indication as to whether the prototype is able to response to changing levels of SpO_2. To address this, we performed hypoxia tests in which we saw the SpO_2 level drop to around 90 and plotted those results.

Figures 7.8 and 7.9 depict the SpO_2 and PR measurements during the 6 minute testing period respectively. Although the only information we can obtain from Figure 7.8 is that the SpO_2 remained constant throughout the entire measurement, Figure 7.9 shows the prototypes response to changing levels of PR. One feature that was observed was that at times when the PR would ramp up, the prototype would instead ramp downwards towards a smaller PR. In fact, it was observed that this occurred 5 times during the measurement period.

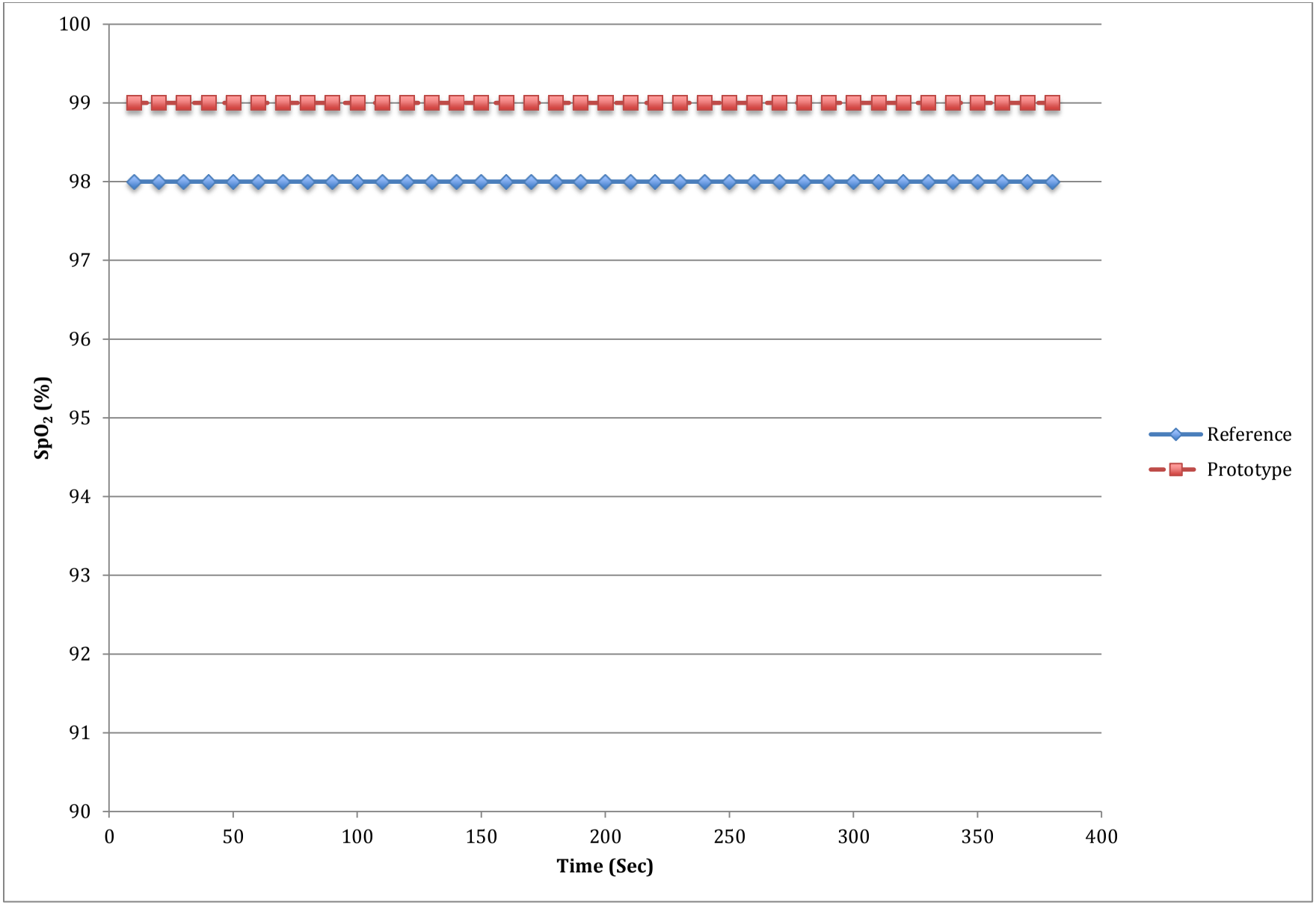

Figure 7.8: Oxygen saturation measurement validation plot for the chest standing test

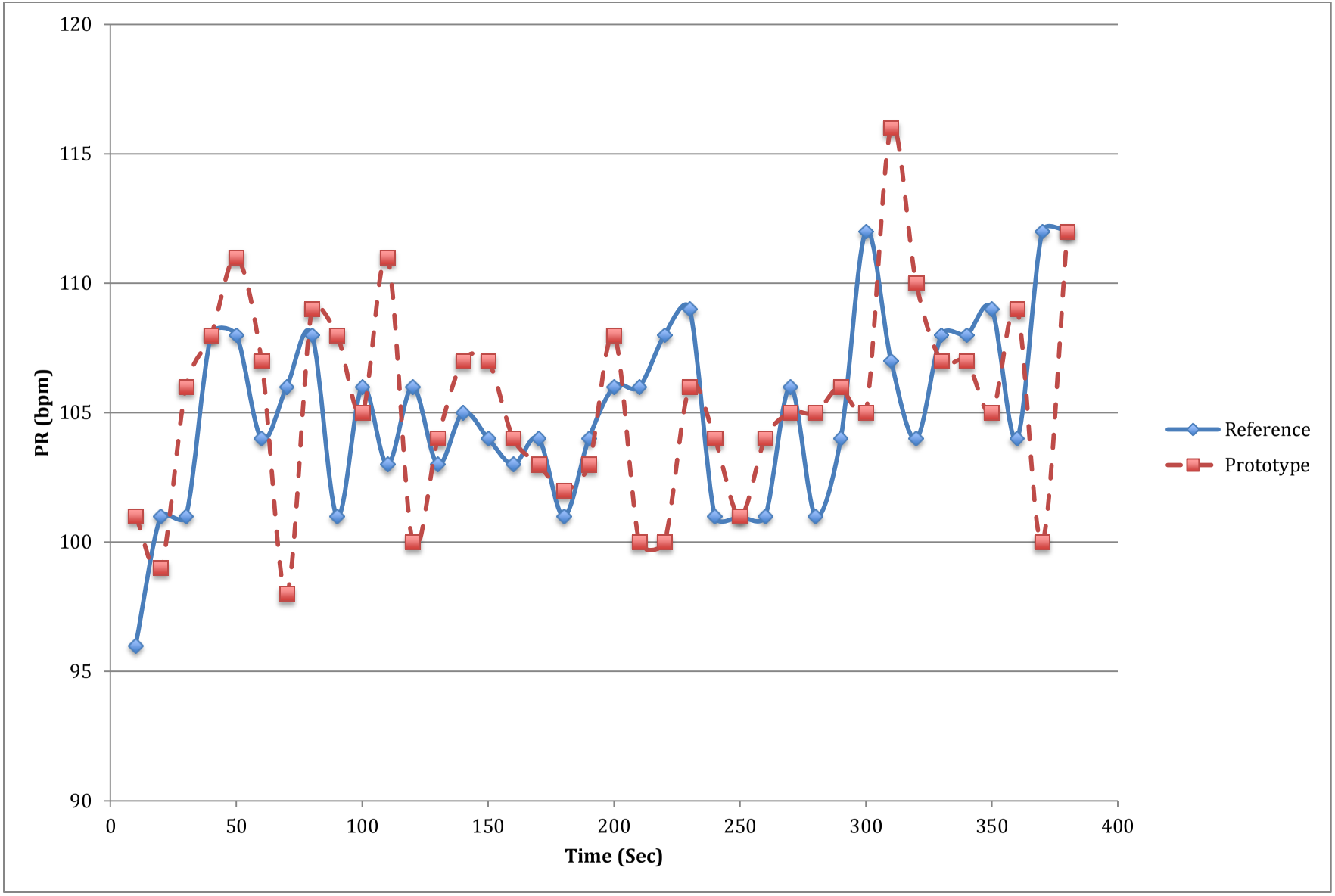

Figure 7.9: Pulse rate measurement validation plot for the chest standing test

Figures 7.10 and 7.11 display the dynamic response plots for the chest measurements of one subject while sitting. Although it was observed that the prototype's measurements bounced around 98% and 99%, this still doesn't give us any real interpretations as to how the prototype can handle different values of SpO_2. Figure 7.11 displays the changing PR measurements over time, depicts the variations in PR of an individual at rest. We did notice from this chart that while our prototype appeared to be following the general trend of data and PR variability, there was indeed quite a number of errors in the measurements. Some cases of overshooting and undershooting were observed as well as certain data points which appeared to almost be delayed PR values of the reference pulse oximeter.

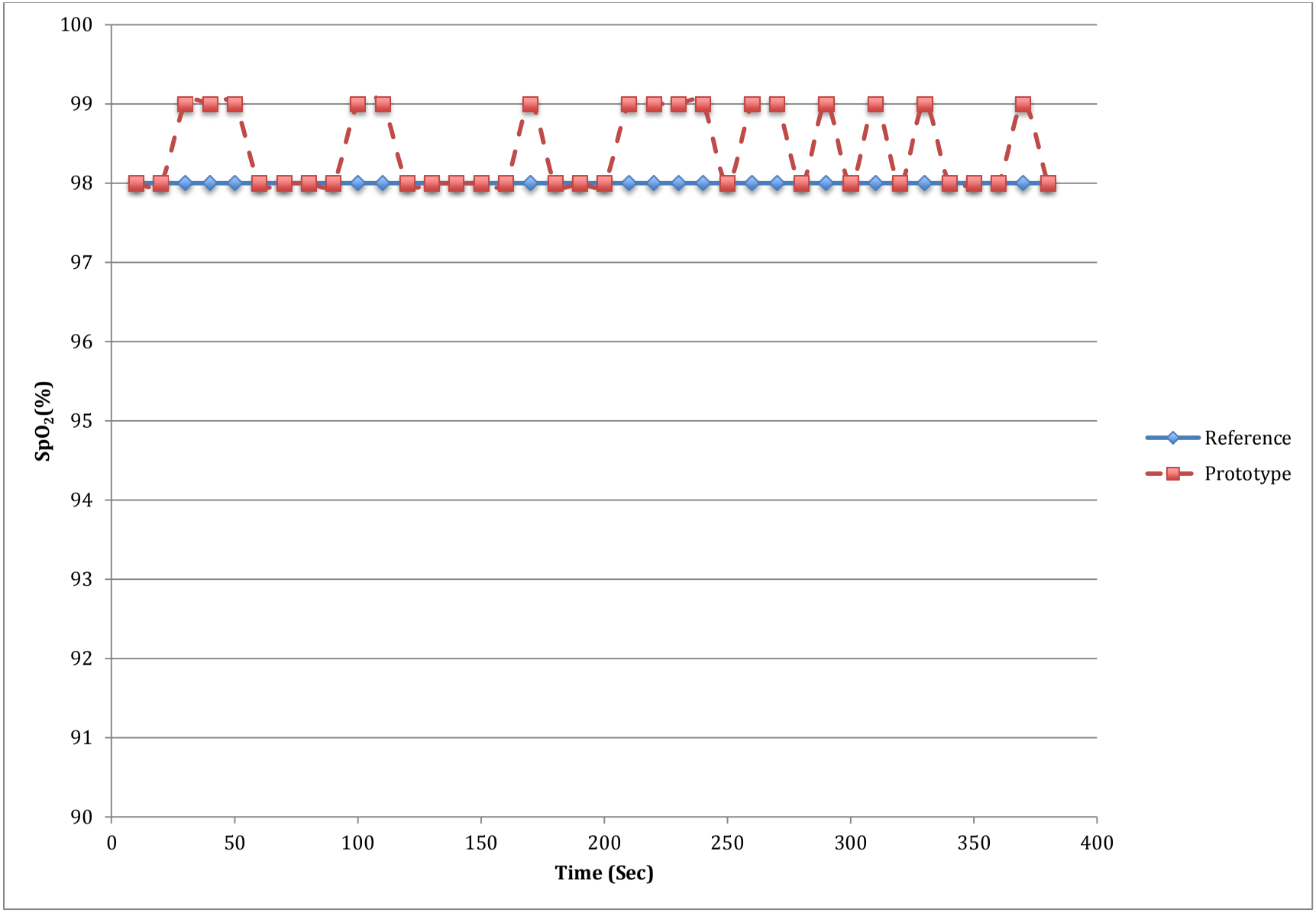

Figure 7.10: Oxygen saturation measurement validation plot for the chest sitting test

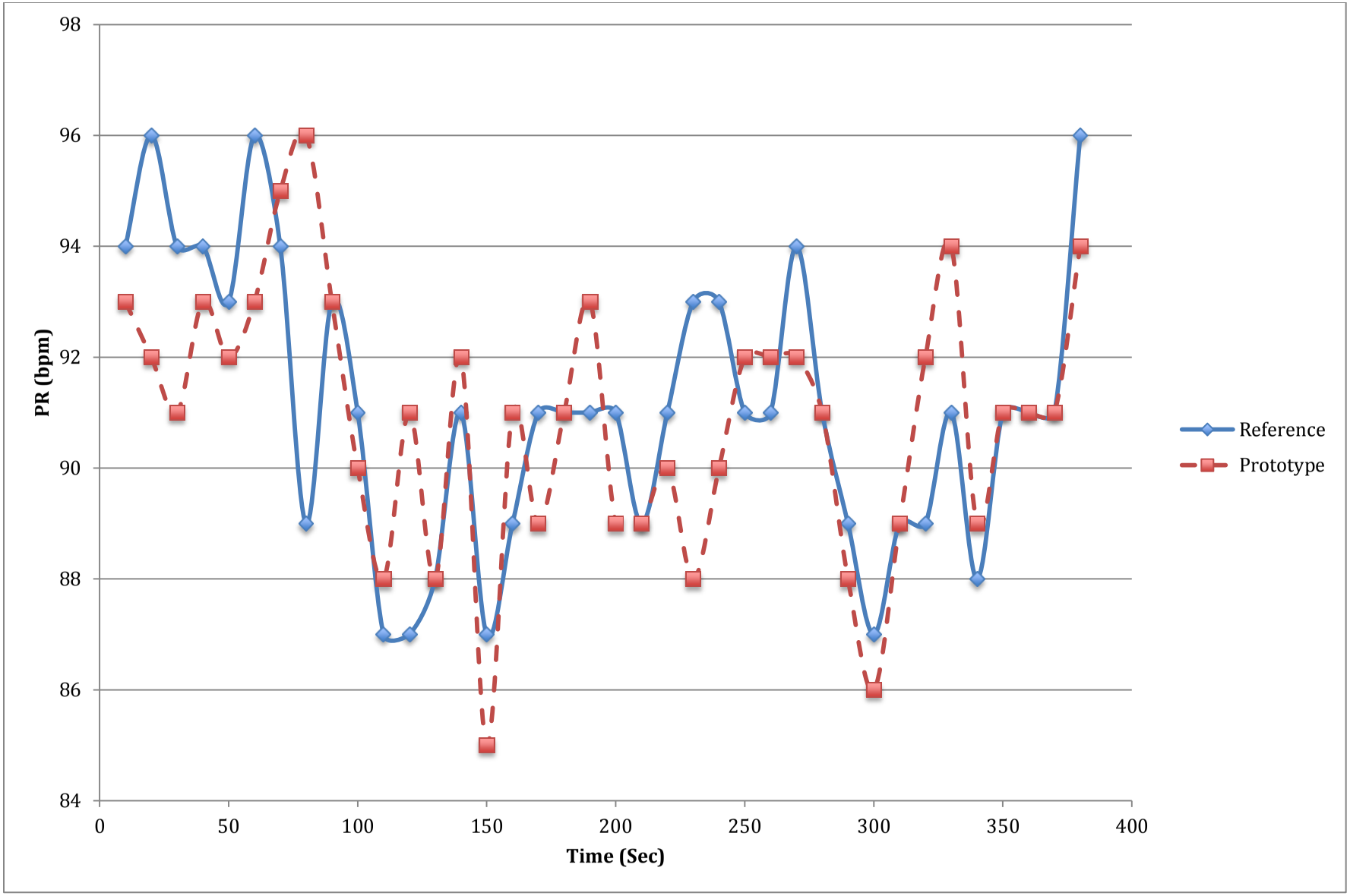

Figure 7.11: Pulse rate measurement validation plot for the chest sitting test

Figures 7.12 and 7.13 display the dynamic response plots for the hyperventilation trials. Both figures display varying PR's for two subjects during the 6 minute measurement period. Plot 1, depicted as Figure 7.12 shows a very high correlation between the prototype and the reference pulse oximeter. This is evident in the proximity of the data points between the prototype and reference pulse oximeter as well as the general trend that the chart follows. However, it was noticed that at 80 seconds, there was an unexplained drop in PR from the 75-80 range to a PR value of 53. The reason for this was believed to be due to corrupted PPG signals during that 10 second duration of measurements. Figure 7.1 shows how a corrupted PPG signal appears. Since our method for calculating PR is by searching for the highest amplitude around a specific frequency, any high frequency noise presented either through ambient light picked up by the sensor or by motion artifacts would slant the power spectrum of the signal which in turn would provide false PR calculations for that interval of data. Figure 7.13 shows similar drops in PR as well due to corrupted PPG signals. One difference observed in Figure 7.13 was that the data were not as closely correlated as in Figure 7.12.

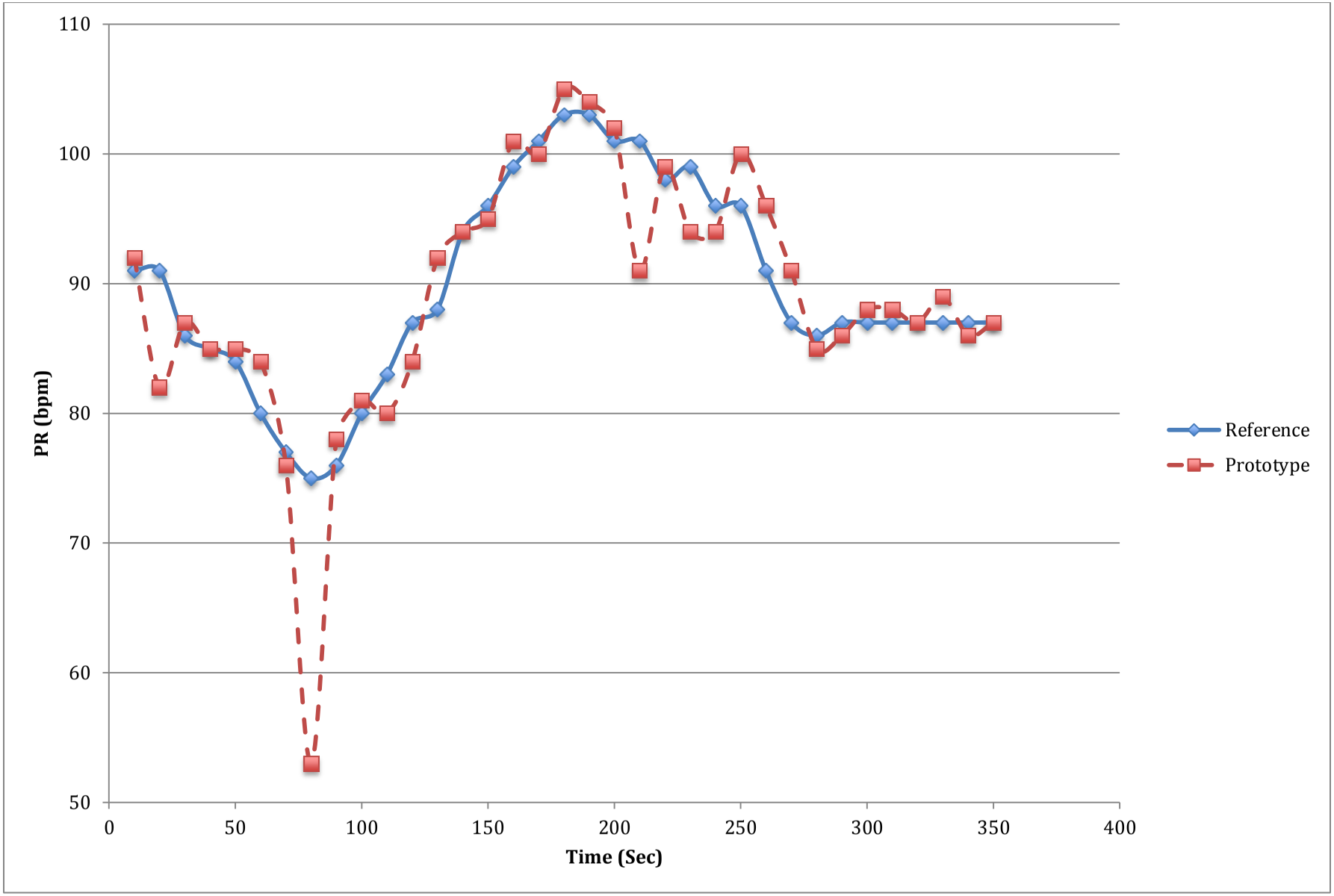

Figure 7.12: Pulse rate measurement validation plot 1 for hyperventilation test

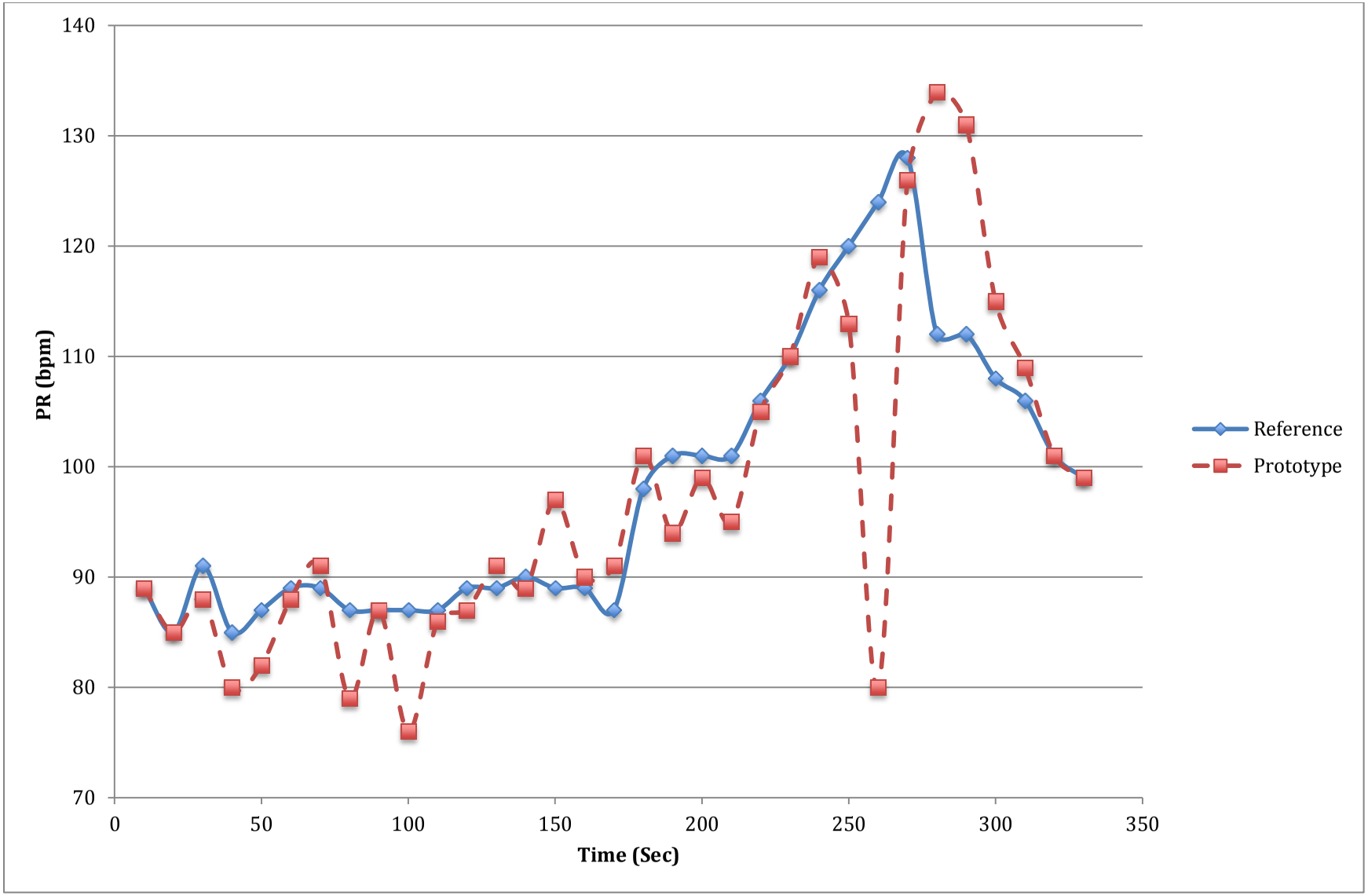

Figure 7.13: Pulse rate measurement validation plot 2 for hyperventilation test

Figures 7.14 and 7.15 depict the PR and SpO_2 measurements during the 6 minute testing period from the wrist as the subject was sitting, respectively. Figure 7.14 shows the prototypes response to changing levels of PR. In general this set of data appears to be very closely correlated and only contains one measurement in which the PR overshoots the reference by about 4bpm. In Figure 7.15 we can observe a small dip at the beginning of the measurements in the SpO_2 but otherwise, the SpO_2 levels stayed constant throughout the entire measurement.

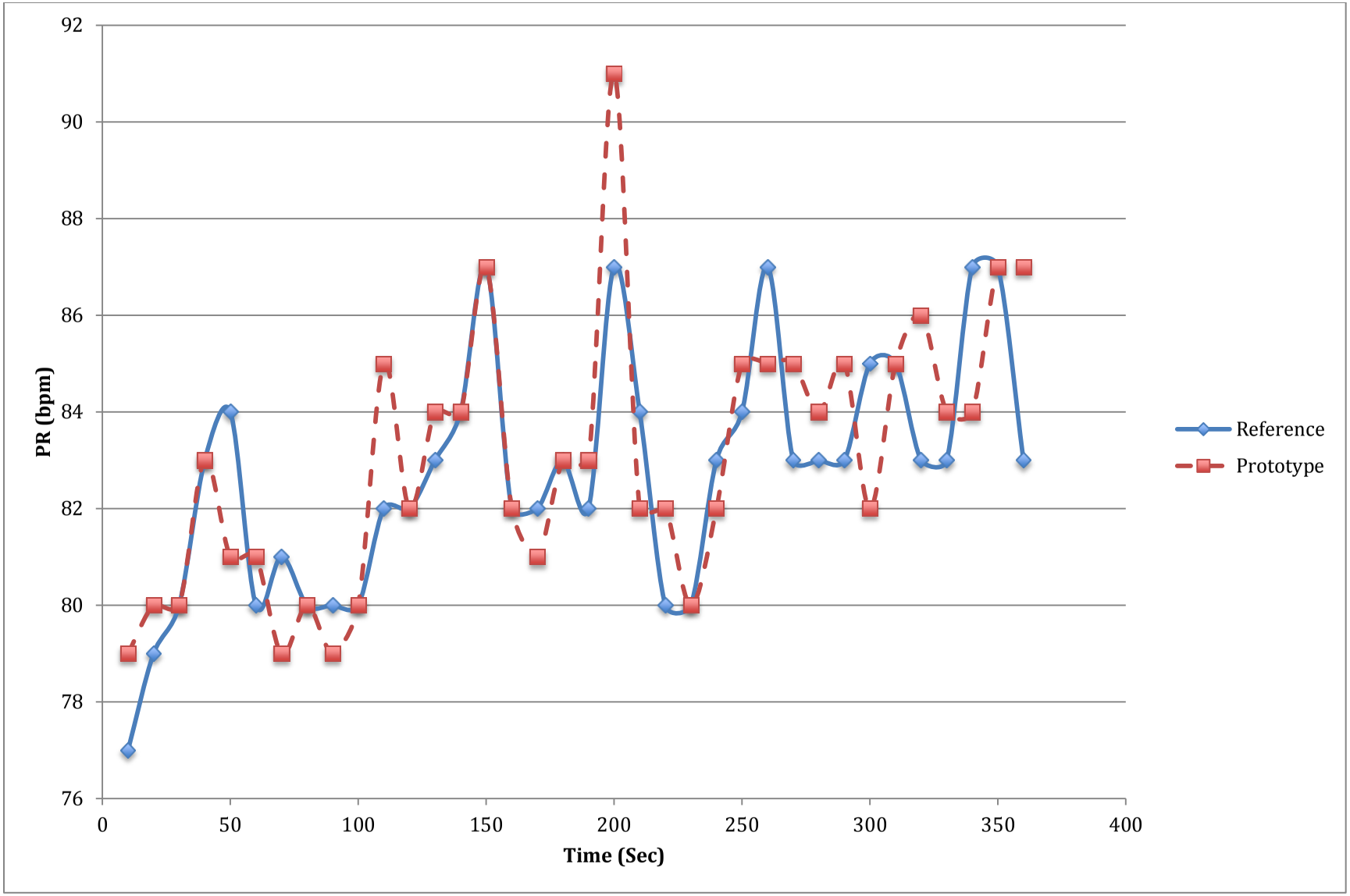

Figure 7.14: Pulse rate measurement validation plot for the wrist sitting test

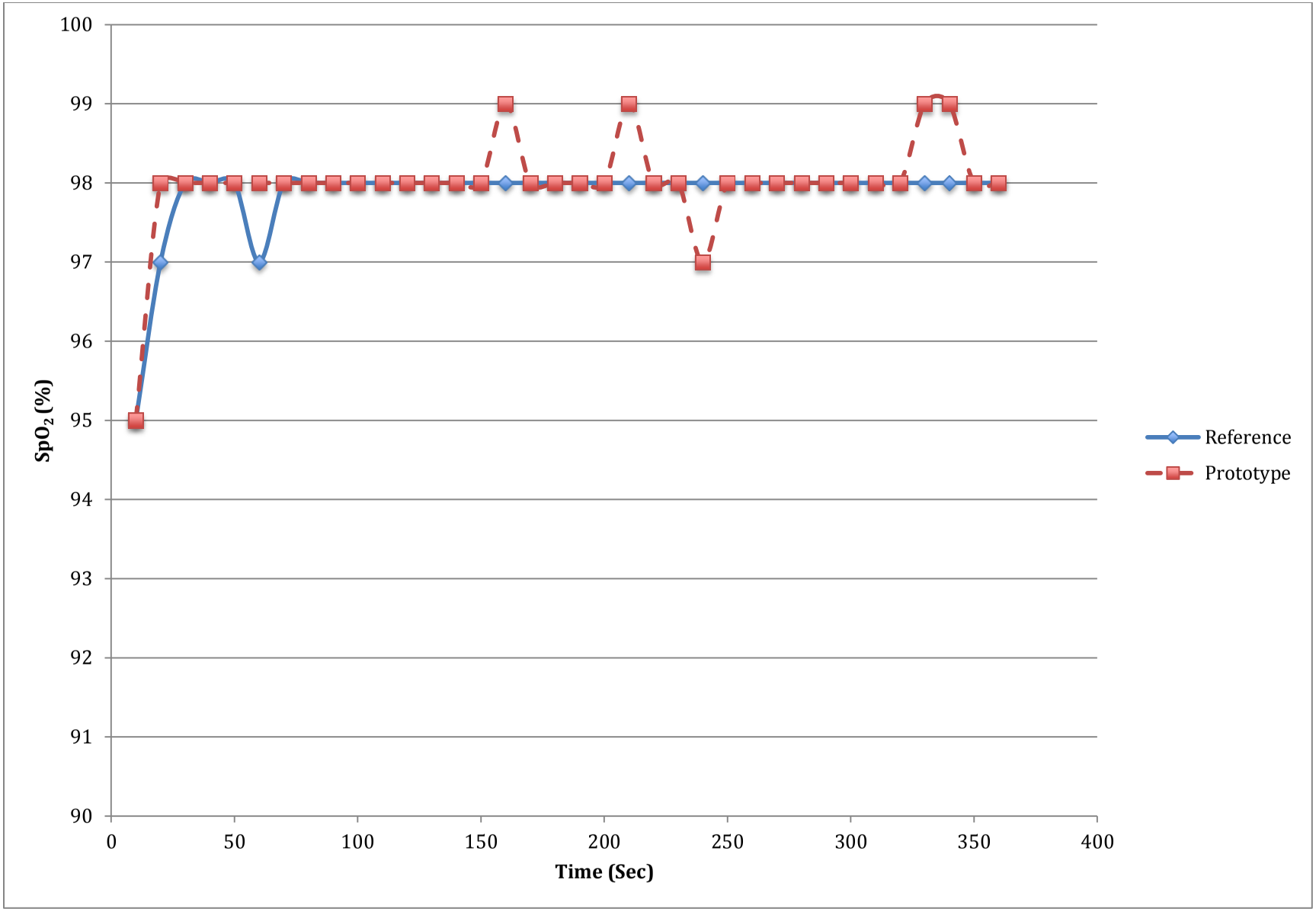

Figure 7.15: Oxygen saturation measurement validation plot for the wrist sitting test

Figures 7.16 and 7.17 depict the SpO_2 and PR measurements during the 6 minute testing period from the wrist as the subject was standing. In Figure 7.16 we observe a constant bouncing of SpO_2 between 98 and 99% for our prototype and a dip in SpO_2 at around 2 minutes into the measurements. Figure 7.17 shows the prototypes response to changing levels of PR while the subject was standing. Apart from two moments of undershooting in which the value displayed on the prototype was lower than the value displayed on the reference device, the rest of the data appeared to be slightly less well correlated than when the subject was sitting.

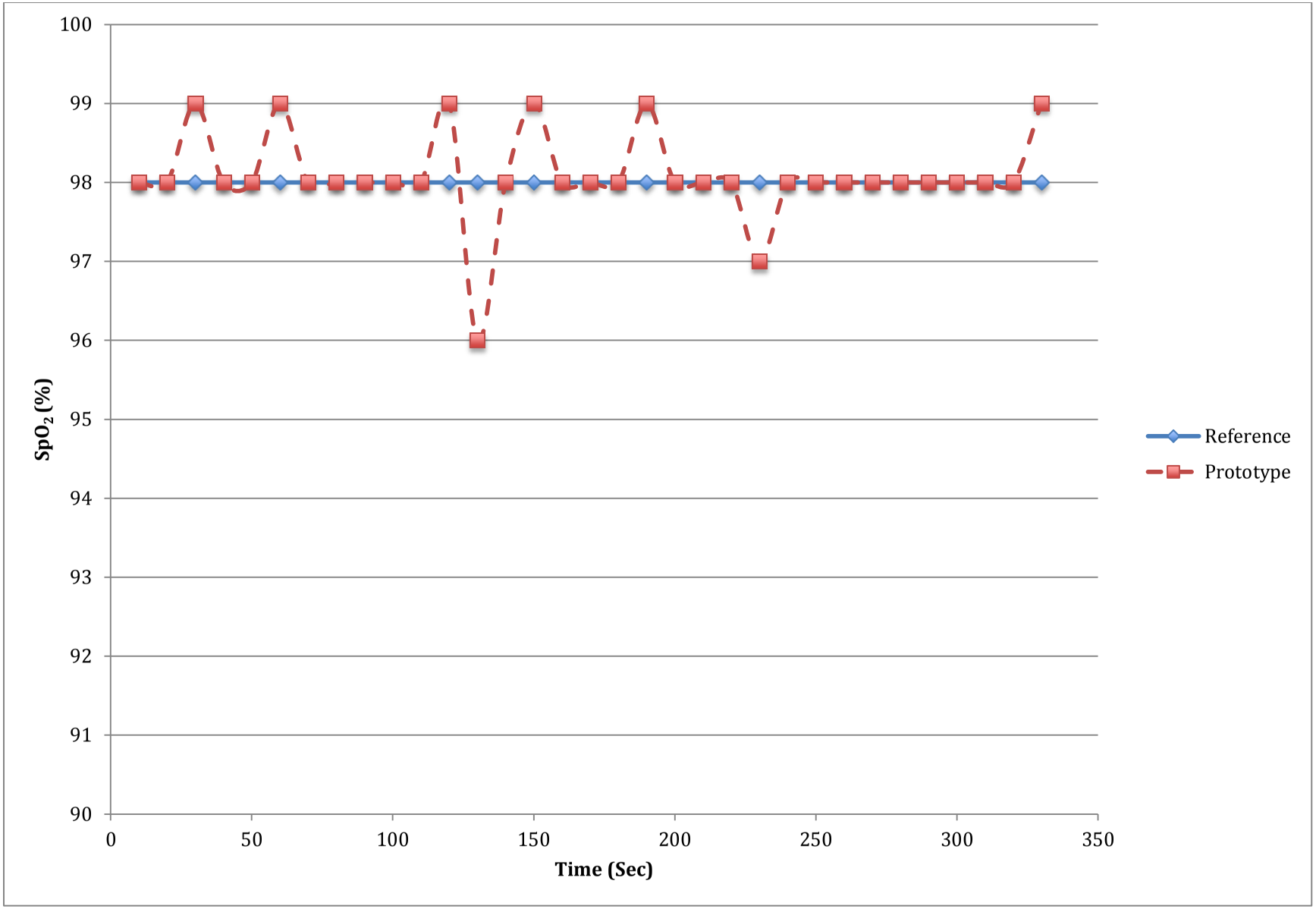

Figure 7.16: Oxygen saturation measurement validation plot for the wrist standing test

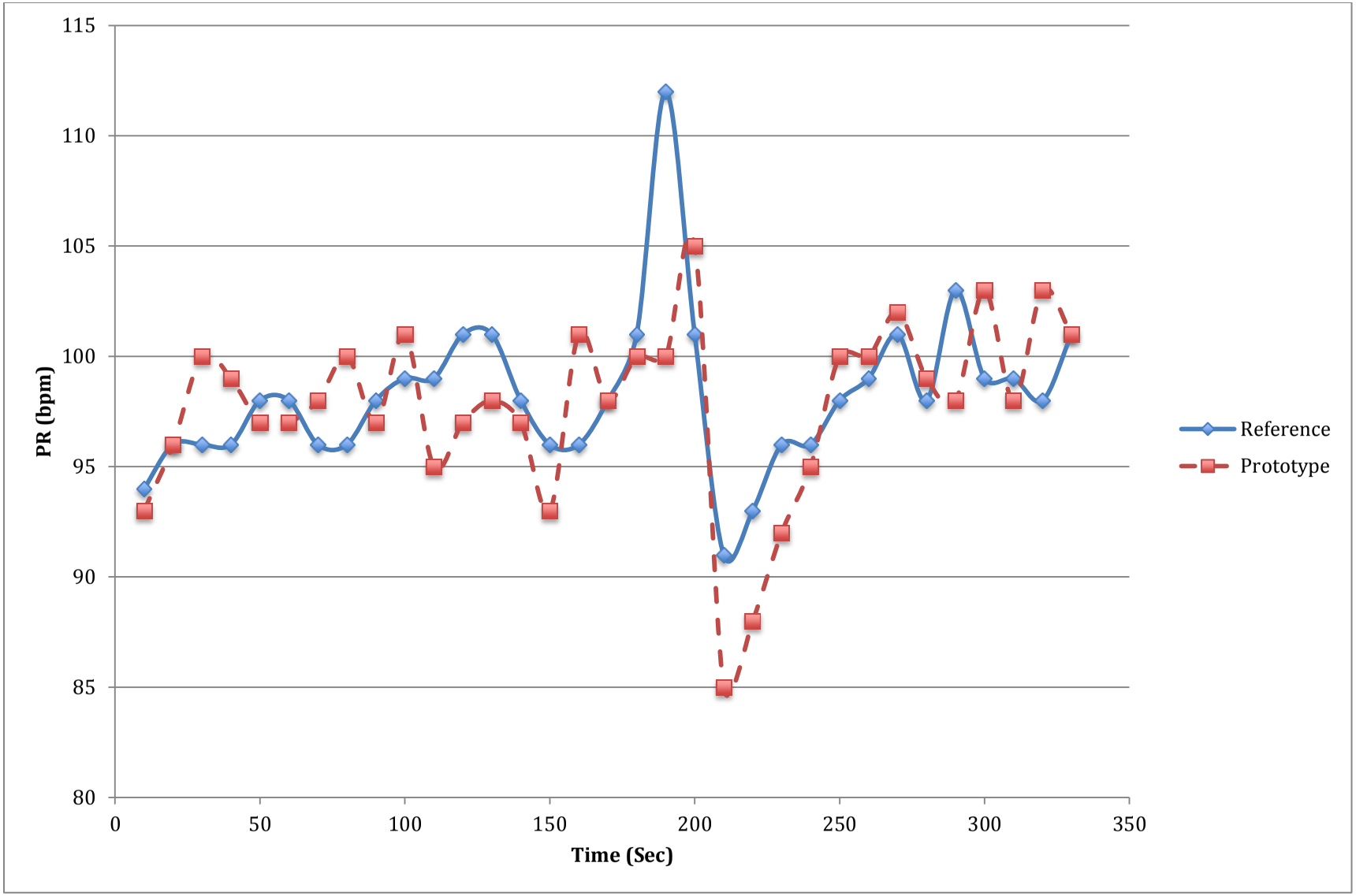

Figure 7.17: Pulse rate measurement validation plot for the wrist standing test

To accurately see how well our device responded to sudden drops in SpO_2 we asked our subjects to hold their breaths for 45 seconds in hopes that a drop in SpO_2 could be observed. Figures 7.18 and 7.19 display two separate plots for induced hypoxia. In Figure 7.18 the moment of induced hypoxia can be observed at around 120-160 seconds in which the SpO_2 dropped from 99 to 91% in the reference pulse oximeter and 97 to 93% for the prototype. While the drop in SpO_2 for the prototype was not as sudden as it was for the reference pulse oximeter, it does in fact validate the claim that our prototype does respond to changing levels of SpO_2. In Figure 7.19 we observe two moments of induced hypoxia, once at 150 seconds and later at 230 seconds. We also observed what appeared to be a delay between our prototype and the reference pulse oximeter when the drops in SpO_2 occurred.

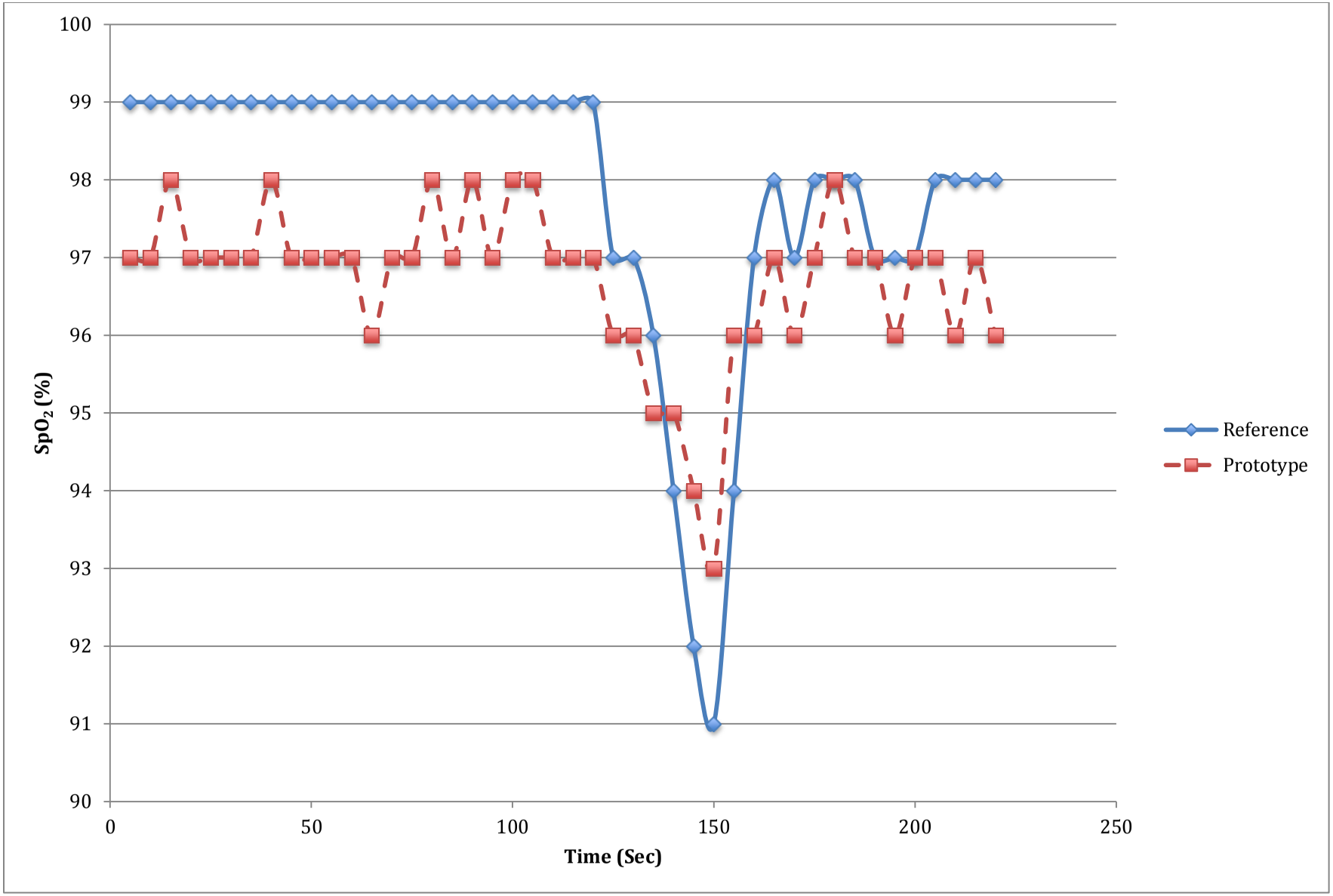

Figure 7.18: Oxygen saturation measurement validation plot 1 for hypoxia test

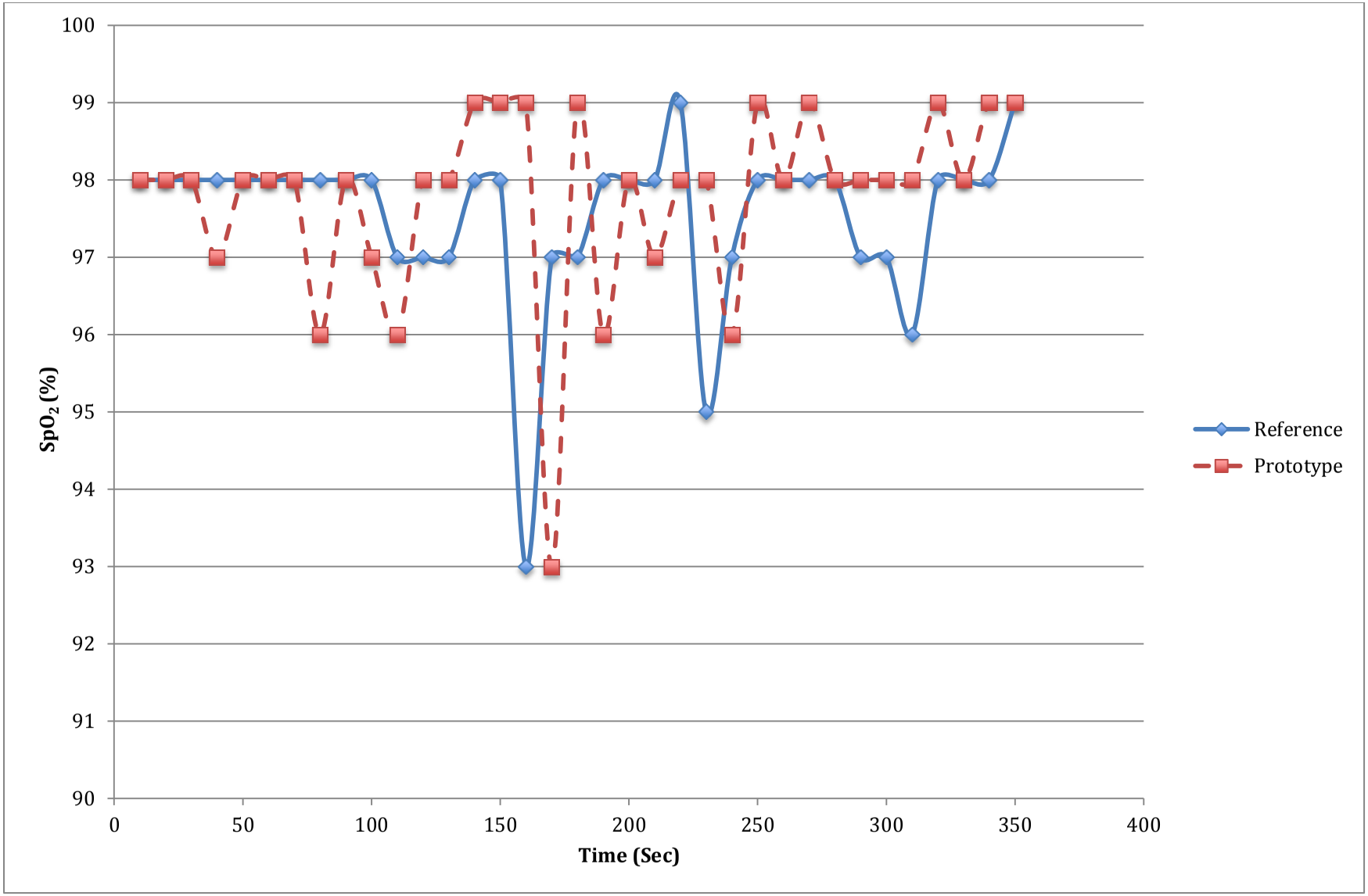

Figure 7.19: Oxygen saturation measurement validation plot 2 for hypoxia test

7.3 Residual Plots

Residual plots were also utilized in analyzing the hypoxia and hyperventilation tests. To graph the residual plots, we calculated the average between the observed measurements from the reference device and our prototype, the difference between each observed measurement, the average of the difference between each observed measurement number, and the standard deviation of the differences. Using these calculations we then plotted the averages of the individual measurements on the horizontal axis and the difference between measurements on the vertical axis. A solid black line was then plotted to represent the average of the differences, and two dashed black lines to represent $\pm$ 2 standard deviations around the average of the difference of measurements. Figures 7.20, 7.21 and 7.22 show the residual plots for the hyperventilation testing. All of these plots show that at least 95% of the data falls within the two standard deviations meaning that the differences between the reference device and the prototype are normally distributed. Although 95% of the data in each figure does fall within the two standard deviations, Figure 7.22 shows the best representation of a high correlation between the reference device and the prototype. Most of the data shown in that plot is much closer to the average of the differences, shown as the black solid line.

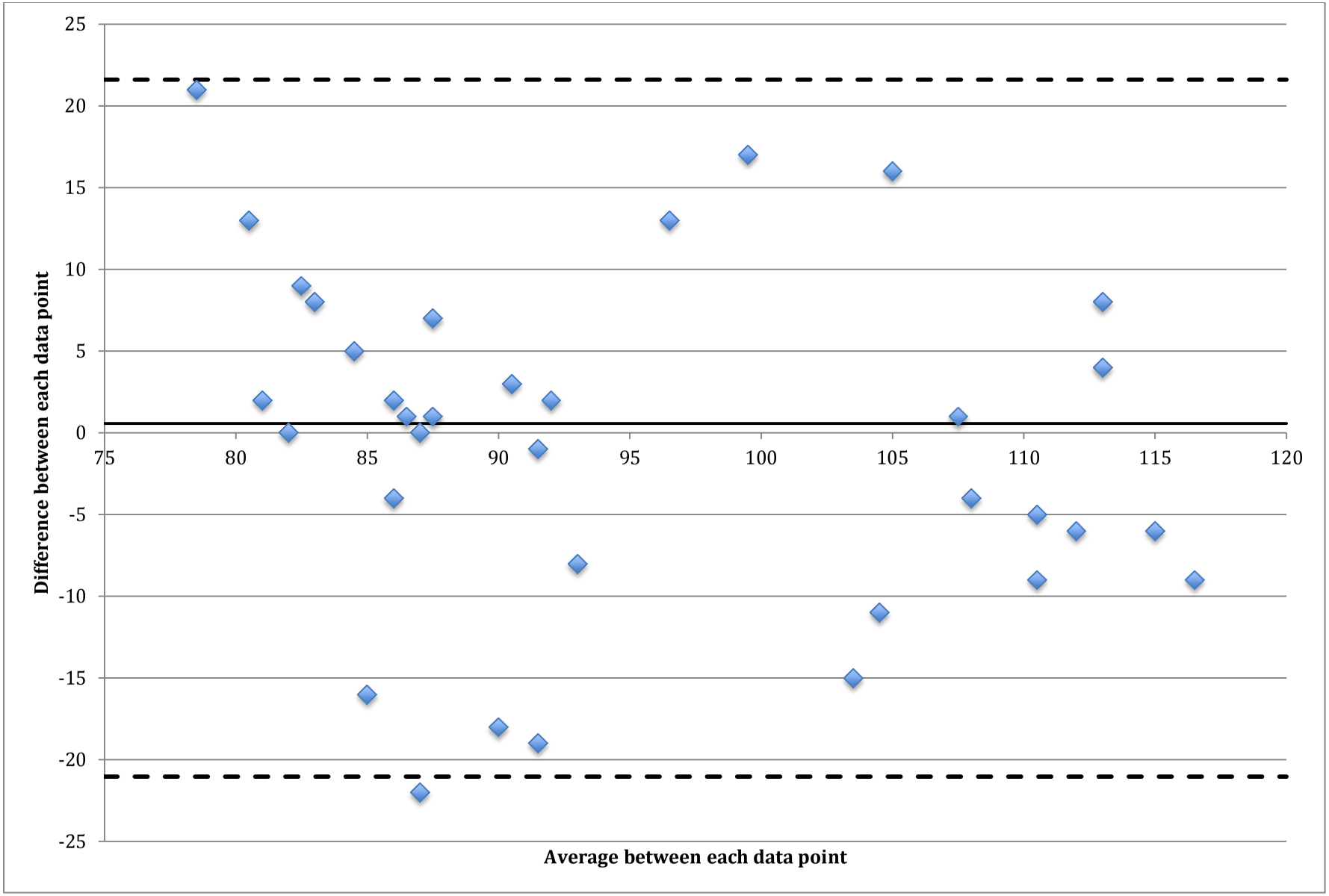

Figure 7.20: Residual plot for hyperventilation testing for data set 1 (dotted lines: ± 2SD, solid line: average of differences)

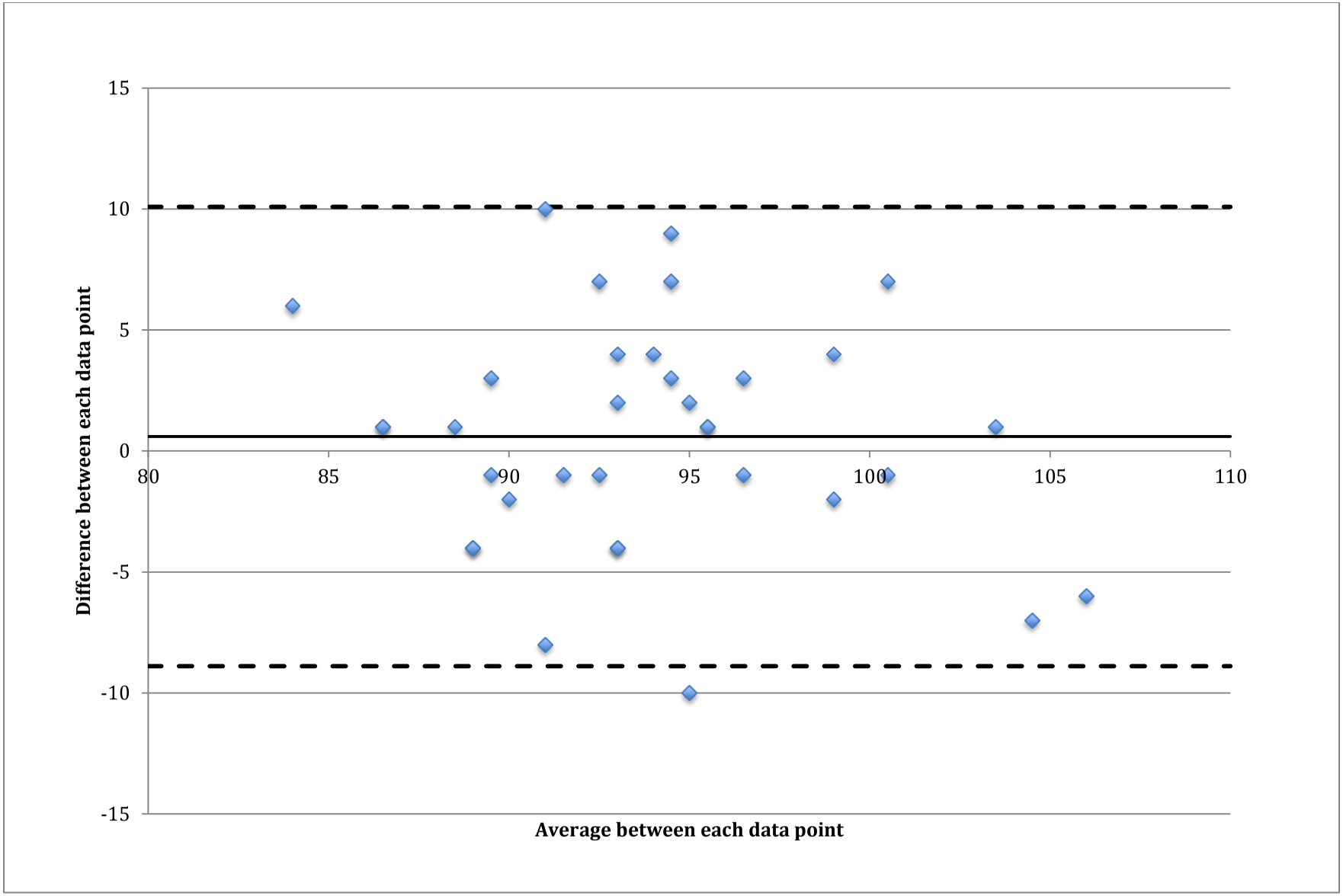

Figure 7.21: Residual plot for hyperventilation testing for data set 2(dotted lines: ± 2SD, solid line: average of differences)

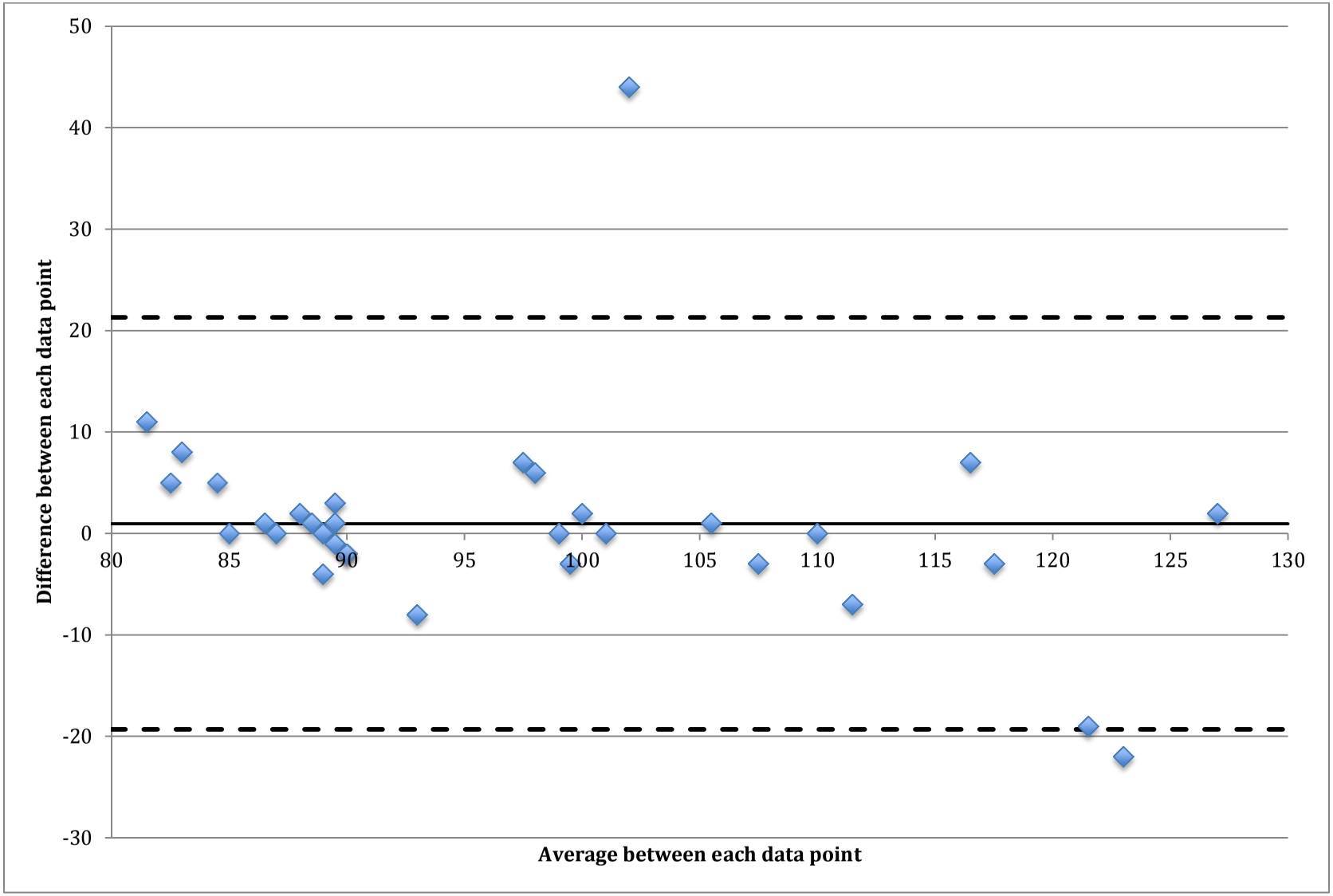

Figure 7.22: Residual plot for hyperventilation testing for data set 3 (dotted lines: ± 2SD, solid line: average of differences)

Figures 7.23 and 7.24 show the residual plots for the hypoxia testing. The data in both plots appear to be slanted to one side due to there not being a large enough SpO_2 range to effectively measure. However, one positive to note from these plots is that the majority of the residuals in both plots appear to fall within two standard deviations of the average difference.

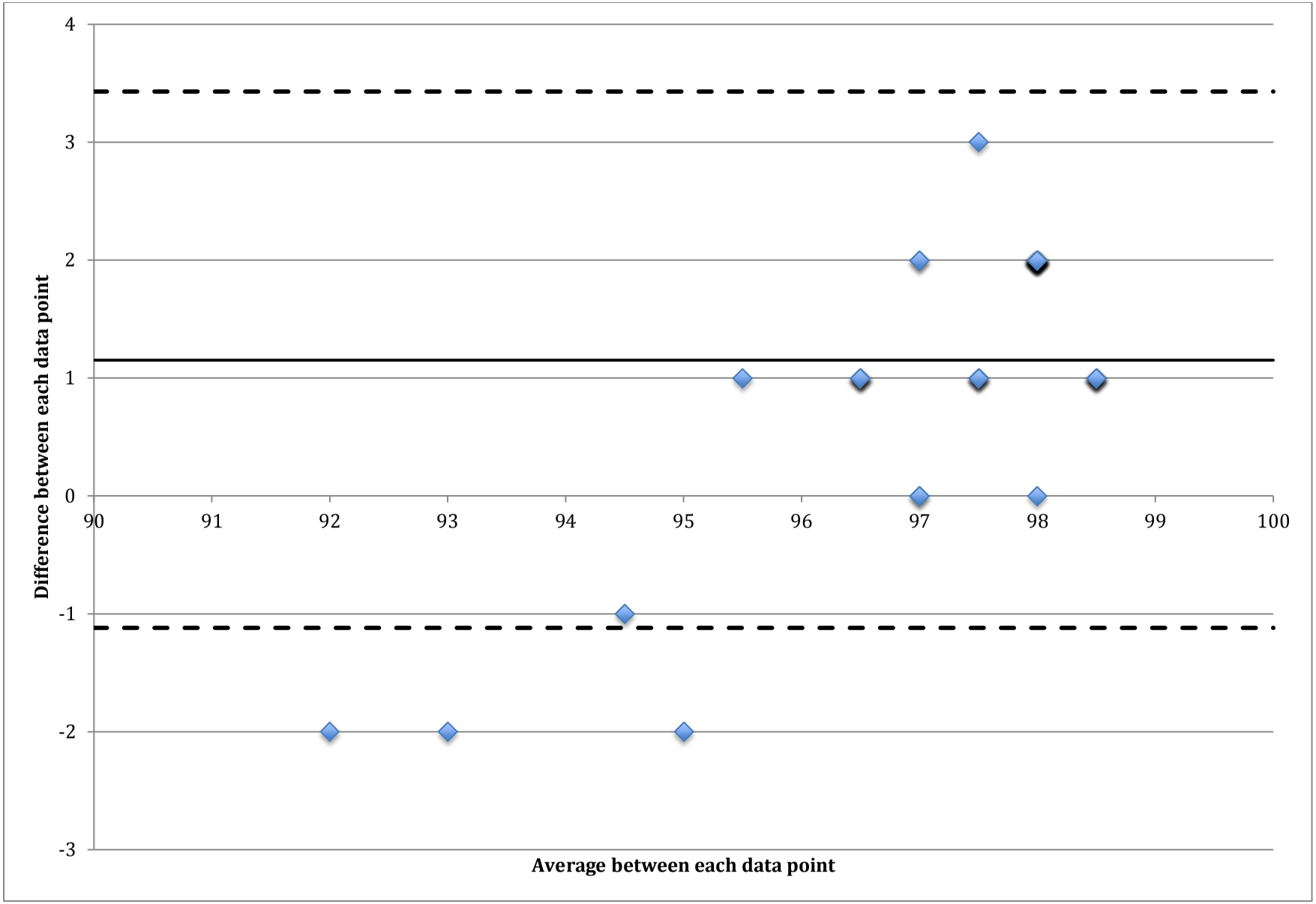

Figure 7.23: Residual plot for hypoxia testing for data set 1 (dotted lines: ± 2SD, solid line: average of differences)

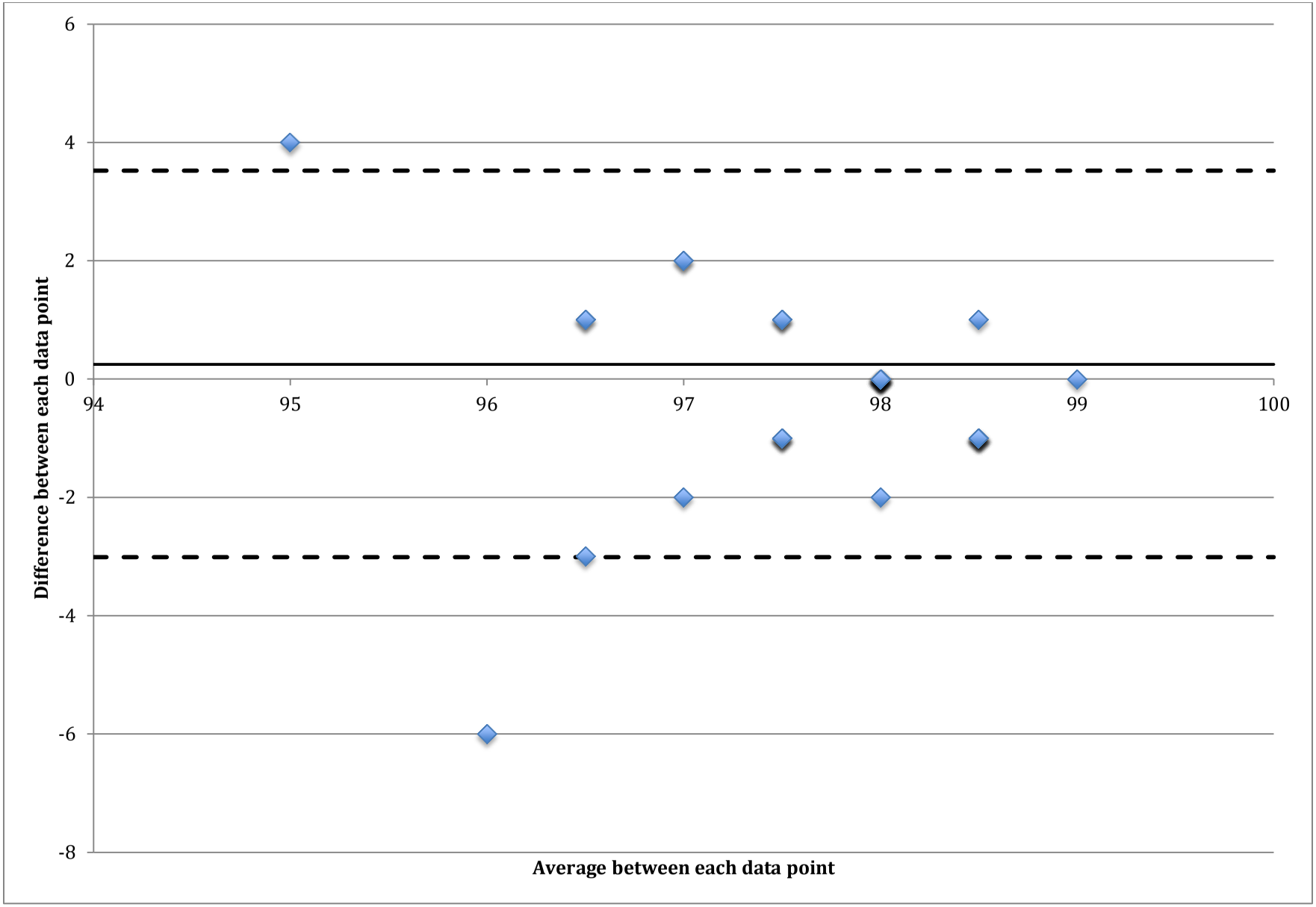

Figure 7.24: Residual plot for hypoxia testing for data set 2 (dotted lines: ± 2SD, solid line: average of differences)

8 Discussion

When creating a device such as a pulse oximeter which requires the acquisition of signals such as PPGs, it is difficult to ensure the integrity of the signals that are acquired. This causes the placement of the sensor on the wrist and chest to be very important. We were able to obtain fairly strong PPGs from the wrist and chest because of the stronger signals due to the high levels of bone and subcutaneous tissues in these locations.

The summarized results suggest that recorded wrist measurements were more accurate than chest measurements. For the standing and sitting measurement tests obtained from the wrist, the errors obtained were 0.6%, and 0.2% for SpO_2 and 0.2%, 1.1% for the PR, respectively. While the measurements from the chest obtained errors of 0.4% and 0.3% for SpO_2 and 0.1%, and 0.7% for the PR, respectively for the same test conditions. There are many factors that could contribute to the difference in the percent errors for the two different locations. When the sensor was placed on the wrist, it was placed over the radial artery which could have given stronger signals as opposed to those gathered from the chest where the sensor was simply placed over the sternum. One factor noticed was when the sensor is placed on the chest, the device became subject to increased motion artifact from breathing. The motion the chest makes when each subject took a breath in some cases moved the device on the skin and could have also prevented it from being in constant contact with the skin. Another factor that could have affected this is the pressure at which the device was strapped on. If there was too much or too little pressure, the signal strength could change, in turn changing the results. For this device to be considered a success, the percent error for all tests must remain at ±3. Although these factors did not affect the accuracy of the device in an extremely negative way as displayed in the results, they were cause for a slightly higher percent error in data taken from the chest. In these cases it was noticed the sensor would allow ambient light to be picked up by the photodetectors. It was observed that when this occurred, the sensor output would completely saturate due to the high amplification we utilized for signal analysis.

The standard tests of standing and sitting while taking measurements from the chest and wrist showed that the prototype could accurately and continuously measure SpO_2 and PR. While the hypoxia and hyperventilation tests demonstrated that the prototype can respond to various SpO_2 and PR measurements respectively. The comparison graphs were used to plot each set of data for each test on one graph together. In these graphs, the reference device was plotted against our prototype to see the correlation between the two. Each different marker corresponds to a different subjects' data taken. The identity line represents a line with a slope of 1. This was useful to plot in the comparison charts because it represents the slope our data is expected to follow when comparing devices as such. The regression line in these plots models the relationship between the reference device and our prototype. In figures 7.2 and 7.3

displaying PR data, the regression line has a slope of .93 and .93 respectively. These slopes show the high correlation between the reference device and our prototype for both the chest sitting and standing results when measuring PR. In figures 7.4 and 7.5 displaying PR data, the regression lines have a slope of .89 and .73 respectively, also showing a high correlation between the reference device and our prototype for the wrist sitting and standing when measuring PR. When testing the devices ability to detect changing PR and SpO_2, the group only took measurements from the wrist. This was decided because of the increased accuracy in the measurements taken from the wrist. Figure 7.6 displays the PR data for the hyperventilation testing. The slope of the regression line here is .88 showing that our device is able to accurately detect changes in PR that would mimic those of exercise. Figure 7.7 displays the SpO_2 data for hypoxia testing. The slope of the regression line here is .33 which would normally indicate that the device does not have a high correlation with the reference device however, because SpO_2's measurements are on such a small scale, even the slightest of discrepancies would cause a big change in the slope of the regression line. It is for examples like this that it was necessary to analyze the data in more than one way and to have more than one form of graphical representation.

The dynamic response plots were used to see the prototypes response to PR and SpO_2 as opposed to the reference devices response over time. Each graph contains a line representing the prototype and a line representing the reference device. While the plots here for the chest while sitting and standing and the wrist while sitting and standing show that the measurements from our prototype remain in close proximity to those of the reference device, the most valuable plots are those done for hyperventilation and hypoxia. Figures 7.12 and 7.13 show that the prototype can react to changing levels of PR as fast as the reference device does and with high accuracy. In figure 7.12 at about 75 seconds in and in figure 7.13 at about 250 seconds there are noticeable outliers in the PR measurement from the prototype. The outliers for each subject went from a regular PR, around 90bpm, to values of about 40 or 50bpm. To verify whether this was due to abnormal PPG data or the software, the PPG data gathered by the VI was re-examined for the specific periods of time in which the outliers occurred. It was discovered that these outliers were primarily due to corrupted PPG data. Figure 7.1 shows a portion of the PPG data with corrupted readings which could be due to motion artifacts introduced by the subject through sudden movements. Another possibility for the corrupted data could be related to the amount of pressure applied to the sensor when it was placed on the subject. Figure 7.18 shows one drop in SpO_2 during induced hypoxia at about 150 seconds while figure 7.19 shows two drops in SpO_2 during induced hypoxia at 160 seconds and at 230 seconds. Both the prototype and the reference oximeter registered the drops in oxygen saturation, though the drop observed by our prototype was less than that of the reference device. This test demonstrated the prototype's ability to detect a decrease in SpO_2 with some degree of accuracy.

Residual plots were used to show by how much the prototype is likely to differ from the reference device. These plots allow us to see if there are any large discrepancies between the reference device and the prototype that would otherwise not be seen in the comparison charts. Figure 7.22 shows one of the residual plots for hyperventilation testing. In this plot we can see that there is not a large difference in the data gathered from the reference device and the prototype as all the data is fairly close to 0 and well within the 2 standard deviation limits showing that our data is normally distributed. Figures 7.20 and 7.21 show the remaining two residual plots for hyperventilation. These two plots show a much larger range of difference between the reference device and the prototype however, 95% of the values are within the 2 standard deviation limits and that the data is normally distributed as well. Figures 7.23 and 7.24 show the residual plots for hypoxia testing. These two plots show that the differences between the reference device and the prototype are very small ranging from a difference of either 1 or 2 and shows that 95% of these data points are also within the 2 standard deviation limit showing that our data is normally distributed.

From the data presented in Table 7.2, the accuracy of the PR measurements ranged in percent error between 3-5% for every single data set. From this it was concluded that while the tone measurements function in LabVIEW is a simple and effective method for calculated PR, it introduces a high degree of error since it is programmed to seek the highest amplitude frequency. For SpO_2 a low percent error was maintained for all the stationary measurements, but there was a decrease in accuracy when the prototype was experiencing changing SpO_2 levels. To ascertain a more precise accuracy for the prototype, further testing should be done in which the SpO_2 levels range from 70-100%.

10 Summary

This project started with the goal of designing and building a wearable reflectance-based pulse oximeter that could measure SpO_2 and PR accurately from the chest and wrist. A literature search was the conducted exploring pulse oximetry theory, application methods, and commercial products. After which, alternative designs for a reflectance-based pulse oximeter were considered. Assessing the benefits of each alternative design, a design consisting of 8 photodiodes positioned concentrically around 2 LEDs, one red and one infrared at wavelengths of 660nm and 940nm, respectively, was selected. In the circuitry, an Arduino Duo microprocessor was used as the LED driver and the logic driver. Sample-and-Hold circuits were utilized to separate the appropriate signals for red and infrared light with analog bandpass filters implemented to isolate the AC component of the PPG waveforms from the DC component. Stages of operational amplifiers were also used to amplify the original signal created by the sensor and amplify the AC signals which were representative of the PPG fluctuations.

The software for this project was developed in the program LabVIEW to further filter the signals and calculate SpO_2 and PR. For the calculation of PR, tone measurement function was used inside of LabVIEW which searches for the highest amplitude signal around a custom set frequency. Expecting the frequency of the range of PRs to lie between 1Hz and 3Hz, the function was set to search around 2Hz with a window of $\pm$ 50%. This method was very effective in calculating the PR frequency and chose to stay with it rather than opting for a peak to peak analysis. The PR frequency was then multiplied by 60 to have the final PR values in beats per minute.

For the calculation of SpO_2 several functions inside of LabVIEW were used to obtain these values. For the AC signals, a function called AC & DC estimator which effectively measured the amplitude of every single amplified PPG fluctuation and then averaged this amplitude over 10 seconds worth off PPG data. To obtain a DC value for both red and infrared signals, the amplitude and level measurements function was used to average 10 seconds worth of data and come up with a constant value for the DC. These methods were found to be satisfactory for calculating the red and infrared AC and DC values due to the small variation in the signal once placed on the skin of an individual. Variations in the signal were only noticeable if the sensor was moved or if the subject moved during testing. For calculating SpO_2, equation 2 was used with variables A= 110 and B = -25. The value for SpO_2 was then normalized so that it is out of 100% and then plotted on a chart as well as having a visual gauge as a reference with a range from 0-100% SpO_2.

Tests were performed using our prototype and a HOMEDICS Deluxe Pulse Oximeter as a reference. For the chest measurements, the sensor was placed directly over the sternum while for the wrist measurements the sensor was worn on the left arm over the radial artery. Depending on the signal

intensity for each subject there were variations in the specific location over the radial artery in which the sensor was placed on to collect measurements. The pressure of the sensor on the skin was adjusted using a Velcro strap which went around the wrist and chest. The testing performed allowed for the collection of measurements from the chest and wrist while sitting and standing. Tests of hypoxia and hyperventilation were also performed to observe the responds of the prototype to changing levels of SpO_2 and PR. Many of the subjects had trouble holding their breaths for the allotted 45 seconds thus the lowest SpO_2 levels observed were 91%. From the gradual increase and decrease of PR, the prototypes response to changing PRs was observed. The VI was set to sample at 25 samples per second for 250 samples each measurement. Every 10 seconds, the VI would display 10 seconds worth of PPG waveforms, as well as the calculated PR and SpO_2 for the last 10 seconds. To maintain the same sampling rate as the prototype, the SpO_2 was also sampled and PR values of the reference pulse oximeter every 10 seconds to coincide with the results picked up by the VI.

Once all of the measurements were taken, the data were analyzed using several different techniques. The averages of each data set were taken for both measurants from which the accuracy of the prototype to that of the reference pulse oximeter was calculated and comparative graphs were created. Regression lines were also calculated and plotted for each set of measurements and compared to an identity line with a slope of 1 and a y-intercept of 0.

The hypoxia and hyperventilation measurements demonstrated how the device would perform with changing SpO_2 and PR levels. To this effect, dynamic response graphs were plotted for each measurement. For the hypoxia and hyperventilation tests, respective prototype and reference pulse oximeter SpO_2 values over time were plotted. Induced hypoxia resulted in lowered levels of SpO_2 and showing a similar response in both the prototype and the reference pulse oximeter. During hyperventilation, rising PR on each subject were observed with the prototype and reference pulse oximeter. Lastly, residual plots were also created for the hypoxia and hyperventilation tests to investigate how our device differs from the reference device. This was accomplished by calculating the difference between the prototype and reference pulse oximeter for each measurement.

11 Conclusion

Based on the experimental results derived several conclusions can be drawn. Through the testing performed on the prototype pulse oximeter we observed that it is in fact possible to measure SpO_2 and PR from the wrist and chest with a reasonable level of accuracy. The SpO_2 measurement contained an error of less than $\pm$1% and the PR measurements less than $\pm$4%. However the prototype does still need some improvement to increase the accuracy of the PR. Though simple to implement, the algorithm currently being used in calculating PR did not provide the level of accuracy required for a FDA regulated commercial device.

12 Future Improvements

While the hardware and software components of this project met the project goals in that they were able to measure PR and SpO_2, there are several improvements we could make in the future for the device to meet industry standards. One aspect of the hardware construction which we never really tackled was designing a PCB model. For the purposes of our project it was simpler to use a breadboard since adjustments were constantly being made with the hardware components to test different settings and for troubleshooting. A factory fabricated PCB board would give us the possibility to start planning for portability and how the device could be attached to the patient. While our design for this project involved a separate module for the LED and photodiode sensor from the actual circuitry, it could be possible to integrate everything in one board once a PCB design is fabricated. A PCB design would allow us to use smaller components in the circuit and minimize the size of the sensor as well as the accompanying circuitry.

Another future improvement which could be implemented is the use of a National Instruments LabVIEW embedded microcontroller. This would not only minimize the amount of components used in the circuitry but would also remove our prototypes dependency on being connected to a desktop PC running LabVIEW in order for the device to work. An embedded microcontroller would allow us to add an LCD display which could show both SpO_2 and PR to the patient. Another benefit for using an embedded microcontroller would be that circuit designs such as the Sample-and-Hold and the bandpass filters would no longer be necessary as analog components since these functions can be programmed digitally in LabVIEW.

The hardware casing should also be redesigned to be not only more aesthetically pleasing but also fully wireless so that it can be worn anywhere. Currently as it stands, our prototype is fairly bulky and requires a constant connection to a desktop PC. Weight is also an issue since the enclosure for our circuitry is an aluminum box with dimensions of 5” x 3” x 3”. We feel that with the development of a PCB design, the overall size requirement for the casing would also dramatically decrease. Another aspect of the casing we would like to see changed is using a hard polymer shell instead of an aluminum box. A plastic casing would be easier to design in any modeling software and would be more easily manufactured with the use of molding techniques. Current developments in 3D printers with plastics would also make a plastic casing an easier option for manufacturing.

To make the device fully portable, wireless connectivity should be considered for future improvements. Wireless connectivity, whether through WIFI, Bluetooth or NFC would not only remove from the user the burden of having wires running through the body but would also provide easier access of SpO_2 and PR measurements. Although battery consumption might be an issue, a wireless pulse oximeter would be more user friendly and increase mobility for the user. The possibility of being able to

display these measurements on any smartphone or other portable wireless devices is another advancement that could make this device increasingly valuable for patients and clinicians.

References

(1) Mendelson, Y. “Pulse Oximetry.” Wiley Encyclopedia of Biomedical Engineering (2006): vol. 5. Hoboken, NJ: John Wiley & Sons, Inc. Print.

(2) Pole, Yash. "Evolution of the Pulse Oximeter." International Congress Series 1242 (2002): 137-44. Print.

(3) "Hemoglobin." Encyclopædia Britannica. Encyclopædia Britannica Online Academic Edition. Encyclopædia Britannica Inc., 2012. Web. 15 Sep. 2012. <http://www.britannica.com/EBchecked/topic/260923/hemoglobin>.

(4) Brinkman R., Zijlstra W.G., and Koopmans R.K, “A Method For Continuous Observation Of Percentage O2 Saturation In Patients,” Arch. Chir. Neerl. 1 (1950): 333 - 444. Print.

(5) Mendelson, Y., and B. D. Ochs. "Noninvasive Pulse Oximetry Utilizing Skin Reflectance Photoplethysmography." IEEE transactions on bio-medical engineering (1988): 35, 10, 798-805. Print.

(6) Mendelson, Duckworth, and Comtois. “A wearable reflectance pulse oximeter for remote physiological monitoring.” Conference Proc. IEEE Engineering Medical Biology Soc. (2006): 1:912-5. Print.

(7) Santa Medical. Finger pulse oximeter SM-110 with carry case and neck wrist cord.

(8) Mendelson, Y., et al. "Design and Evaluation of a New Reflectance Pulse Oximeter Sensor." Medical instrumentation 22.4 (1988): 167. Print.

(9) Shelley K. and Shelley S., “Pulse Oximeter Waveform: Photoelectric Plethysmography,” Clinical Monitoring, Carol Lake, R. Hines, and C. Blitt, Eds.: W.B. Saunders Company, (2001): 420-428. Print.

(10) Shelley K. H., Jablonka D. H., Awad A. A., Stout R. G., Rezkanna H., and Silverman D. G., “What Is the Best Site for Measuring the Effect of Ventilation on the Pulse Oximeter Waveform?” Anesth Analg, (2006): vol. 103, 372-377. Print.

(11) Reisner A, Shaltis. P. A., McCombie D., and Asada, H. H., “Utility of the Photoplethysmogram in Circulatory Monitoring, Anesthesiology,” Anesthesiology, (2008): vol. 108, pp. 950-958. Print.

(12) Nogawa, M., Kaiwa, T., and Takatani, S., "A Novel Hybrid Reflectance Pulse Oximeter Sensor With Improved Linearity And General Applicability to Various Portions of the Body," Engineering in Medicine and Biology Society, (1998). Proceedings of the 20th Annual International Conference of the IEEE, vol.4,.1858-1861.

(13) Tilakaratna, Prasanna. "Pulse Oximeter." Equipmentexplained.com. N.p., n.d. Web. 15 Sept. 2012. <http://www.equipmentexplained.com/physics/respi_measurements/oxygen/oximeter/pulse_oximeter .html>.

(14) Dresher RP, Mendelson Y., “Reflectance Forehead Pulse Oximetry: Effects of Contact Pressure During Walking.” Conf Proc IEEE Eng Med Biol Soc. (2006); 1: 3529-32.

(15) Mardirossian, G., and Schneider R. E.. "Limitations of Pulse Oximetry." Anesthesia Progress 39.6 (1992): 194-6. Print.

(16) Cocker, B., Leung J., Cohen C., Goska B., Albright R., House S., and Chiang P.. "Wearable, Wireless Reflectance-Sensing Pulse Oximeter." (2012): 2017-020.

(17) "Neonatal Pulse Oximetry Archives Tag Archive for Baby Heart Screening- Newborn Heart Defect Screening." *Baby Heart Screening Newborn Heart Defect Screening*. N.p., n.d. Web. 23 Apr. 2013.

(18) Online Courses: Medical Equipment Technology, Support and Management. N.p., n.d. Web. 23 Apr. 2013.

(19) Anliker et al. “AMON: A Wearable Multiparameter Medical Monitoring and Alert System.” IEEETrans Inf Technology Biomedical (2004): (4) 415-27. Print.

(20) Mendelson, Y., and M. J. McGinn. "Skin reflectance pulse oximetry: In vivo measurements from the forearm and calf." Journal of Clinical Monitoring and Computing 7.1 (1991): 7-12.

(21) Respironics. WristOx™ Ambulatory Finger Pulse Oximeter.

(22) Crucial Medical Systems. Oled cms50d fingertip pulse oximeter and oxygen meter.

(23) Mendelson Y. and Pujary. “Photodetector Size Considerations in the Design of a Noninvasive Reflectance Pulse Oximeter for Telemedicine Applications.” IEEE Xplore, (2003): 148-149. Print.

(24) Schreiner, C., Catherwood, P., & Anderson, J. “Blood Oxygen Level Measurement with a Chest-Based Pulse Oximetry Prototype System.” Computing in Cardiology (2010). Print.

(25) Li, K., & Warren, S. “A Wireless Reflectance Pulse Oximeter with Digital Baseline Control for Unfiltered Photoplethysmograms.” IEEE Transactions on Biomedical Circuit and Systems (2010). Print.

Appendix A: Description of LabVIEW

Discussed below are the functions used in the construction of the program that was used in this study.

While loop is a structure that allows for the continuous sampling of input signals and the application of the diagrams placed within it.

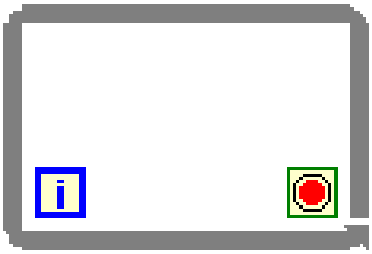

Figure A.1: While loop

When placed in the block diagram, the DAQ assistant launches creating a new task. The task was to identify the signal provided by the external DAQ and set sampling parameters. The task can be edited by double-clicking the DAQ assistant. For continuous measurement a while loop should be placed around the DAQ assistant.

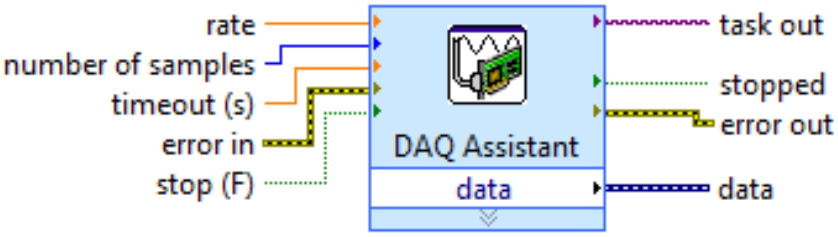

Figure A.2: DAQ Assistant

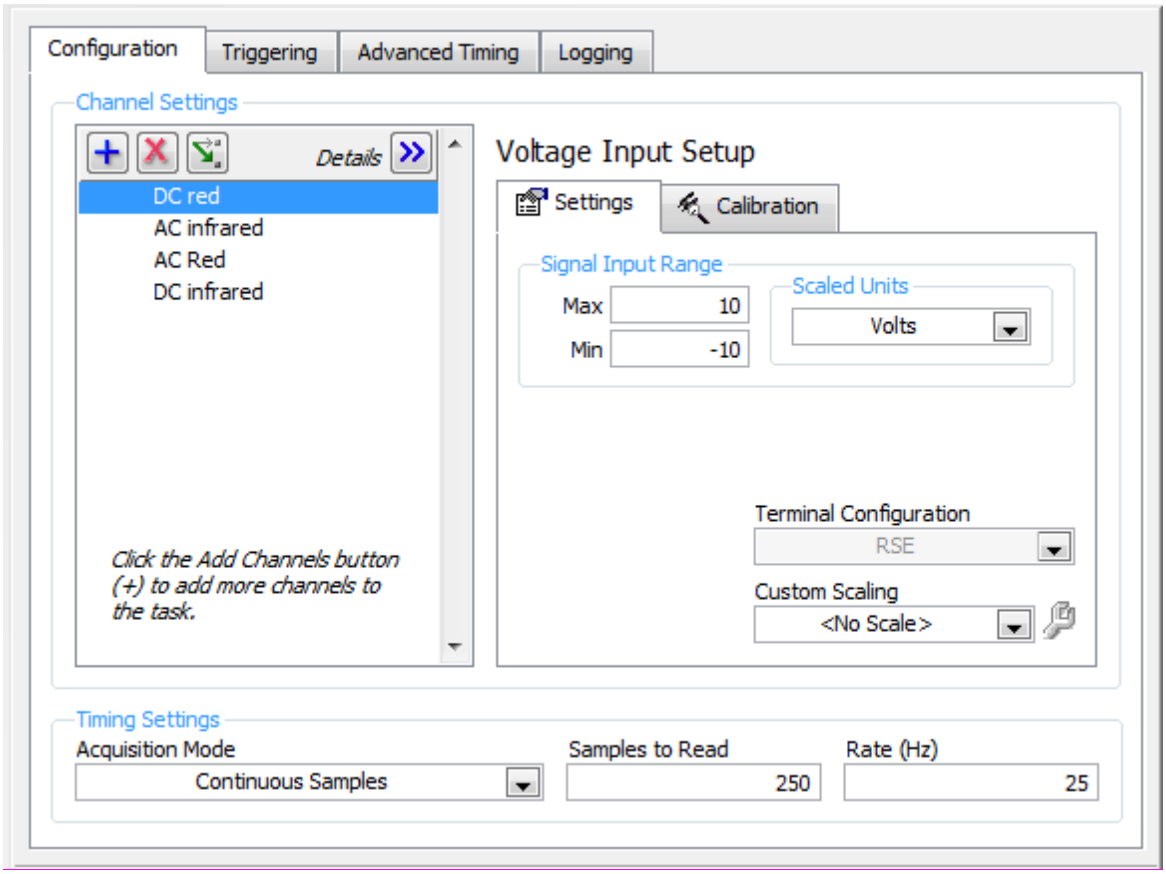

Figure A.3: DAQ assistant task

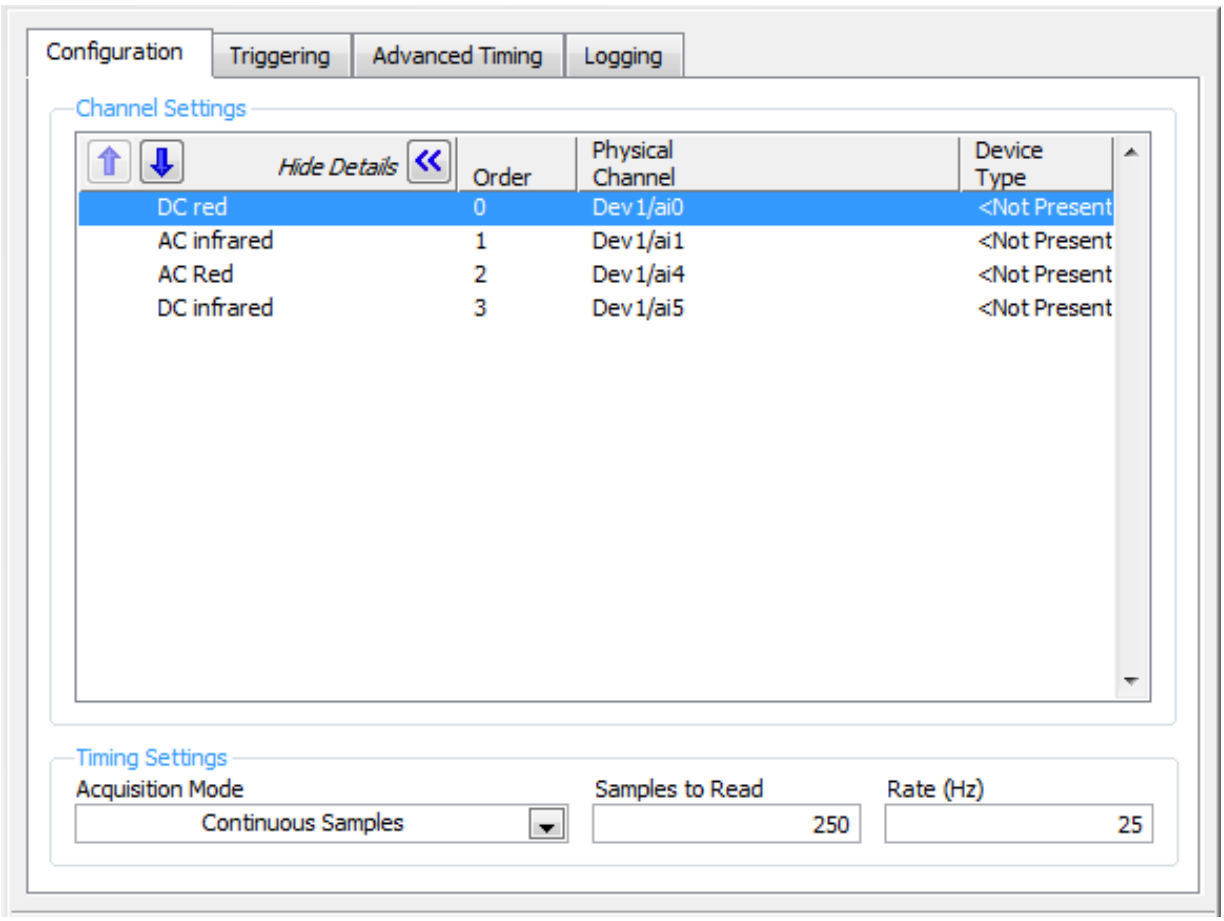

Figure A.4: DAQ assistant task with open details

Select signals accepts multiple signals as inputs and returns only the signals selected allowing the user to specify which signals to include in the output.

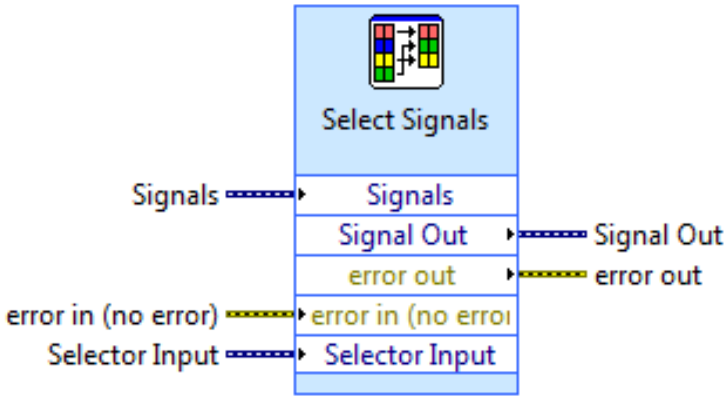

Figure A.5: Select signals

The filter function filters a signal using an infinite impulse response or finite impulse response filter which removes or attenuates unwanted frequencies from a signal using various standard filter types and

topologies continuously. In this instance the Chebyshev filter was used because Chebyshev filters minimize the error between the idealized and the actual filter characteristic over the range of the filter.

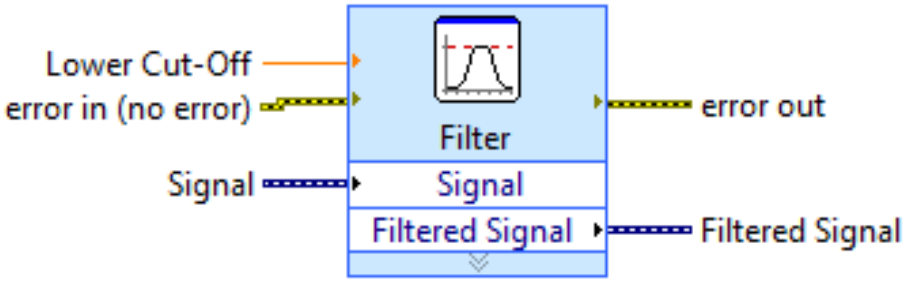

Figure A.6: Filter function

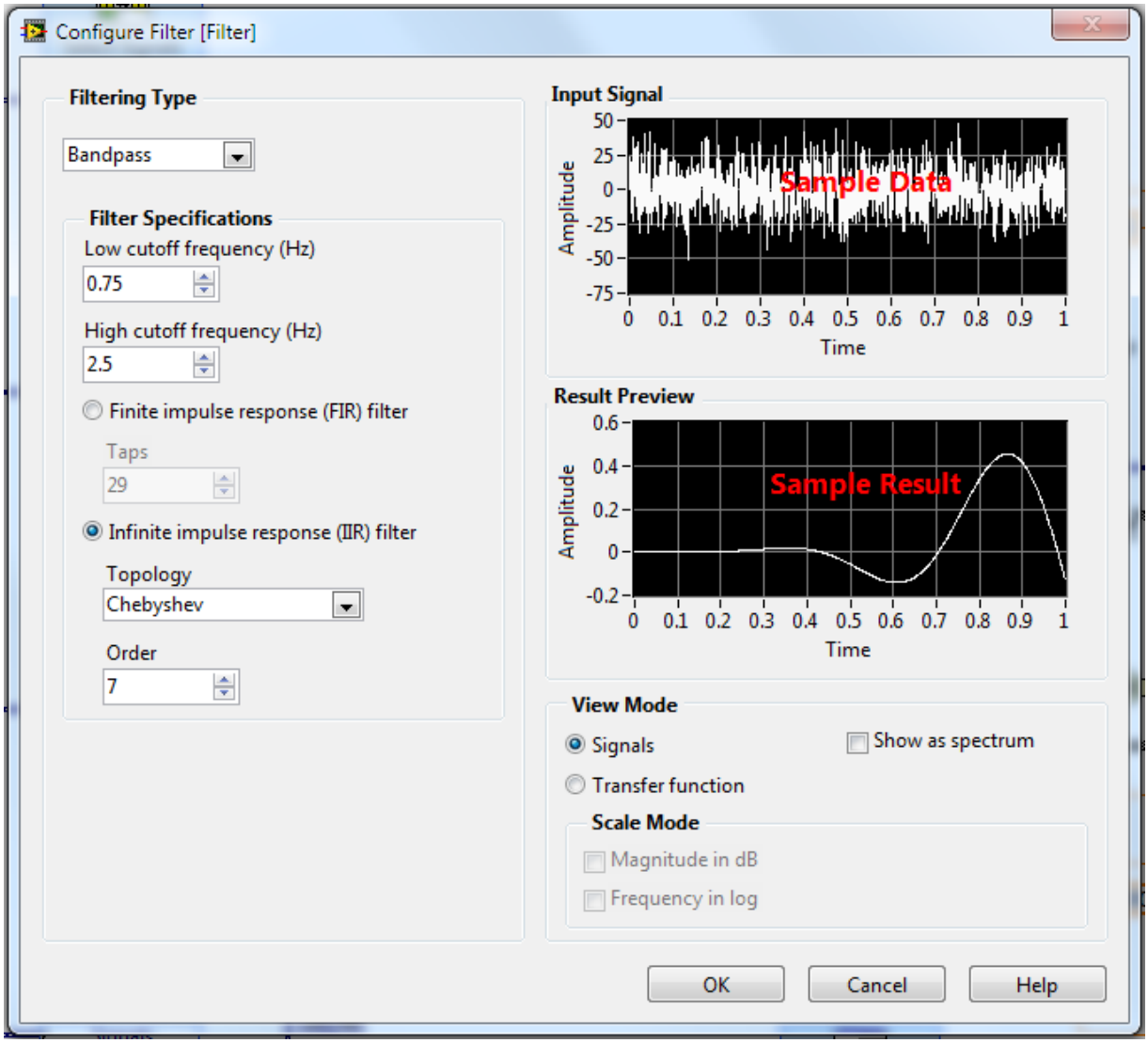

Figure A.7: Filter function parameters

The *tone measurements* function finds the signal with the highest amplitude or searches a specified frequency range to find the single tone with the highest amplitude and also can find the frequency and phase. In this instance, this function is used to find frequency.

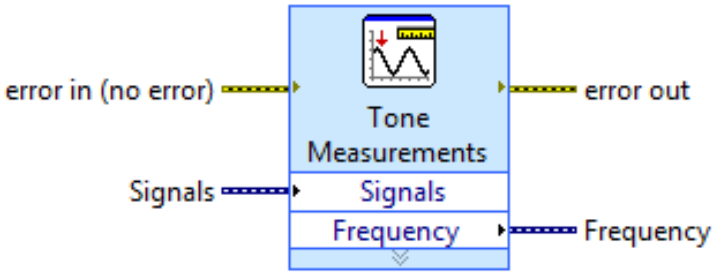

Figure A.8: Tone measurements function

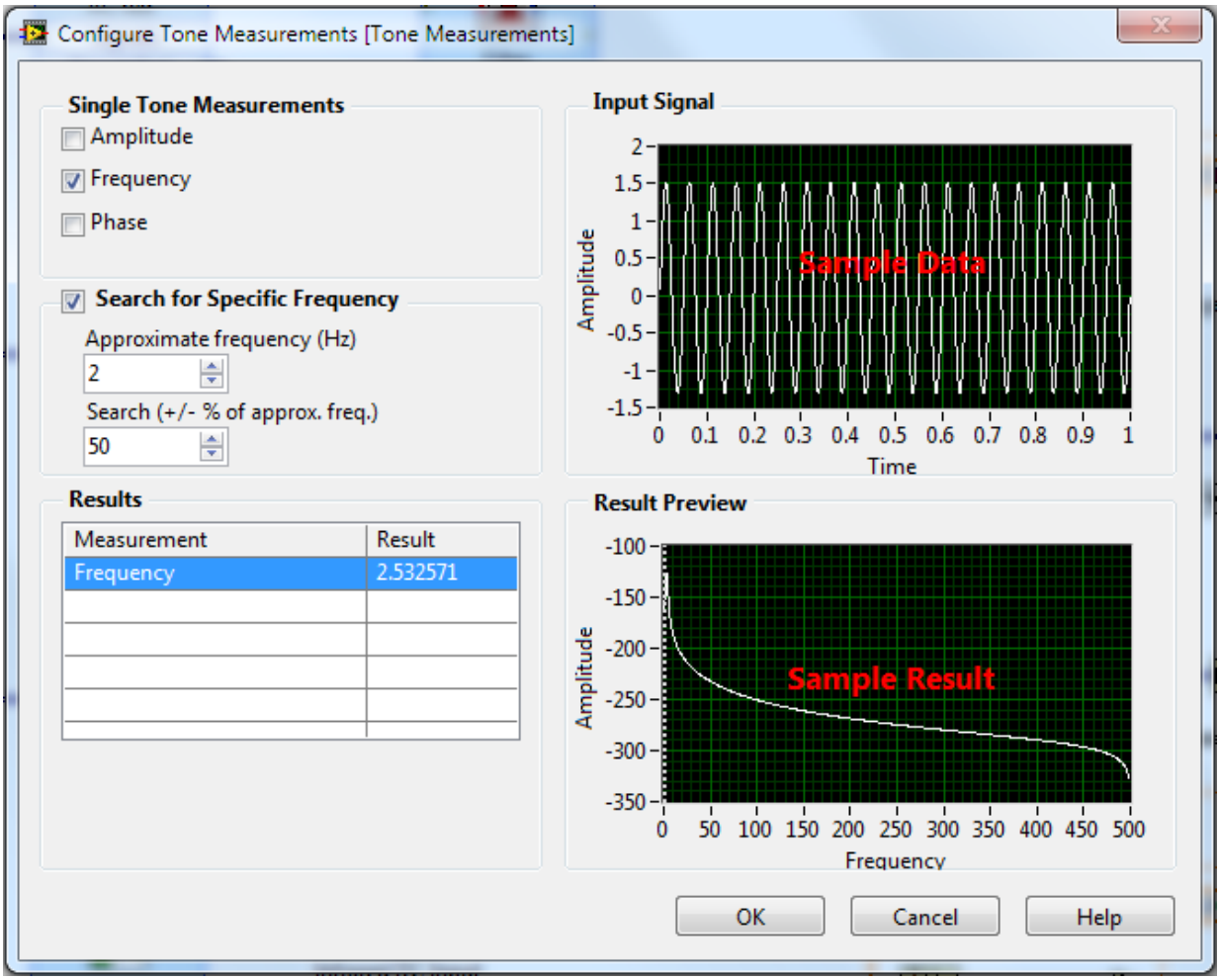

Figure A.9: Configuration of the tone measurements function

Amplitude and level measurements performs voltage measurements on a signal, such as an average of the DC component of the signal, the maximum peaks, and the mean level of one complete period of a periodic input signal.

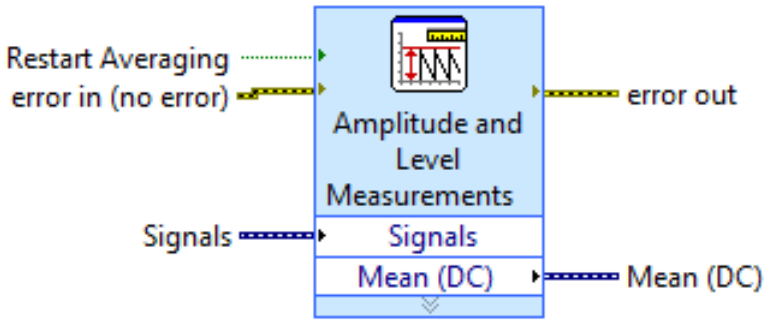

Figure A.10: Spectral measurement function

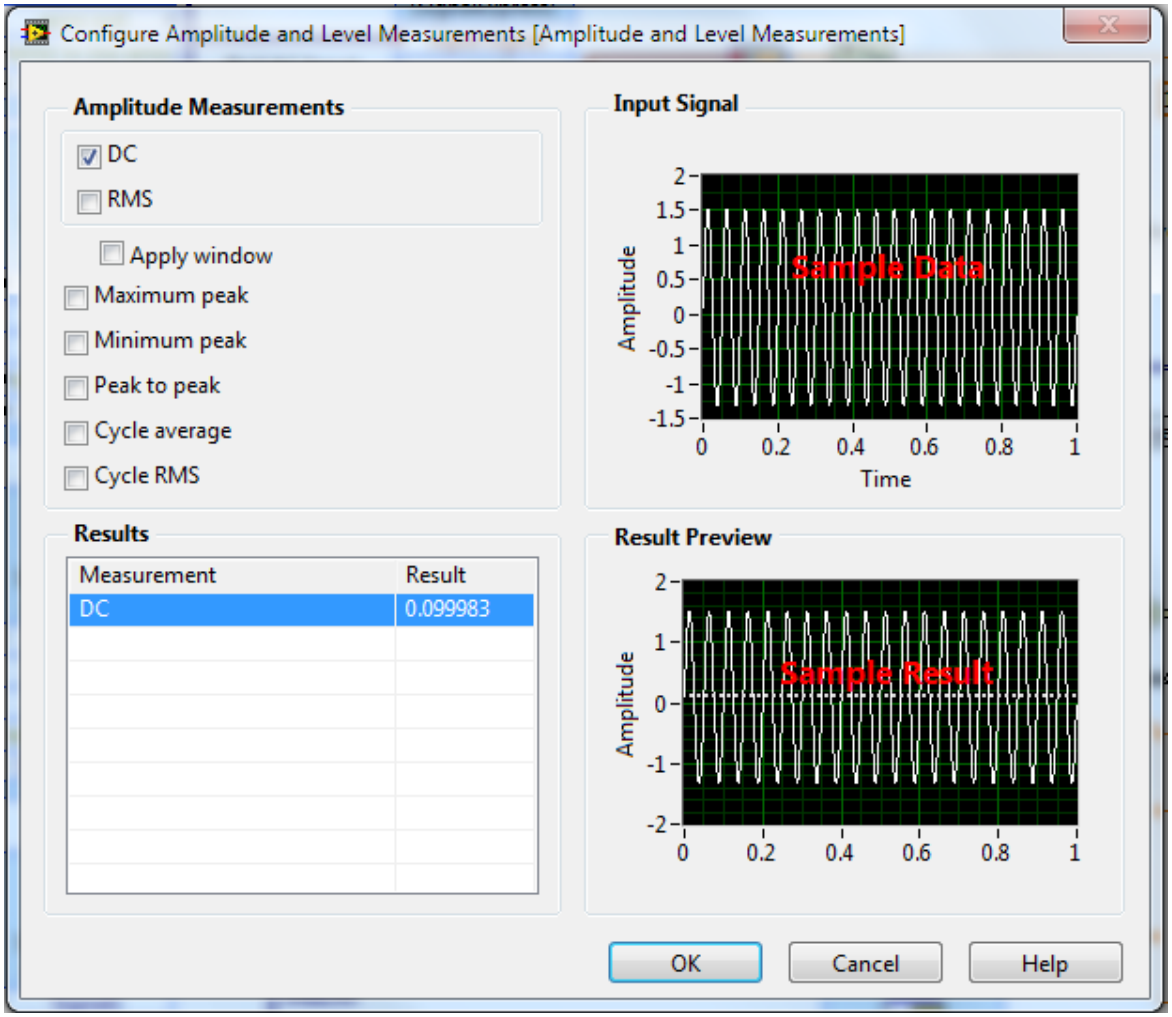

Figure A.11: Configuration of the spectral measurements

The AC&DC estimator.vi applies the Hanning window, which separates most of the AC energy from the DC bin, allowing the estimation the AC and DC levels of the input signal.

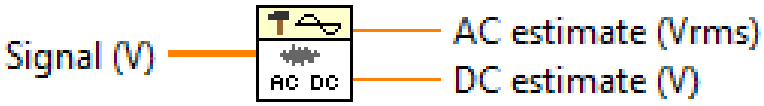

Figure A.12: AC & DC estimator.vi

Divide computes the quotient of the inputs.

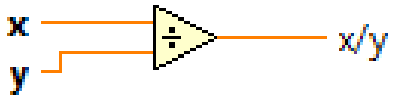

Figure A.13: Division

Round to nearest integer rounds the input to the nearest integer. If the value of the input is midway between two integers, the function returns the nearest even integer.

Figure A.14: Round to nearest integer

Multiply returns the product of the inputs.

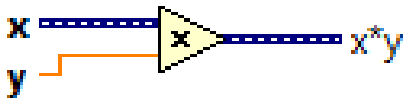

Figure A.15: Multiply

Add computes the sum of the inputs.

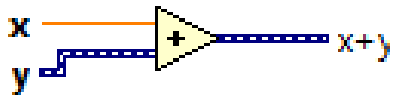

Figure A.16: Add

The *greater than function* returns TRUE if x is greater than y and returns FALSE if y is greater than x.

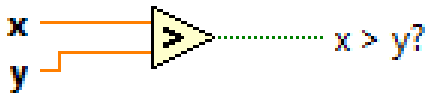

Figure A.17: Greater than function

The *less than function* returns TRUE if x is less than y and returns FALSE if y is greater than x.

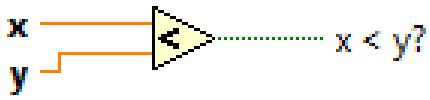

Figure A.18: Less than function

The *and function* computes the logical AND, meaning if both inputs are TRUE, the function returns TRUE and otherwise it returns FALSE.

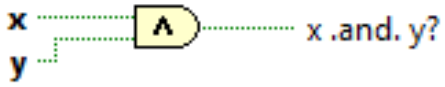

Figure A.19: And function

Case structure has multiple sub diagrams, or cases, with only one case executing when the structure executes. The execution can be controlled by wiring a value to the case structure which will determine which case to use.

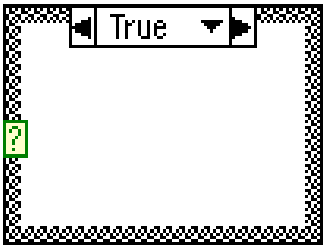

Figure A.20: Case structure

Above is the *numeric indicator* that displays values continuously. The image on the left represents the function in the block diagram while the image on the right represents the function in the front panel that displays the commuted values.

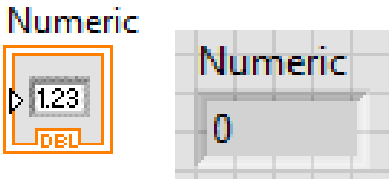

Figure A.21: Numeric indicator (left: block diagram, right: front panel)

The *gauge indicator* is a continuous numeric indicator. The image on the left represents the function in the block diagram while the image on the right represents the function in the front panel that displays the commuted values.

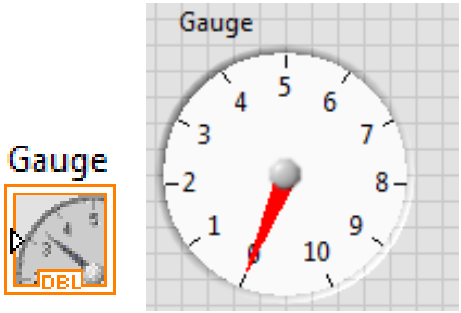

Figure A.22: Gauge indicator (left: block diagram, right: front panel)

Waveform graph is a graphic indicator that evenly plots sampled measurements. The image on the left represents the function in the block diagram while the image on the right represents the function in the front panel that graphs the commuted values.

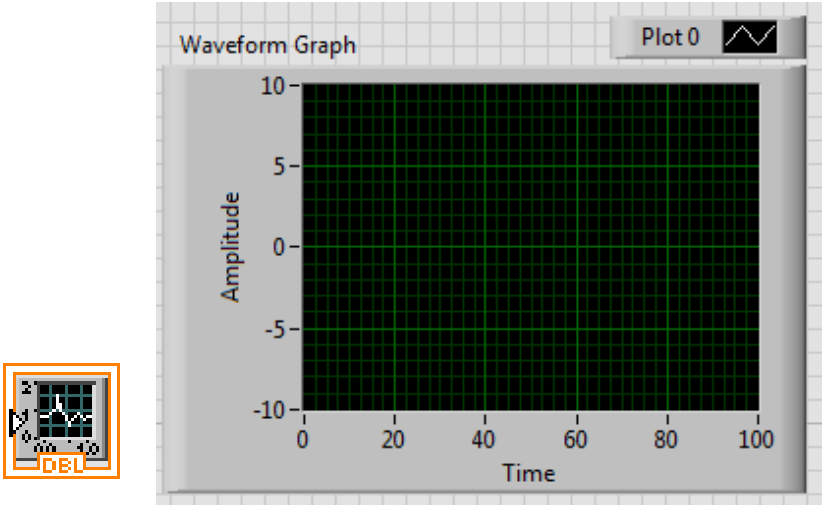

Figure A.23: Waveform graph (left: block diagram, right: front panel)

Waveform chart is a numeric indicator that plots data at a constant rate and maintains a history of the data. The image on the left represents the function in the block diagram while the image on the right represents the function in the front panel that graphically records the commuted values.

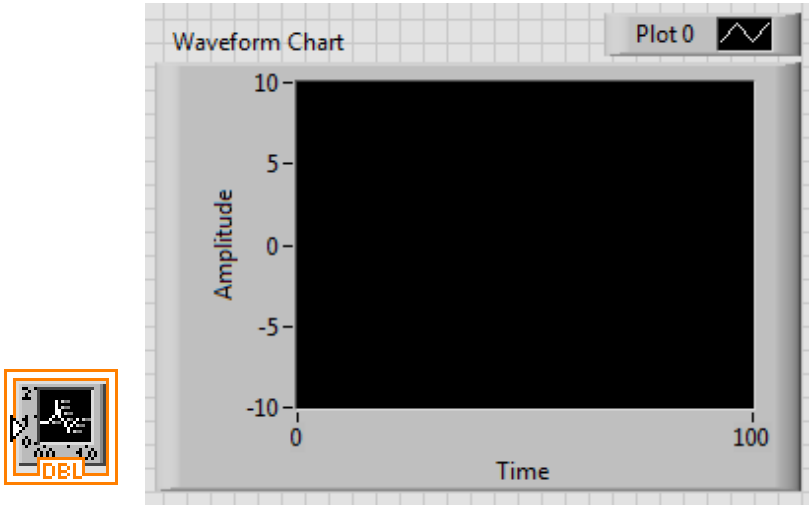

Figure A.24: Waveform chart (left: block diagram, right: front panel)

Appendix B: Bill of Materials

Item	Vendor	Part Number	Quantity	Price
Photodiodes	Allied Electronics	BPW34	8	$18.80
940nm Infrared LED	Radioshack	276-143	1	$2.49
660nm Red LED	Radioshack	55050641	1	$1.44
Round Fiberglass Copper Boards	Radioshack	276-004	1	$5.49
Bread Board	Radioshack	276-003	1	$9.99
LF398LN	Mouser	LF398N/NOPB	2	$3.08
LM348 Quad Op-Amp	Obtained from BME Lab		3	$1.99
Velcro Strap	Home Depot	90340	1	$9.27
Aluminum Box Enclosure	Radioshack	270-238	1	$3.49
Double sided tape	Home Depot	285189	1	$6.97
Arduino Duo Microcontroller	Radioshack	276-128	1	$29.99
			SUM	$93.00

Appendix C: Data Sets

Table C.1: Sitting chest data set

Subject 1 Sitting Chest				Subject 2 Sitting Chest				Subject 3 Sitting Chest				Subject 4 Sitting Chest			
Reference Oximeter		Prototype		Reference Oximeter		Prototype		Reference Oximeter		Prototype		Reference Oximeter		Prototype	
SpO2	PR	SpO2	PR	SpO2	PR	SpO2	PR	SpO2	PR	SpO2	PR	SpO2	PR	SpO2	PR
98	62	99	65	98	94	98	93	97	92	99	88	98	80	96	92
98	60	99	63	98	96	98	92	98	94	99	99	98	80	98	82
98	59	99	60	98	94	99	91	97	90	96	92	98	83	98	85
98	60	99	60	98	94	99	93	98	93	95	91	98	86	98	87
98	61	99	61	98	93	99	92	98	94	95	94	98	87	98	88
98	60	99	62	98	96	98	93	97	91	95	94	98	87	98	87
98	60	99	64	98	94	98	95	97	93	96	93	98	87	98	86
98	63	99	63	98	89	98	96	97	93	95	94	98	85	98	86
98	64	99	63	98	93	98	93	97	91	95	93	98	87	98	85
98	61	99	64	98	91	99	90	97	91	96	92	98	91	98	89
98	65	99	63	98	87	99	88	98	96	96	94	98	87	98	88
98	68	99	64	98	87	98	91	98	98	95	94	98	89	98	91
98	65	99	68	98	88	98	88	97	96	94	94	98	91	98	87
98	61	99	63	98	91	98	92	97	94	95	97	98	83	98	89
98	58	99	61	98	87	98	85	97	99	95	62	98	87	98	88
98	60	99	59	98	89	98	91	97	97	98	101	98	82	98	81
98	60	99	60	98	91	99	89	97	96	97	97	98	87	98	83
98	59	99	64	98	91	98	91	97	96	97	95	98	87	98	86
98	58	99	60	98	91	98	93	97	96	98	98	98	85	98	84
98	58	99	59	98	91	98	89	97	91	97	97	98	86	98	88
98	60	99	58	98	89	99	89	97	91	97	96	98	88	99	89

98	63	99	61	98	91	99	90	97	93	98	93	98	91	98	90
98	73	99	63	98	93	99	88	97	94	98	99	98	87	98	89
98	72	99	71	98	93	99	90	97	96	98	96	98	87	98	90
98	79	99	71	98	91	98	92	97	99	98	68	98	87	98	85
98	70	99	81	98	91	99	92	97	96	99	103	98	86	98	85
98	68	99	71	98	94	99	92	97	98	97	96	98	88	98	93
98	63	99	65	98	91	98	91	97	99	97	100	98	83	99	86
98	59	99	64	98	89	99	88	97	96	98	99	98	85	98	83
98	58	99	60	98	87	98	86	97	98	98	97	98	87	99	85
98	56	99	59	98	89	99	89	98	98	97	99	98	82	98	88
98	56	99	56	98	89	98	92	98	94	98	95	98	80	99	84
98	58	99	59	98	91	99	94	98	98	98	94	98	89	98	90
98	60	99	59	98	88	98	89	97	99	99	99	98	86	98	87
98	60	99	62	98	91	98	91	97	101	98	99	98	87	99	89
98	62	99	61	98	91	98	91	97	104	99	101	98	89	98	91
98	62	99	61	98	91	99	91	97	101	98	101				
				98	96	98	94	97	98	99	99				

Table C.2: Standing chest data set

Subject 1 Standing Chest				Subject 2 Standing Chest				Subject 3 Standing Chest				Subject 4 Standing Chest			
Reference Oximeter		Prototype		Reference Oximeter		Prototype		Reference Oximeter		Prototype		Reference Oximeter		Prototype	
SpO2	PR	SpO2	PR	SpO2	PR	SpO2	PR	SpO2	PR	SpO2	PR	SpO2	PR	SpO2	PR
98	96	99	101	98	96	96	93	98	91	99	87	98	98	98	98
98	101	99	99	98	94	98	92	98	91	99	89	98	94	98	97
98	101	99	106	98	98	98	89	98	87	98	92	98	100	97	103
98	108	99	108	98	101	98	92	98	87	99	94	98	99	95	100

98	108	99	111	98	93	97	93	97	87	99	82	98	98	98	98
98	104	99	107	98	94	99	92	98	87	99	87	98	96	98	97
98	106	99	98	98	96	99	94	98	88	99	85	98	96	99	102
98	108	99	109	98	91	99	93	98	91	99	87	98	99	98	104
98	101	99	108	98	96	99	95	98	84	99	89	98	96	98	95
98	106	99	105	98	96	99	93	97	84	98	92	98	98	98	100
98	103	99	111	99	94	99	93	98	86	99	83	98	99	98	103
98	106	99	100	99	91	99	94	98	87	99	88	98	99	98	101
98	103	99	104	99	91	98	90	98	84	99	85	98	98	98	97
98	105	99	107	98	91	99	92	98	87	98	86	98	94	99	95
98	104	99	107	98	91	99	92	98	87	99	84	98	99	98	103
98	103	99	104	98	89	99	93	98	86	98	90	98	101	98	101
98	104	99	103	98	89	99	92	98	87	99	88	98	99	98	101
98	101	99	102	99	88	99	89	98	87	98	87	98	96	98	99
98	104	99	103	98	87	99	91	98	91	98	86	98	98	98	98
98	106	99	108	99	88	99	91	98	87	98	92	98	101	98	103
98	106	99	100	99	94	99	90	98	89	98	92	98	101	97	99
98	108	99	100	99	93	98	92	98	91	98	90	98	98	98	92
98	109	99	106	98	96	99	95	98	87	98	87	98	101	98	100
98	101	99	104	99	96	98	92	98	89	98	87	98	101	97	103
98	101	99	101	99	96	99	94	98	87	99	84	98	104	97	106
98	101	99	104	99	96	99	88	98	87	98	85	98	105	98	107
98	106	99	105	99	94	99	92	98	87	98	87	98	106	98	106
98	101	99	105	99	93	99	98	98	89	98	88	98	106	98	107
98	104	99	106	99	91	99	95	98	92	98	89	98	112	99	108
98	112	99	105	99	93	99	92	98	91	98	89	98	96	97	99
98	107	99	116	99	94	98	92	98	87	98	92	98	101	98	99
98	104	99	110	99	91	99	94	98	89	98	91	98	101	98	102

98	108	99	107	99	94	99	94	98	89	98	90	98	104	98	106
98	108	99	107	99	94	99	94	98	92	98	89	98	105	98	106
98	109	99	105	99	93	99	69	98	87	99	87	98	109	97	106
98	104	99	109	99	94	99	94	98	88	99	88	98	101	98	100
98	112	99	100	98	96	98	74					98	106	97	107

Table C.3: Sitting wrist data set

Subject 1 Sitting Wrist				Subject 2 Sitting Wrist				Subject 3 Sitting Wrist				Subject 4 Sitting Wrist			
Reference Oximeter		Prototype		Reference Oximter		Prototype		Reference Oximeter		Prototype		Reference Oximeter		Prototype	
SpO2	PR	SpO2	PR	SpO2	PR	SpO2	PR	SpO2	PR	SpO2	PR	SpO2	PR	SpO2	PR
95	77	95	79	98	106	98	104	98	85	99	84	99	62	98	60
97	79	98	80	98	106	98	107	98	87	99	88	99	61	99	63
98	80	98	80	98	101	98	103	98	85	99	89	99	62	99	62
98	83	98	83	98	101	98	101	98	85	99	89	99	62	99	59
98	84	98	81	98	96	98	102	98	87	98	86	99	66	99	64
97	80	98	81	98	98	98	101	98	87	99	89	99	62	99	74
98	81	98	79	98	99	98	102	98	88	99	86	99	58	99	61
98	80	98	80	98	96	98	99	98	91	99	91	99	58	99	58
98	80	98	79	98	98	98	99	98	91	98	92	99	59	99	59
98	80	98	80	98	99	98	101	98	92	98	89	99	58	99	59
98	82	98	85	98	101	98	102	98	87	98	86	99	60	99	59
98	82	98	82	98	106	99	61	98	87	99	89	99	63	99	66
98	83	98	84	98	96	98	98	98	87	98	92	99	62	99	63
98	84	98	84	98	96	98	99	98	87	99	86	99	67	99	63
98	87	98	87	98	101	98	102	98	86	99	90	99	83	99	64
98	82	99	82	98	87	98	98	98	89	99	90	99	60	99	63

98	82	98	81	98	88	98	96	98	91	98	89	99	60	99	61
98	83	98	83	97	91	98	94	98	89	98	87	99	68	99	60
98	82	98	83	98	101	98	104	98	85	99	87	99	59	99	69
98	87	98	91	98	99	98	98	98	89	99	86	99	58	99	62
98	84	99	82	98	96	98	99	98	91	98	86	99	59	99	59
98	80	98	82	98	96	98	100	98	87	98	92	99	59	99	59
98	80	98	80	98	99	98	100	98	88	98	83	99	60	99	60
98	83	95	82	98	101	98	101	98	87	99	85	99	60	99	61
98	84	98	85	98	101	98	101	98	83	99	87	99	57	99	61
98	87	98	85	98	99	98	101	98	85	98	88	99	58	99	59
98	83	98	85	98	101	98	103	98	91	98	89	99	66	99	58
98	83	98	84	98	98	98	96	98	89	98	86	99	60	99	67
98	83	98	85	98	98	97	100	98	85	99	84	99	59	99	60
98	85	98	82	98	98	98	99	98	83	99	82	99	59	99	58
98	85	98	85	98	96	98	98	98	84	99	86	99	53	99	61
98	83	98	86	98	99	98	101	98	87	99	86	99	53	99	107
98	83	99	84	98	98	98	95	98	83	98	86	99	63	99	68
98	87	99	84	98	99	98	99	98	87	98	89	99	69	99	61
98	87	98	87	98	99	98	102	98	87	99	86	99	65	99	69
98	83	98	87	98	101	98	102	98	87	99	92	99	61	99	67

Table C.4: Standing wrist data set

Subject 1 Standing Wrist				Subject 2 Standing Wrist				Subject 3 Standing Wrist				Subject 4 Standing Wrist			
Reference Oximeter		Prototype		Reference Oximeter		Prototype		Reference Oximeter		Prototype		Reference Oximeter		Prototype	
SpO2	PR	SpO2	PR	SpO2	HR	SpO2	PR	SpO2	HR	SpO2	PR	SpO2	Heart Rate	SpO2	PR
98	94	98	93	98	99	98	108	98	98	98	96	98	71	94	69

98	96	98	96	98	101	98	99	98	98	95	97	98	77	98	73
98	96	99	100	98	99	98	99	98	94	95	100	98	71	98	69
98	96	98	99	98	103	98	98	98	96	95	100	98	79	98	80
98	98	98	97	98	103	98	101	98	99	95	91	98	84	98	83
98	98	99	97	98	96	98	101	98	99	95	99	98	76	98	75
98	96	98	98	98	101	98	97	98	94	95	96	98	75	98	77
98	96	98	100	98	94	96	95	98	96	97	97	98	80	98	82
98	98	98	97	98	95	97	88	98	94	95	96	98	77	98	79
98	99	98	101	98	96	97	98	98	96	95	98	98	80	98	78
98	99	98	95	98	97	98	96	98	96	96	99	98	80	98	81
98	101	99	97	98	99	98	97	98	91	95	100	98	79	98	78
98	101	96	98	98	101	98	101	98	94	95	92	98	75	98	80
98	98	98	97	98	100	98	99	98	99	95	95	97	83	98	82
98	96	99	93	98	98	99	94	98	93	95	91	98	83	98	81
98	96	98	101	98	101	98	97	98	91	95	87	98	80	98	85
98	98	98	98	98	103	98	99	98	88	97	106	98	77	98	82
98	101	98	100	98	101	97	104	98	89	96	93	97	78	98	85
98	112	99	100	98	99	97	100	98	93	95	98	97	78	98	85
98	101	98	105	98	102	98	99	98	92	95	95	97	80	98	83
98	91	98	85	98	103	98	104	98	96	96	95	98	78	98	73
98	93	98	88	98	101	97	103	98	96	95	93	98	76	98	78
98	96	97	92	98	99	98	99	98	91	96	88	98	78	98	81
98	96	98	95	98	101	98	98	98	96	95	94	98	77	98	76
98	98	98	100	98	104	98	100	98	90	97	88	98	83	98	86
98	99	98	100	98	106	98	107	98	91	98	61	98	80	98	77
98	101	98	102	98	101	98	99	98	86	99	93	98	75	98	79
98	98	98	99	98	99	96	99	97	96	96	93	98	80	98	87
98	103	98	98	98	99	97	99	97	91	96	91	98	76	98	81

98	99	98	103	98	103	98	98	97	91	95	93	98	80	98	81
98	99	98	98	98	101	97	105	98	89	95	97	98	80	97	85
98	98	98	103	98	104	98	100					98	79	98	81
98	101	99	101	98	108	98	105					98	76	98	80
				98	106	98	110					98	73	98	79
				98	96	98	105					98	73	98	80
				98	103	98	95					98	81	98	80

Table C.5: Standing wrist data set

Subject 1 Hyperventilation		Subject 2 Hyperventilation		Subject 3 Hyperventilation		Subject 4 Hyperventilation	
Reference Oximeter	Prototype	Reference Oximeter	Prototype	Reference Oximeter	Prototype	Reference Oximeter	Prototype
PR	PR	PR	PR	PR	PR	PR	PR
91	92	91	92	82	82	89	89
91	82	89	88	81	99	85	85
86	87	89	91	82	80	91	88
85	85	87	86	88	87	85	80
84	85	87	86	84	88	87	82
80	84	87	91	87	87	89	88
77	76	87	91	87	85	89	91
75	53	89	90	87	78	87	79
76	78	94	92	87	86	87	87
80	81	96	95	87	74	87	76
83	80	96	93	87	82	87	86
87	84	98	100	87	79	89	87
88	92	100	101	77	93	89	91
94	94	96	89	76	98	90	89
96	95	96	94	82	101	89	97

99	101	96	92	96	111	89	90
101	100	91	95	99	110	87	91
103	105	91	88	106	110	98	101
103	104	87	95	108	107	101	94
101	102	87	81	108	113	101	99
101	91	92	93	106	115	101	95
98	99	95	91	109	115	106	105
99	94	96	97	112	118	110	110
96	94	96	95	112	121	116	119
96	100	98	95	115	111	120	113
91	96	98	91	117	109	124	80
87	91	99	90	113	97	128	126
86	85	104	97	108	91	112	134
87	86	104	103	103	90	112	131
87	88	103	109	93	91	108	115
87	88	101	108	91	92	106	109
87	87	101	97	89	97	101	101
87	89	91	95	91	84	99	99
87	86	90	100	92	89		
87	87	96	86	89	68		

Table C.6: Hyperventilation data set

Subject 1		Subject 2	
Reference Oximeter	Prototype	Reference Oximeter	Prototype
SpO2	SpO2	SpO2	SpO2
99	97	98	98
99	97	98	98
99	98	98	98

99	97	98	97
99	97	98	98
99	97	98	98
99	97	98	98
99	98	98	96
99	97	98	98
99	97	98	97
99	97	97	96
99	97	97	98
99	96	97	98
99	97	98	99
99	97	98	99
99	98	93	99
99	97	97	93
99	98	97	99
99	97	98	94
99	98	98	98
99	98	98	97
99	97	99	98
99	97	95	98
99	97	97	96
97	96	98	99
97	96	98	98
96	95	98	99
94	95	98	98
92	94	97	98
91	93	97	98
94	96	96	98

97	96	98	99
98	97	98	98
97	96	98	99
98	97		
98	98		
98	97		
97	97		
97	96		
97	97		
98	97		
98	96		
98	97		
98	96		

Appendix D: Filter Bode Plots

The bode plot in *Figure D.1* was generated online using an online filter calculator which allows you to input the filter characteristics and the calculator will output appropriate resistor and capacitor values. In the case above, the filter was a bandpass filter utilized in analog form in the circuitry directly after the Sample-and-Hold circuits. The filters consisted of a frequency cutoff of 2Hz and a bandwidth of 2Hz to effectively cover a range between 1Hz and 3Hz.

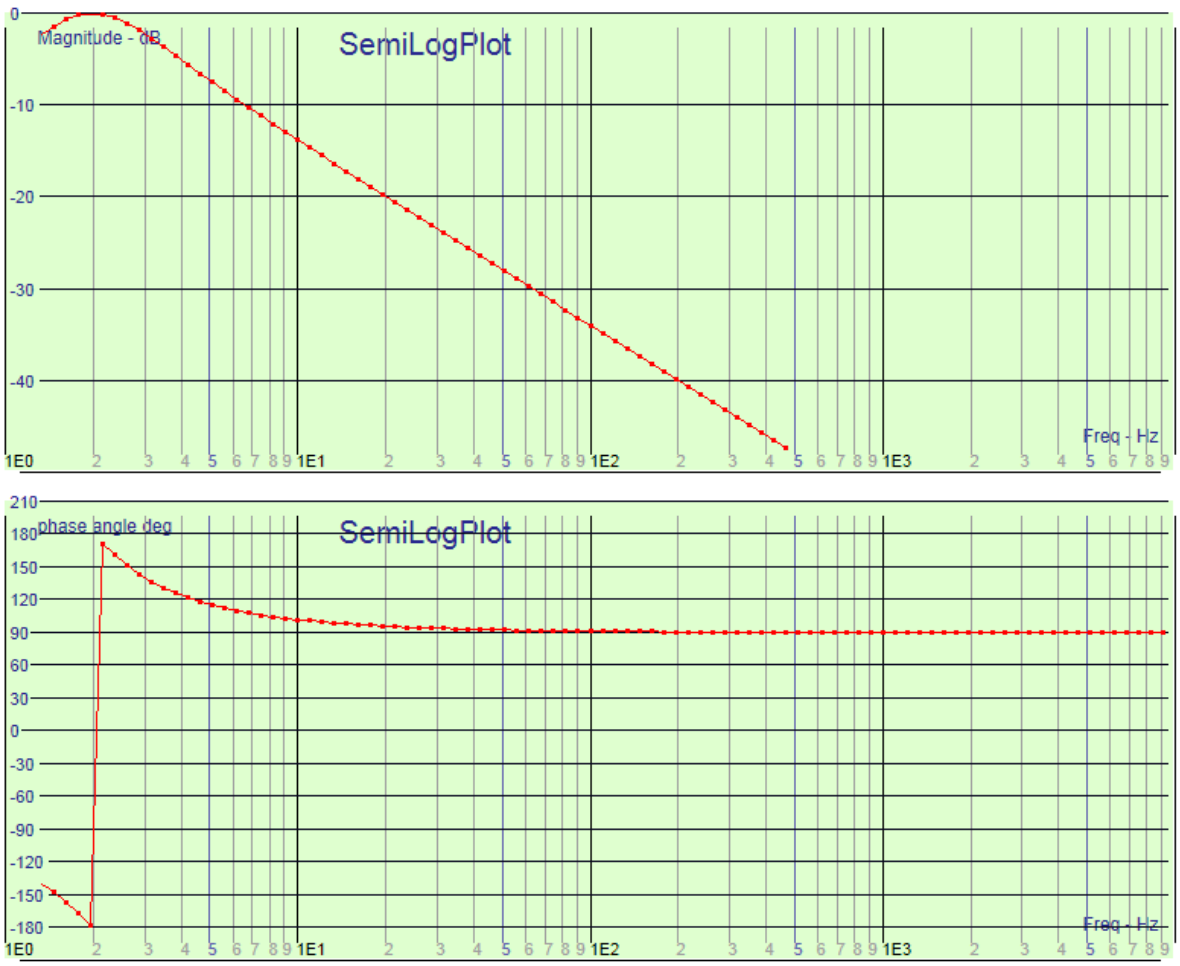

Figure D.1: Active analog bandpass filter plot

In *Figures D.2* and *D.3* we show two analog filters that were implemented in the circuitry for the red AC signal. We noticed that the red AC signal still contained a DC offset even after the bandpass filter and as a result decided to implement two more analog passive filters, one a high pass filter with an fc of 0.1Hz and the other a low pass filter with a fc of 5.3Hz. This not only reduced the DC offset that was present in the red AC signal but also reduced any noise present.

Both Bode plots and phase diagrams were generated online through a similar calculator for RC Lowpass and RC High pass filters. The calculations for these filters were also done to check for errors.

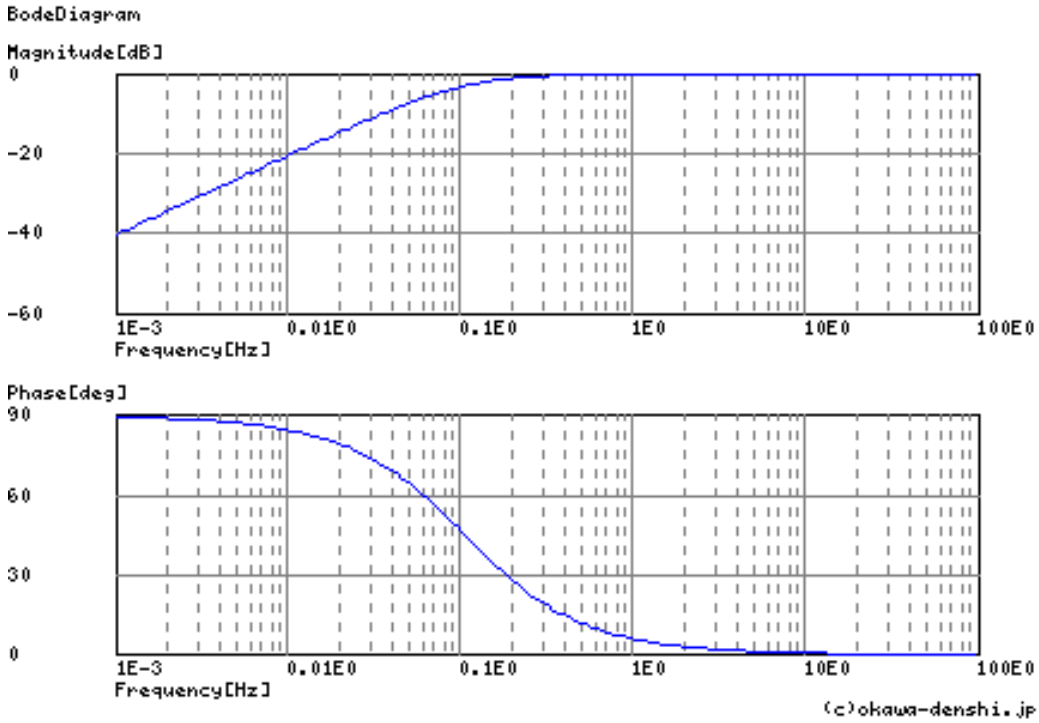

Figure D.2: High pass filter with fc of 0.1 Hz

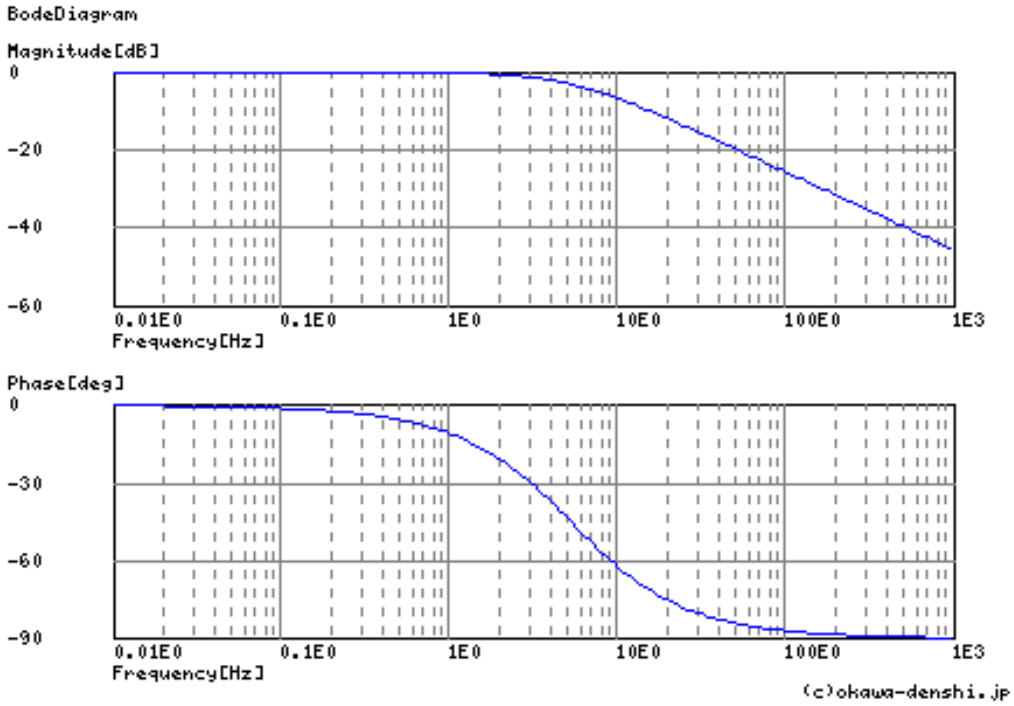

Figure D 3: Low pass filter with fc of 5.3 Hz

In *Figure D.4* we show the magnitude response and the phase response of a 7th order Chebyshev digital filter which was implemented in LabVIEW for the purpose of cleaning up the red AC signal to a further extent. This Bode Plot and phase diagram was generated using the Signals Toolbox in LabVIEW which allows one to see the magnitude response and the phase response of a filter as its being developed.

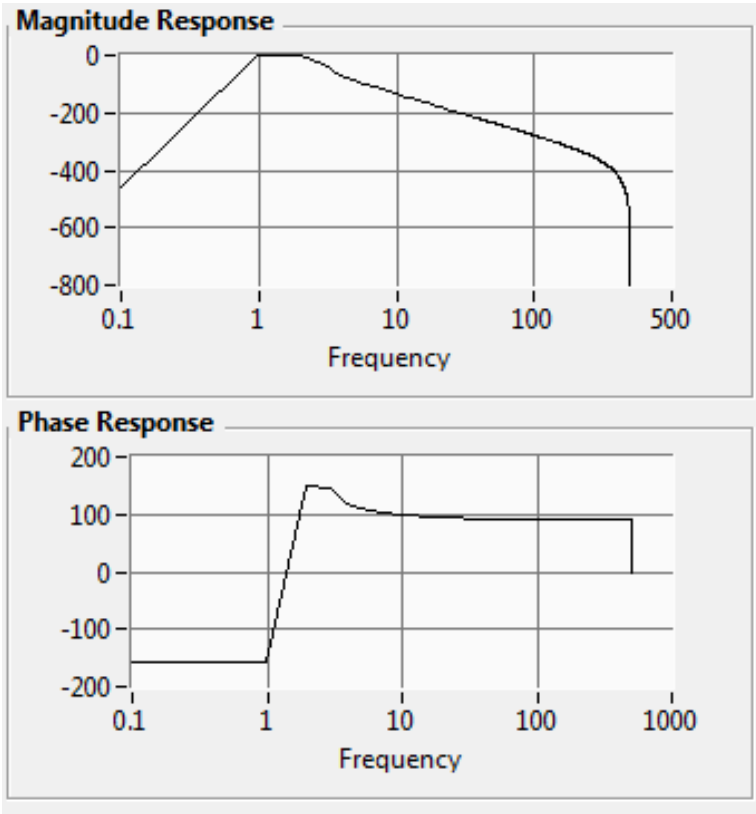

Figure D.4: 7th order Chebyshev digital filter with low fc of 0.75 and high fc of 2.5